A wide field view of the population of X-ray bursters in the Galaxy

A wide field view of the population of X-ray bursters in the Galaxy

Een wijde blik op de populatie van röntgenflitsers in de melkweg
(met een samenvatting in het Nederlands)

Proefschrift

ter verkrijging van de graad van doctor aan
de Universiteit Utrecht op gezag van de
Rector Magnificus, Prof. Dr. W.H. Gispen, ingevolge
het besluit van het College voor Promoties in het
openbaar te verdedigen op
woensdag 15 januari 2003 des middags te 12.45 uur

door
Rémon Cornelisse
geboren op 15 augustus 1974, te Vlaardingen

promotoren: Prof. Dr. Frank Verbunt
Faculteit Natuur- en Sterrenkunde, Universiteit Utrecht

Prof. Dr. John Heise
Stichting Ruimteonderzoek Nederland
Faculteit Natuur- en Sterrenkunde, Universiteit Utrecht

co-promotor: Dr. Jean in 't Zand
Stichting Ruimteonderzoek Nederland

Contents

Chapter 1

Introduction

1.1 Brief history on X-ray binaries

In 1962 the first extra-solar X-ray source was discovered during a rocket flight (Giacconi et al. 1962). For this work Giacconi was awarded part of the Nobel prize in physics in 2002. In 1966 it was suggested that this source, named Scorpius X-1 (Sco X-1, first X-ray source detected in the constellation Scorpius), was a member of a binary system with a period of 18.9 hrs and an optical counterpart of V=12.6±0.2 mag (Gottlieb et al. 1975; Gursky et al. 1966; Sandage et al. 1966). During the period between 1962 and 1966 it was realized that binary systems could emit X-rays, through accretion onto a compact object (Hayakawa & Matsuoka 1963; Salpeter 1964; Zel'Dovich 1964), either a neutron star or black hole. Cyg X-1 was the first binary system for which the compact object was suggested to be a black hole (Webster & Murdin 1972, Bolton 1972). The radial velocity of the supergiant showed a 5.6 day orbital period, imlying a mass for the compact object in excess of $\simeq 7\ M_\odot$. Since then, approximately 230 X-ray binaries have been detected in our Galaxy. An excellent overview on the topic of X-ray binaries is the book 'X-ray binaries' edited by Lewin, van Paradijs, & van den Heuvel (1995).

1.2 X-ray binaries

X-ray binaries are traditionally divided in two classes; those with companion stars which have masses above $10M_\odot$, the so-called high mass X-ray binaries

(HMXBs), or those with companion stars which have masses below $1M_{\odot}$, the so-called low mass X-ray binaries (LMXBs). Only later it was realized that a few binaries have intermediate mass, for example Cygnus X-2 and Hercules X-1 (e.g. Podsiadlowski & Rappaport 2000; Reynolds et al. 1997), and that a class of intermediate mass X-ray binaries exists (e.g. Davies & Hansen 1998; Kolb 1998)

The X-rays from HMXBs are thought to be due to either accretion from the wind of the O or B type companion (e.g. Vela X-1) or a disk that is fed by Roche lobe overflow of the supergiant companion (e.g. Cen X-3). The neutron stars in HMXBs have strong magnetic fields ($B \gtrsim 10^{12}$ G) that disrupt the accretion flow and funnel the material on the magnetic poles (e.g. Pringle & Rees 1972; Davidson & Ostriker 1973). This causes hot-spots at the magnetic poles which are observed as X-ray pulsations when they rotate through the line of sight. Their X-ray to optical flux ratio ranges from $\sim 10^{-3}$ to $\sim 10^{1}$ and their orbital periods from 4.8 hrs to 187 days.

The compact object in LMXBs accretes matter through a disk that is fed by Roche lobe overflow of the secondary. The magnetic fields from LMXBs are much lower ($B \lesssim 10^{10}$ G) and the accretion disk can come close to, or connect to the compact object through a boundery layer. The energy released from the inner parts of the disk is observable in X-rays, and gives rise to a significantly softer X-ray spectrum compared to HMXBs. The optical counterparts of LMXBs are faint ($M_V > 0$), making detection difficult. The LMXBs that are optically identified have X-ray to optical flux ratios ranging from 10^{2} to 10^{4} while their orbital periods range between 0.19 and 398 hrs. The outer regions of the accretion disk outshine the secondary, and completely dominate the optical flux. Recently signatures of the mass donor of Sco X-1 were revealed (Steeghs & Casares 2002).

1.3 Low Mass X-ray binaries

Most bright X-ray sources ($\gtrsim 10^{-10}$ erg cm^{-2}s^{-1} (2-10 keV), corresponding to $\gtrsim 10^{34}$ erg s^{-1} for a source at 8 kpc distance) in the sky are LMXBs, and about 160 have been detected so far (Liu et al. 2001). As can be seen from Fig. 1.1 the population of LMXBs is concentrated towards the Galactic center. The fact that LMXBs are found towards the Galactic center or in globular clusters, together with the fact that they have low-mass companions points towards an old population.

The creation of a LMXB is very hard. It is not easy to understand why the
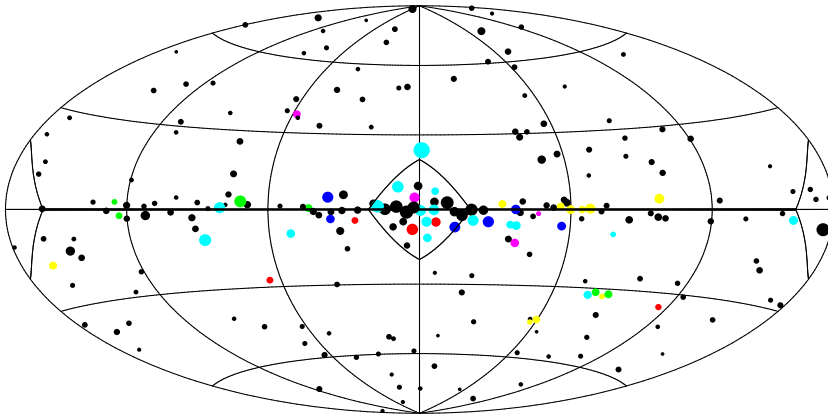
Ariel V 3rd Catalogue

Figure 1.1: Distribution of X-ray sources in Galactic coordinates as observed with the Ariel V satellite. The Galactic center is in the middle of the figure. The size of a dot gives the relative brightness of the X-ray source. The field of view of the BeppoSAX Wide Field Cameras is indicated with a square centered around the Galactic center and anti-center.

system is not disrupted during the supernova explosion which forms the neutron star. Two solutions have been suggested (see, e.g., Verbunt 1993 for a review). The exchange of the neutron star during the encounter with a binary or tidal capture are thought to be the most important formation mechanisms in globular clusters (Hut et al. 1992). This could explain the large fraction ($\simeq 10\%$) of X-ray binaries in globular clusters; e.g. in 47 Tuc and NGC 6440 the Chandra satellite recently detected 2 and 4 LMXBs, respectively (Grindlay et al. 2001; Pooley et al. 2001). In the Galactic center region a spiral-in scenario where the binary lost most of its initial mass and angular momentum is most likely (van den Heuvel et al. 1983). A third scenario, the collapse of a white dwarf induced by accretion, is not thought to be a likely scenario anymore (Verbunt 1993).

The discovery of the first millisecond pulsar, PSR 1937+21, triggered the idea of 'recycled' pulsars (Backer et al. 1982). These pulsars have low magnetic fields (10^{8-9} Gauss) and are often found in binary systems. They are thought to be spun-up by the accretion of $\simeq 0.1 \ M_{\odot}$ from the companion star (see e.g.
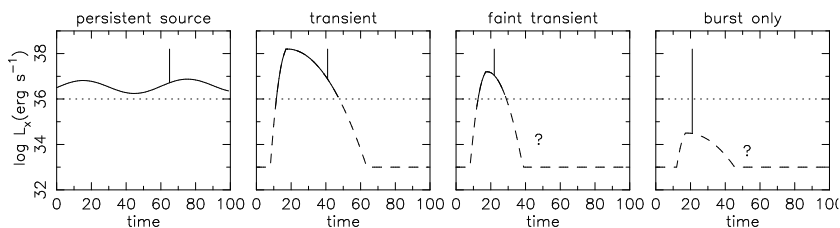
Figure 1.2: The four different classes of low mass X-ray binaries. The last two classes, the faint transients and burst-only, were discovered with BeppoSAX. The solid line sketches the typical observed behaviour of the persistent emission for the different classes. The horizontal dotted line indicates the typical sensitivity for survey instruments. The dashed line indicates the behavior of the persistent emission below this limit. A question mark indicates that the behavior of the persistent emission is not known. The spike denotes the occurrence of a type I X-ray burst (see below). They do not occur in all sources. No physical value is attached to the timescales, although days is a good approximation.

reviews by Bhattacharya & van den Heuvel 1991). This makes LMXBs very good candidates of being the progenitor of millisecond pulsars. But it was only until the discovery of coherent millisecond pulsations in SAX J1808.4−3658 that this connection was confirmed (Wijnands & van der Klis 1998). So far, only three accreting millisecond pulsars have been detected, and all of them are very close binaries and have extremely low mass transfer rates (Markwardt et al. 2002, Galloway et al. 2002).

The population of LMXBs can be further divided in four subclasses as indicated in Fig. 1.2. Easiest to detect are the persistent sources which are always 'on' at luminosities of 10^{36-38} erg s^{-1}. In this class a distinction is made between so-called Z-sources with persistent emission levels roughly at the Eddington limit (10^{38} erg s^{-1}), and the so-called Atoll sources which emit well below the Eddington limit ($\sim 10^{36-37}$ erg s^{-1}; Hasinger & van der Klis 1989). The distinction between these two groups is made by the different tracks they follow in X-ray color-color diagrams. However, recently it was suggested that over long periods of time some Atoll sources follow the same track as the Z-sources (Muno et al. 2002; Gierlinski & Done 2002).

The (soft) X-ray transients are most of the time not visible to survey instruments. Only sometimes do they brighten by several orders of magnitude and rise above the detection thresholds. The peak luminosity of their outbursts is

10^{37-38} erg s^{-1}, as was the case with e.g. Aql X-1 and Cen X-4 (see Campana et al. 1998 for an overview). Thereafter their luminosities slowly decay over a period of weeks to months, back to a quiescent level of 10^{32-33} erg s^{-1} for neutron stars systems (Campana et al. 1998) and $\lesssim 10^{32-33}$ erg s^{-1} for black hole systems (Campana et al. 2001).

A class of faint transients was established by the BeppoSAX Wide Field Cameras (Heise et al. 2000; in 't Zand 2001). The cameras detected about a dozen transients with outburst peak luminosities of 10^{36-37} erg s^{-1} and outburst durations of only a few weeks, i.e. much shorter and fainter than the classical bright transients. One of the conclusions in this thesis is that the distribution of these faint transients is clearly more concentrated towards the Galactic center as compared to the persistent sources, pointing towards a separate class of the LMXBs.

Finally, there is the class of burst-only sources (in 't Zand et al. 1998; Cocchi et al. 2001). These sources are always below 10^{36} erg s^{-1} (the detection limit of most survey instruments) and probably above 10^{32} erg s^{-1} (the level of known neutron star soft X-ray transients in quiescence). Not much is known about the behaviour of these objects, because they are detected during a type I X-ray burst only (see below). The fact that these objects show a type I X-ray burst is a clear indication that the object is a LMXB containing a neutron star. Chapters 6 and 7 of this thesis discuss the class of burst-only sources in more detail.

1.4   Type I X-ray burst theory

Hansen & van Horn (1975) were the first to investigate the stability of a neutron star envelope assuming steady accretion rates and nuclear burning in thin shells. For most of the models they reviewed it was noticed that the nuclear fusion time became shorter than the cooling time, i.e. the shells become thermally unstable with growth rates ranging between milliseconds and months. A few months after the publication of their paper the Astronomical Netherlands Satellite (ANS) discovered intense X-ray bursts from the globular cluster NGC 6624 (Grindlay & Heise 1975, Grindlay et al. 1976). The connection between these X-ray bursts, later named type I X-ray bursts (Hoffman et al. 1978), and thermally unstable shell burning was later independently realized by Maraschi & Cavaliere (1976) and Woosley & Taam (1975). Since then about 65 type I X-ray bursters have been discovered. Type II X-ray bursts are only observed from the Bursting Pulsar (GRO J1644-28) and the Rapid Burster (MXB 1730−335) and are thought to be due to spasmodic accretion onto the neutron star surface (see Lewin et al.
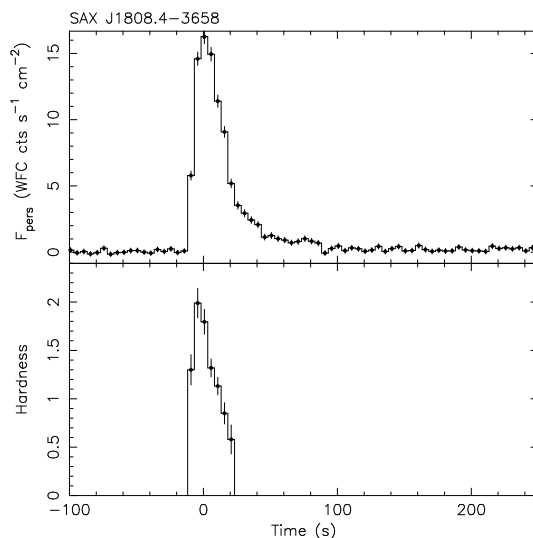
Figure 1.3: A typical X-ray burst as observed with the Wide Field Cameras. In the top panel the lightcurve of the source SAX J1808−3658 is shown with a resolution of 5 seconds. In the bottom panel the hardness, an indication for the temperature, during the burst is shown.

1995 for more information).

In Fig. 1.3 a typical example of a type I X-ray burst is shown. The shape of type I bursts is best described by a fast rise ($< 1 - 10$ s), during which the photoshere is heated, and an exponential-like decay (seconds to tens of minutes). During the decay the spectrum becomes softer, which is explained as the cooling of the neutron star photosphere. The burst spectrum is best bescribed by black body radiation with a peak temperature of $\simeq 2.5$ keV and a radius of $\simeq 10$ km (see Lewin et al. 1993 for a review).

The neutron star accretes hydrogen and/or helium rich material from the companion star, and a layer of fresh material is built up on the neutron star surface. If the temperature reaches about 10^8 K and a density of about 10^5 g cm^{-3} the hydrogen starts burning in a stable manner in the hot CNO cycle. This will create successive shells where the burning processess slowly changes the composition of the accreted matter. The shells at the bottom are increasingly difficult to cool. When the cooling rate becomes lower than the energy

production rate an instable situation arises, and thermonuclear runaway processes may start. Within a few milliseconds the temperature of this thin shell increases above the ignition temperature of helium. The helium rapidly starts burning in various shells via the triple alpha process. This is the start of the type I X-ray burst. Extensive overviews of the physics of X-ray bursts are given by Fujimoto et al. (1981) and Bildsten (1998). The fact that a surface is needed to start thermonuclear runaway processes gives direct prove that the compact object is a neutron star instead of a black hole (which has no surface). This makes X-ray bursts one of the best tools to unambiguously identify the compact object.

Differences in burst durations are explained by different fuel compositions which are basically caused by different accretion rates (see e.g. Fujimoto 1981). At the highest accretion rates ($0.05 \lesssim \dot{M}/\dot{M}_{\mathrm{Edd}} \lesssim 1$) hydrogen is accreted at a higher rate than can be burned in a stable fashion. This causes the unstable helium burning to take place in a hydrogen rich environment. Consequently, rapid proton capture can take place on the ashes of the helium burning, creating proton-rich elements up to Tellurium (^{107}Te; Schatz et al. 2001). The extra energy released due to the proton capture processes plus the β-decay processes, which are very slow compared to the other nuclear processes, extends the duration of the burst to at least tens of seconds. At intermediate accretion regimes ($0.01 \lesssim \dot{M}/\dot{M}_{\mathrm{Edd}} \lesssim 0.05$), hydrogen is burned in a stable manner at the same rate as it is accreted. As a result a helium layer is formed below the hydrogen burning shell. This layer is heated by the inward heat flow of the hydrogen burning shell until the critical temperature for unstable helium burning is reached. Due to the lack of protons only 3α and αp processes can take place (and not the β-decay processes), creating elements up to Titanium (^{42}Ti). This gives rise to bursts with durations shorter than 10 s. In the lowest accretion regime ($5 \times 10^{-7} \lesssim \dot{M}/\dot{M}_{\mathrm{Edd}} \lesssim 0.01$) the stable hydrogen burning is extinghuised during the inter-flash phase. When the temperature at the bottom of this hydrogen-rich envelope reaches $\sim 10^7$ K unstable hydrogen burning takes place triggering the X-ray flash. In this case the accreted helium burns in a hydrogen rich environment, giving rise to bursts with durations of tens of seconds. However, one must note that these different regimes only exists if hydrogen-rich material is accreted. For pure helium accretors, e.g. 4U 1820−30, only flashes in a pure helium environment can occur that last seconds, increasing to tens of seconds at very low mass accretion rates (Bildsten 1995).

After an X-ray burst in a hydrogen-rich environment the composition of the ashes consists mainly of heavy elements (e.g. ^{104}Ru) with a few % of Carbon (^{12}C; Schatz 2001). The amount of carbon gradually increases due to the X-ray

bursts until it can burn in an unstable fashion in the ocean of heavy element ashes (Cumming & Bildsten 2001). This is observed as the so-called superbursts, as discussed in chapter 4 and 5 of this thesis.

1.5 Observations of type I X-ray bursters

If the mass accretion rate is constant, the same amount of matter is accreted during equal intervals and the instability should occur after equal waiting times. The waiting time between bursts should in principle decrease linearly with increasing accretion rate. However, in many sources the opposite behaviour is observed, e.g. 4U 1705−44 and EXO 0748−676 show increasing waiting times with higher accretion rates (Langmeier 1987; Gottwald 1986). This was explained by Marshall (1982) and Bildsten (2000) by considering the local accretion rate instead of the global accretion rate. They suggest that, when the accretion rate gets higher, the burning area of the neutron star increases in such a way that the accretion rate per unit area actually decreases. Another explanation was given by van Paradijs et al. (1988). They suggested that more helium is burned in a stable manner with increasing mass accretion rate.

The energy released during an X-ray burst is in principle related to the amount of matter accreted and to the composition of the fuel. This is expressed by the so-called α-parameter, i.e. the ratio of the total emitted flux between bursts and the total flux emitted during a burst. For hydrogen-dominated bursts (at high and low accretion regimes; see above) a value of $\simeq 40$ and for pure helium bursts (middle accretion regime) a value of $\simeq 200$ is predicted. These values are confirmed by long term observations of e.g. 4U 1705−44, EXO 0748−676 and GS 1826−24 (Gottwald 1986; Gottwald 1989; Ubertini et al. 1999).

It is possible to make an estimate of the distance to a LMXB using X-ray bursts, and one may even get an indication on the ratio of the mass and radius of the neutron star. The peak-flux of an X-ray burst can never exceed the Eddington-limit of 2×10^{38} erg s^{-1} (assuming standard neutron star parameters and solar abundances). When a burst reaches this Eddington-limit, the photosphere, through which the luminosity is transported, expands due to radiation pressure and the effective temperature decreases. After the luminosity decreases below the Eddington limit the temperature increases and the radius decreases again to their original value; at that point the neutron star atmosphere starts cooling. This is observed during so-called photospheric radius expansion bursts. One can use the fact that for these bursts the peak luminosity equals the Eddington limit to estimate the distance. For non radius expansion bursts, where

the peak luminosity is below the Eddington Limit an upper-limit to the distance can be estimated. During radius expansion bursts the gravitational redshift can in principle be estimated, and from this the ratio of the mass and radius of the neutron star (see Lewin et al. 1993 for a detailed overview). However, the uncertainties on these parameters are still very large.

For a long time radius expansion bursts were the only method to estimate the gravitational redshift, and thus the ratio on the mass and radius of a neutron star. Only recently the XMM-Newton satellite observed absorption lines from EXO 0748−676 (Cottam et al. 2002), giving a direct measurement of the gravitational redshift. This is the first measurement of absorption lines in a neutron star atmosphere. High resolution spectra of other sources, like the isolated neutron stars RX J1856.5−3754, showed no spectral lines (Drake et al. 2002). For RX J1856.5−3754 the spectrum could very well described by pure black body radiation from an object with a radius of 3.8-8.2 km, inconsistent with the radius derived from optical and infra red observations (15±6 km; Kaplan et al. 2002).

The RXTE satellite discovered nearly coherent X-ray oscillations during thermonuclear X-ray bursts (Strohmayer 1996). For ten sources such oscillations have been detected, so far (see Strohmayer 2001). They are thought to be caused by a burning hot-spot on the neutron star surface rotating in and out of the line of sight near the neutron star spin frequency. One of these 10 sources, SAX J1808.4−3658 has a known spin frequency (401 Hz; Wijnands & van der Klis 1998) that corresponds to the observed burst oscillations (in 't Zand et al. 2001). The observed frequencies for the other nine sources are between 270 and 620 Hz, which is consistent with estimates of the spin periods reached by accretion-induced spin-up (Webbink et al. 1983). In principle these oscillations can tell us something about the propagation of the nuclear burning on the neutron star surface and again on the radius and mass of the neutron star.

1.6   Outline of this thesis

When I started the research for this thesis the main goal was to analyse the X-ray sources observed with the Wide Field Cameras (WFC) onboard the BeppoSAX satellite, resulting in a catalogue. The catalogue has not been completed due to all kinds of interesting discoveries during the analysis. Therefore, this thesis has become a compilation of these discoveries. The main theme is about low mass X-ray binaries, and more particular the type I X-ray bursters.

The first chapters of this thesis (3-5) discuss individual sources. Then there are two chapters (6+7) that treat several sources, and finally in chapter 8 a large set of X-ray bursters that are the most frequent bursters of the total population is discussed. The emphasis of this thesis is on the topics of superbursts (chapters 4+5) and the burst-only sources (chapters 6+7). These are two new developments in the area of X-ray bursters to which this thesis adds a significant contribution.

Most of the data presented in this thesis are from the WFC. Therefore, a description of the satellite and in particular the WFC is given in chapter 2.

In chapter 3 the discovery is described of SAX J1750.8−2900, a new member of the class of faint transients. The outburst lasted for $\simeq 2$ weeks before the source disappeared below the detection limit of the WFC. Seven type I X-ray bursts were observed during the outburst and two after the end of the outburst, proving that the compact object is a neutron star.

The discovery of the first so-called superburst is described in chapter 4. An hours long flare-like event was detected from the known X-ray burster 4U 1735−44. This event showed all the characteristics of thermonuclear X-ray bursts. However, no explanation could be given for the long duration and the large amount of energy released; both are an order of magnitude larger than typical type I X-ray bursts.

The discovery of this first superburst triggered an archival search for other such events in the WFC database. Two such superbursts were found; one in Serpens X-1 which is described in chapter 5 of this thesis. The third superburst, from KS 1731−260, is reported by Kuulkers et al. (2002). In the meantime two theoretical models were developed to explain these superbursts: unstable carbon burning in the deeper layers of a neutron star (Cumming & Bildsten 2001; Strohmayer & Brown 2002) and electron capture on heavy elements in the deeper layers of the neutron star (Kuulkers et al. 2002). Interestingly, according to the newest ideas most of the energy of a superburst is released due to photo-dissociation of heavy elements (Schatz 2002), making superbursts the only known process in astronomy where nuclear fission is the dominant energy source!

In chapter 6 five new discoveries of burst sources are reported. Four of these sources are burst-only sources, strengthening the proof of existence of this class. Chapter 7 describes follow-up observations with the Chandra X-ray satellite on five burst-only sources. No X-ray counterparts could unambiguously be identified, and the inferred persistent luminosity of $\sim 10^{32}$ erg s^{-1} shows that these sources are probably connected with the soft X-ray transients in quiescence.

General properties of the population of X-ray bursters are derived in chap-

ter 8. The nine of the most frequent bursters, as observed with the WFC are discussed. They appear to show the same burst behaviour when they are at the same luminosity. At the lowest luminosities there is a linear increase in burst rate with increasing luminosity. At 3×10^{37} erg s^{-1} there is a drop by a factor of five in burst rate observed, connected to the transition of burst in a hydrogen-rich environment to pure helium bursts. At higher luminosities the burst rate becomes irregular and no clear trend is observed with increasing luminosity.

references

Bhattacharya, D., van den Heuvel, E.P.J. 1991, Physics Report 203, 1

Bildsten, L. 1995, ApJ 438, 852

Bildsten, L. 1998, in Buccheri, R., van Paradijs, J., Alpar, M.A. (eds.), The many faces of neutron stars, Kluwer, p. 419

Bildsten, L. 2000, in Holt, S.S., Zhang, W.W. (eds.), Cosmic explosions, AIP, p. E65

Campana, S., Colpi, M, Mereghetti, S., Stella, L., & Tavani, M. 1998, A&AR 8, 279

Campana, S., Parmar, A.N., Stella, L. 2001, A&A 372, 241

Maraschi, L., Cavaliere, A. 1976 in Müller, E. (ed.), Highlights of Astronomy, Vol. 4, IAU, 127

Cocchi, M., Bazzano, A., Natalucci, L., et al. 2001, A&A 378, L71

Cottam, J., Paerels, F., & Mendez, M. 2002, Nature 420, 51

Cumming, A., & Bildsten, L. 2001, ApJ 559, L127

Davidson, K., & Ostriker, J.P. 1973, ApJ 179, 585

Davies, M.B., & Hansen, B.M.S. 1998, MNRAS 301, 15

Drake, J.J., Marshall, H.L., Dreizler, S., et al. 2002, ApJ 572, 996

Fujimoto, M.Y, Hanawa, T., Miyaji, S. 1981, ApJ 247, 267

Galloway, D.K., Chakrabarty, D., Morgan, E.H., Remillard, R.A. 2002, ApJ 576, 137

Giacconi, R., Gursky, H., Paolini, F.R., & Rossi, B.B. 1962, Phys. Rev. Lett. 9, 439

Gierlinski, M., & Done, C. 2002, MNRAS 331L, 47

Gottlieb, E.W., Wright, E.L., Liller, W. 1975, ApJ 195L, 33

Gottwald, M., Haberl, F., Parmar, A.N., & White, N.E. 1986, ApJ 308, 213

Gottwald, M., Haberl, F., Langmeier, A., et al. 1989, ApJ 339, 1044

Grindlay, J., Gursky, H., Schnopper, H., et al. 1976, ApJ 205, L127

Grindlay, J., & Heise, J. 1976, IAUC 2929

Grindlay, J., Heinke, C., Edmonds, P.D., & Murray, S.S. 2001, Science 292, 2290

Gursky, H., Giacconi, R., Gorenstein, P., et al. 1966, ApJ 146, 310

Hansen, C.J., & van Horn, H.M. 1975, ApJ 195, 735

Hasinger, G., & van der Klis, M. 1989, A&A 225, 79

Hayakawa, S., & Matsauka, M. 1963, in Composition, Origin, and Prehistory Proceedings from the 8th International Cosmic Ray Conference, Vol. 3, p. 213

Heise, J., in 't Zand, J.J.M., & Kuulkers, E. 2000, HEAD 32, 28.03 van den Heuvel, E.P.J. 1983, In Accretion Driven Stellar X-ray Sources, Ed. W.H.G. Lewin, E.P.J. van den Heuvel, Cambridge Univeristy press, p. 189

Hoffman, J.A., Marshall, H.L., & Lewin, W.H.G. 1978, Nature 271, 630

Hut, P., McMillan, S., Goodman, J., et al. 1992, PASP 104, 981

Kaplan, D.L., van Kerkwijk, M.H., & Anderson, J. 2002, ApJ 571, 447

Kolb, U. 1998, MNRAS 297, 419

Kuulkers, E., van der Klis, M., & van Paradijs, J. 1995, A&A 297, 141

Kuulkers, E., in 't Zand, J.J.M., van Kerkwijk, M.H., et al. 2002, A&A 382, 503

Langmeier, A., Sztajno, M., Hasinger, G., Trümper, J., & Gottwald, M. 1987, ApJ 323, 288

Lewin, W.G., van Paradijs, J., & van den Heuvel, E.P.J. 1995, in: X-ray binaries, Cambridge Univerity Press

Lewin, W., van Paradijs, J., Taam, R. 1993, Space Sci. Rev., 62, 223

Lewin, W., van Paradijs, J., Taam, R. 1995, in Lewin, W.G., van Paradijs, J., & van den Heuvel, E.P.J. 1995, in: X-ray binaries, Cambridge Univerity Press, p. 175

Liu, Q.Z., van Paradijs, J., & van den Heuvel, E.P.J. 2001, A&A 368, 1021

Markwardt, C.B., Swank, J.H., Strohmayer, T.E., in 't Zand, J.J.M., Marshall, F.E. 2002, ApJ 575L, 21

Marshall, H.L. 1982, ApJ 260, 815

Muno, M.P., Remillard, R.A., & Chakrabarty, D. 2002, ApJ 568L, 35

van Paradijs, J., Penninx, W., & Lewin, W.H.G. 1988, MNRAS 233, 437

Podsiadlowski, Ph., Rappaport, S. 2000, ApJ 529, 946

Pooley, D., Lewin, W.H.G, Verbunt, F., et al. 2002, ApJ 573, 184

Pringle, J.E., & Rees, M.J. 1972, A&A 21, 1

Reynolds, A.P., Quaintrell, H., Still, M.D., et al. 1997, MNRAS 288, 43

Salpeter, E.E. 1964, ApJ 140, 499

Sandage, A., Osmer, P., Giacconi, R., et al. 1966, ApJ 146, 316

Schatz, H. Aprahamian, A., Bildsten, L., et al. 2001, Phys. Rev. Lett. 86, 3471

Schatz, H. 2002, APS, U2004

Steeghs, D., & Casares, J. 2002, ApJ 568, 273

Strohmayer, T.E., Giles, B., Jahoda, K., & Lee, U. 1996, Bull. of the AAS 28, p. 1425

Strohmayer, T.E. 2001, in Advances in Space Research, Volume 28, Elsevier, p. 511

Strohmayer, T.E., & Brown, E.F. 2002, ApJ 566, 1045

Tawara, Y., Hayakawa, S., Kii, T. 1984, PASJ 36, 855

Ubertini, P., Bazzano, A., Cocchi, M. 1999, ApJ 514L, 27

Verbunt, F. 1993, ARA&A 31, 93

Webbink, R.F., Rappaport, S., Savonije, G.J. 1983, ApJ 270, 678

Webster, B.L., & Murdin, P. 1972, Nature 235, 37

Wijnands, R., van der Klis, M. 1998, Nature 394, 344

Woosley, S.E., Taam, R.E. 1976, Nature 263, 101

in 't Zand, J.J.M., Heise, J., Muller, J.M, et al. 1998, AN 319, p. 112

in 't Zand, J.J.M., 2001, in A. Gimenez, V. Reglero, & C. Winkler (eds.),

in 't Zand, J.J.M., Cornelisse, R., Kuulkers, E., et al. 2001, A&A 372, 916
  Exploring the gamma-ray universe, ESA Pub. Div., p. 463

Zel'Dovich, Ya. B. 1964, Sov. Phys. Dokl. 9, p. 246

Chapter 2

BeppoSAX

2.1 The satellite

The Satellite per Astronomia X (SAX) (Boella et al. 1997a) is an Italian-Dutch X-ray satellite that operated from April 30 1996 to April 30 2002. Fig. 2.1 gives a photograph of the satellite. Shortly after launch the satellite was renamed BeppoSAX in honor of the Italian physicist Giuseppe (Beppo) Occhialini (1907-1993). He was an Italian elementary particle physicist and played a crucial role in starting the European Space Research Organisation, especially in stimulating the scientific program.

The satellite had a low-earth circular orbit of 600 km, with an inclination of $3°9$. It had an orbital period of 96 min; however, the observing efficiency was on average 50% due to earth eclipses and South Atlantic Anomaly passages. The satellite was stabilized in three axes with a pointing accuracy of about $1'$. The solar panel needed to be oriented within $30°$ from the sun, with occasional excursions of upto $5°$ possible. Due to these solar constraints about 50% of the sky was accessible at any given time.

The main scientific characteristic of the satellite was the wide spectral coverage, from 0.1 to to 300 keV. The scientific payload consisted of four Narrow Field Instruments (NFI), the Gamma Ray Burst Monitor and two Wide Field Cameras (WFC). The WFCs will be discussed separately in section 2.2. The NFI were co-aligned with the Z-axis of the satellite (see Fig. 2.2) and consisted of the following instruments:

- Low Energy Concentrator Spectrometer (LECS): grazing incidence tele-

15

Figure 2.1: The BeppoSAX satellite before launch at ESTEC, Noordwijk

scope with a position sensitive gas scintillation proportional counter in its focal plane (Parmar et al. 1996).

- Medium Energy Concentrator Spectrometers (MECS): three identical grazing incidence telescopes, identical to the LECS, with position sensitive gas scintillation proportional counters in their focal planes (Citterio et al. 1985; Conti et al. 1994; Boella et al. 1997).

- High Pressure Gas Scintillation Proportional Counter: non-imaging device (HPGSPC; Manzo et al. 1996).

- Phoswich Detector System: non-imaging device (PDS; Frontera et al. 1997).

In Table 2.1 we summarize the main characteristics of each instrument. The four lateral active shields of the PDS were used to detect gamma-ray bursts (with a temporal resolution up to 1 ms) in the range of 40-700 keV (Frontera et al. 1997).

2.2 Wide Field Cameras

The Wide Field Cameras were developed by the Space Research Organization Netherlands in Utrecht (Jager et al. 1997). In Fig. 2.3 one of the WFCs is

16
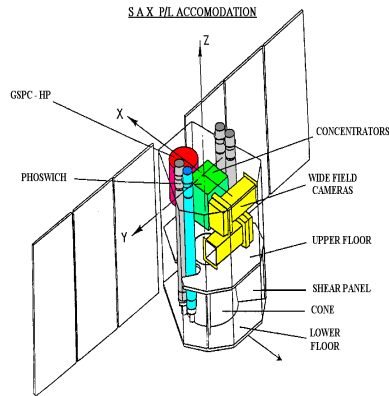
Figure 2.2: An schematic drawing of the BeppoSAX satellite showing the scientific instruments accommodation

shown. They are identical coded mask cameras that are mounted in opposite directions and perpendicular to the pointing directions of the NFI (see Fig. 2.2). In Table 2.2 the characteristics of the instrument are given.

The main scientific goal of the WFC was the study of transient X-ray phenomena at unexpected positions in the sky. It therefore continuously monitored (except for earth occultations and South Atlantic Anomaly passages) during the so-called WFC secondary mode observations the region in the sky dictated by the NFI observing program. The instrument could also carry out spatially-resolved simultaneous monitoring of compact X-ray sources in crowded fields like the Galactic center. Therefore, each spring and fall a monitoring program was carried out on the Galactic center region, so-called WFC primary mode

Table 2.1: Characteristics of the NFI.

instrument	energy range (keV)	field of view (°) FWHM	resolution (′)	area cm^2
LECS	0.1-10	0.5	3.5	50
MECS	1.3-10	0.5	1.2	150
HPGSPC	4-120	1.1		240
PDS	15-300	1.3		600

17
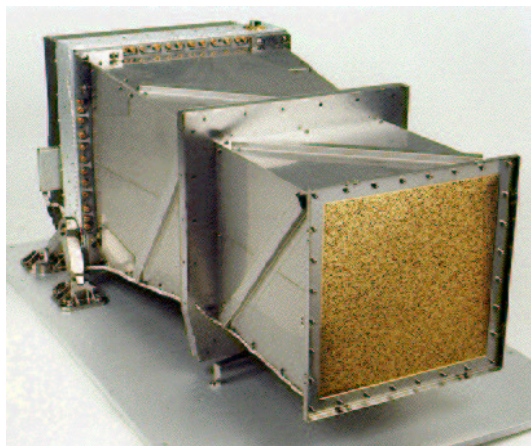
Figure 2.3: One of the Wide Field Cameras

observations. In total 8% of the observing time was dedicated to these primary mode observations.

During the visibility windows in which the Galactic center was observable with the WFC, a program was carried out that on average monitored this region one day per week. In Fig 1.1 the WFC field of view of the X-ray sky is over-layed on about the Galactic center region (and the anti-center). From Fig 1.1 we notice that 50% of the low mass X-ray binary population can be observed simultaneously. The brightest source, Sco X-1, was kept out of the field of view on purpose. This source is so bright that it prevents the detection of weak sources over large portions of the field of view (see below).

Table 2.2: Characteristics of the Wide Field Cameras

Field of View	$40° \times 40°$
Energy range	1.8-28 keV (31 channels)
Effective area @6 keV	140 cm^2
Angular resolution	$5'$
source location accu.	$< 1'$
sensitivity	few mCrab in 10^5 s
time resolution	0.5 ms

2.3 Coded aperture imaging

In Fig. 2.4 the mask pattern that is used for the WFC is shown. It is basically a semi-random pattern (Dicke 1968) of equal sized squares that are either transparant or opaque to photons between 2 to 28 keV. The WFC mask has 256×256 elements of 1 mm^2 each. Behind the mask there is an equally sized $(25.6 \times 25.6$ cm$^2)$ detector. This detector is a two-dimensional position-sensitive multi-wire proportional counter (Mels et al. 1995).

Photons from a certain direction in the sky project the mask pattern on the detector. The direction of the photons gives the projected mask pattern a unique shift relative to the central position. During an observation the detector collects the sum of mask patterns equal to the number of point sources in the sky. The amplitude of the mask pattern encodes the intensity. The mask pattern should, therefore, satisfy the conditions that the auto-correlation function of the mask pattern is a single peak with flat side-lobes, and that the signal-to-noise ratio of a coded sky source is optimum. Semi-random patterns exist that fulfill these requirements (e.g. Fenimore & Cannon 1978). In the case of the WFC, where one of the objectives was the observation of crowded fields like the Galactic Center, an open fraction of the pattern between 0.25 and 0.33 was found to be optimum. However, a pattern with an open fraction around 0.33 which fulfills the above conditions does not exist, so a pattern was chosen for the WFC as close as possible to an optimum one (in 't Zand et al. 1994). An extensive overview of the principles of coded mask imaging is given by in 't Zand (1992).

After an observation the image of the detector must be decoded to reconstruct an image of the observed sky. For the WFC this is done by the process of Iterative Removal Of Sources (IROS; Hammerslay et al. 1992). In the first stage a cross-correlation between the mask and the detector image is made for each sky position, meaning that all counts from the detector pixels that are illuminated for a sky position are summed. This total derived flux for a sky position is a combination of the photons from a potential source at this position, the background photons plus the contribution of all other sources that illuminated these detector pixels. To estimate the contribution from the background and the other sources, the inverted mask (i.e. transparent squares are taken as opaque and vice versa) is correlated with the detector. One now knows that the measured flux at each sky position is only a combination of the background and other sources illuminating these pixels, the contribution from a potential source at this sky position should be zero. By subtracting the two fluxes derived above, and after accounting for the different numbers of open and closed mask elements, it gives an estimate for the flux from a potential source at each sky
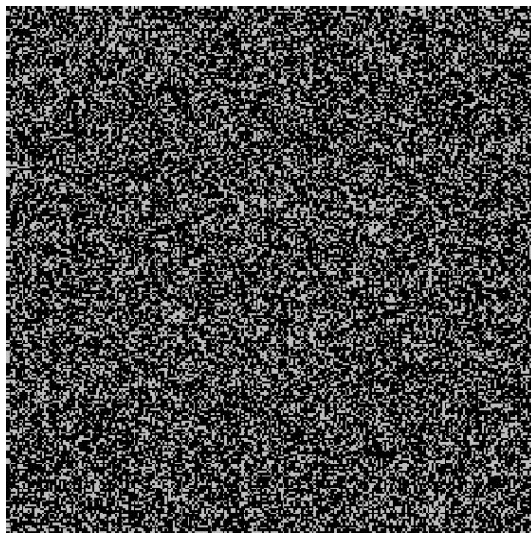
Figure 2.4: The Wide Field Cameras coded mask pattern.

position.

If the flux for each sky position is estimated IROS considers the brightest 100 sky postions in more detail (IROS takes into account that the point spread function of a real source is usually distributed over several sky positions, so the number of considered sky positions drops to $\simeq 20$). These positions are compared with a catalogue of X-ray sources, and the positions coinciding with catalogued sources are taken as a detection. For each of the detections the position (not taking into account the catalogued position) and the flux (plus error) are estimated. These fluxes are subtracted from the original detector image, and a background level is determined assuming that it is homogeneous over the detector.

After the detected sources are subtracted the second iteration starts in the same way as the first. The only difference is when IROS evaluates the brightest sky positions. Then it takes into account the sources found previously (to get a better flux and position estimate) and sources not listed in the catalogue (detection of new transient sources). This process is repeated until no new sources at 10σ significance are detected.

In principle IROS should find all sources up to the poisson noise. However,

due to the support structure of the WFC and the non perfect response of the detector pixels some extra flux is left in the image after all sources are removed. Especially at the edges of the detector some structure is still visible, making it impossible to detect weak sources on the edge of the field of view. Also, a very bright source (like Sco X-1) in the field of view degrades the detection limit significantly. The poisson noise of this source is so high that weaker sources do not belong to 100 brightest sky positions, and therefore can not be detected. This problem is solved by removing the part of the detector illuminated by this bright source, and thus lowering the noise level of the rest of the detector significantly.

The final result of IROS is a list of detected sources with their positions and average flux. The list of positions can be used to derive lightcurves for each individual source. For each time interval a detector image is created. Correlating the source positions in the sky with the mask gives for the photons in each detector pixel a weighted distribution over the sources. Applying this to all detector images in time gives a lightcurve. With this method the directional information of individual photons is lost, however. But this is an intrinsic problem of the coded mask. The advantage is that for a large part of the sky all (bright) sources can be observed simultaneously. To create a spectrum of an individual source one takes the position derived with IROS (for the total energy passband) as fixed and performs IROS for each of the 31 energy channels seperately.

References

Boella, G., Butler, R.C., Perola, G.C., et al. 1997a, A&AS 122, 299

Boella, G., Chiappetti, L., Conti, G., et al. 1997b, A&AS 122, 327

Citterio, O., Conti, G., Mattaini, E., Santambrogio, E., Sacco, B. 1985, SPIE Proc. 597,102

Conti, G. 1994, SPIE Proc. 2279, 101

Dicke, R.H. 1968, ApJ 153L, 101

Fenimore, E.E., & Cannon, T.M. 1978, Appl. Opt. 17, 337

Frontera,F., Costa, E., dal Fiume, D., et al. 1997, A&AS 122, 357

Hammerslay, A.P., Ponman, T.J., Skinner, G.K., et al. 1992, Nuc. Instr. Meth. Phys. Res. A311, 585

Jager, R., Mels, W.A., Brinkman, A.C., et al. 1997, A&AS 125, 557

Manzo, G., Giarrusso, S., Santangelo, A., et al. 1997, A&AS 122, 341

Mels, W.A., Buurmans, H.B., Jager, R., et a;. 1995, SPIE 2517, 269

Parmar, A.N., Martin, D.D.E., Bavdaz, M., et al. 1997, A&AS 122, 309

in 't Zand, J.J.M. 1992, Ph.D. thesis, University Utrecht

in 't Zand, J.J.M., Heise, J., Jager, R. 1994, A&A 288, 655

Chapter 3

SAX J1750.8-2900

A new bursting X-ray transient

L. Natalucci, R. Cornelisse, A. Bazzano, M. Cocchi, P. Ubertini, J. Heise,
J.J.M. in 't Zand and E.Kuulkers

Abstract– We have analysed in detail the discovery measurements of the X-ray
burster SAX J1750.8−2900 by the Wide Field Cameras on board BeppoSAX in
spring 1997, at a position ∼1.2 degrees off the Galactic Centre. The source was
in outburst on March 13th when the first observation started and showed X-ray
emission for ∼ 2 weeks. A total of 9 bursts were detected, with peak intensities
varying from ≈0.4 to 1.0 Crab in the 2-10 keV range. Most bursts showed a
fast rise time (≈1 s), an exponential decay profile with e-folding time of ≈5 s,
spectral softening during decay, and a spectrum which is consistent with few
keV blackbody radiation. These features identify them as type I X-ray bursts
of thermonuclear origin. The presence of type I bursts and the source position
close to the Galactic Centre favours the classification of this object as a neutron
star low mass X-ray binary. X-ray emission from SAX J1750.8−2900 was not
detected in the previous and subsequent Galactic bulge monitoring, and the
source was never seen bursting again.

3.1   Introduction

A long term program to survey the 40×40 degrees around the Galactic Centre started on mid 1996 with the large field of view instruments on board the BeppoSAX satellite (Wide Field Cameras, hereafter WFC). Previous surveys of the region with similar instruments were limited by the lack of the combination of sufficiently long, repeated exposures and the wide angular coverage. In the last 10 years, however, the use of the coded mask imaging technique increased the total number of known X-ray emitters in the region (Skinner et al. 1993; Vargas et al. 1997) stimulating detailed measurements of individual sources and in turn their identification at different wavelengths.

The Galactic Bulge monitoring program carried out by BeppoSAX WFC in the energy range 2-30 keV has been especially prolific in the study of X-ray burst sources, increasing substantially (by about 50% in 2.5 years) the number of objects of this type which were known originally in this region. As of January 1999 it led to the discovery of 6 new burst sources and, in addition, found burst emission from 7 already known sources (Heise et al. 1999; Ubertini et al. 1999a; Cocchi et al. 1998a for earlier results) in a total time exposure of $\approx$2.5×10^6s. The new transient sources show dim X-ray outburst episodes during $\sim$1 to a few weeks, with peak fluxes generally below a few 10^{37} erg s^{-1} at 10 kpc distance (Heise et al. 1999). From one of these sources, SAX J1808.4-3658 (in 't Zand et al. 1998) a modulation period of 2.5 ms was discovered by RXE during a second outburst (Wijnands & van der Klis 1998; Chakrabarty & Morgan 1998).

Here we report results of one of these previously unknown transients showing bursting behaviour, discovered by the WFC on March 18th, 1997 (Bazzano et al. 1997a; Heise et al. 1997) in a celestial position 1.2 degrees off the Galactic Center. In particular, we analyse the spectral and temporal behaviour of the persistent emission and characterise the burst emission properties to determine the nature of the transient.

3.2   Observations and data analysis

The Wide Field Cameras experiment on board the BeppoSAX satellite comprises 2 identical coded aperture multi-wire proportional counter detectors viewing opposite sky directions (Jager et al. 1997), each one featuring a field of view of 40×40 degrees full width to zero response (i.e., 3.7% of the sky) and an angular resolution of 5 arcmin. The source location accuracy depends on the signal-to noise ratio and is 0.7 arcmin at best (99% confidence level). The en-

ergy range is 2-30 keV on-axis and the time resolution is 0.5 ms. The field of view (FOV) is the largest of any flown X-ray imaging device with arcmin resolution, which allows for the search of short duration and/or weak transient events. The on-axis sensitivity for the Galactic Bulge field is $\approx$10 mCrab in 10^4s observing time. Detector data contain a superposition of background and of multiple source shadowgrams, the latter resulting from the coding of the sky object image with the instrument aperture pattern. The reconstruction of the sky image for point-like sources involves an algorithm that consist of a cross correlation of the detector data with the aperture (see e.g. Caroli et al. 1987). The position and intensity of any point source is determined by folding a sky model distribution through a point spread function (PSF), using iterative χ^2 minimisation (Jager et al. 1997). For WFC this can be carried out in each individual energy channel. The full-width at half maximum of the PSF is smallest on axis at $\approx$5 arcmin. SAX J1750.8−2900 is located only 1.2 degrees off the Galactic Centre and so in the most sensitive region for this type of observations. The Galactic Bulge was observed during spring 1997 for 5×10^5 s, spread out along 28 days.

Burst phenomena are systematically searched in data from both cameras using time profiles of the total detector over the entire energy range with a time resolution of 1 s. When a burst occurs a reconstructed sky image is generated for the burst duration and different sky images corresponding to longer time exposure are generated for intervals just before and after burst. This allows to resolve the point source responsible for the intensity increase revealed in detector ratemeters. In crowded fields and in some not evident case an image subtraction is necessary to facilitate identification of bursting sources in the FOV.

3.3   Transient source position and lightcurve

Fig. 3.1 shows the error region for SAX J1750.8-2900. The best fit position is R.A. = 17h 50m 24s, Dec = -29° 02' 18" (equinox 2000.0), with an error radius of 1 arcmin (99% confidence). This is a position refined from the previously published value which resulted from a quick-look analysis (Heise et al. 1997). The deviation between both values is 0.4 arcmin. Also shown are the positions of two X-ray bursts that were observed simultaneously with the active phase of SAX J1750.8-2900, showing that they result from a position coincident with the transient. In March 1992 the ROSAT/PSPC observed the region around SAX J1750.8−2900 four times (between MJD 48685.09 and MJD 48691.63 with exposure times up to 1976 s), during a raster scan of the Galactic Centre region.
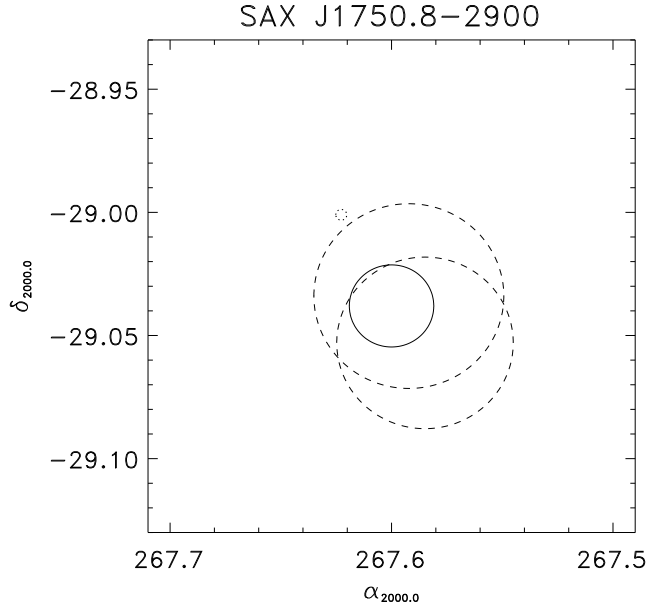
Figure 3.1: Position of SAX J1750.8-2900 computed by analysis of both persistent and burst images. Dashed contours are the source positions estimated from two X-ray bursts, and the solid line circle (1 arcmin radius) is the error circle of the transient source. Also shown (dotted circle) is the position of the ROSAT source 1RXP J175029-2859.9. All contours represent 99% confidence.

No source was detected during these observations within the 99% confidence error box of SAX J1750.8−2900. The source 1RXP J175029-2859.9 lies 1.5 arcmin outside the SAX J1750.8−2900 error box. This close-by source was marginally detected at $6.2 \pm 1.9 \times 10^{-3}$ counts s^{-1} in the second observation (between MJD 48685.36 and MJD 48685.39). From this result we can derive an upper limit of $\sim 3 \times 10^{-12}$ erg cm^{-2} s^{-1} on the soft X-ray emission (0.5-2.0 keV) of SAX J1750.8−2900 during quiescence.

The RossiXTE All Sky Monitor (RXTE/ASM; Levine et al. 1996) data shows the onset of a fast rise, exponential decay outburst of SAX J1750.8−2900 peaking at $\sim 120\pm40$ mCrab in the 2-10 keV range, starting close to MJD 50518 (two days before the initial WFC observation) and lasting ≈ 2 weeks. This
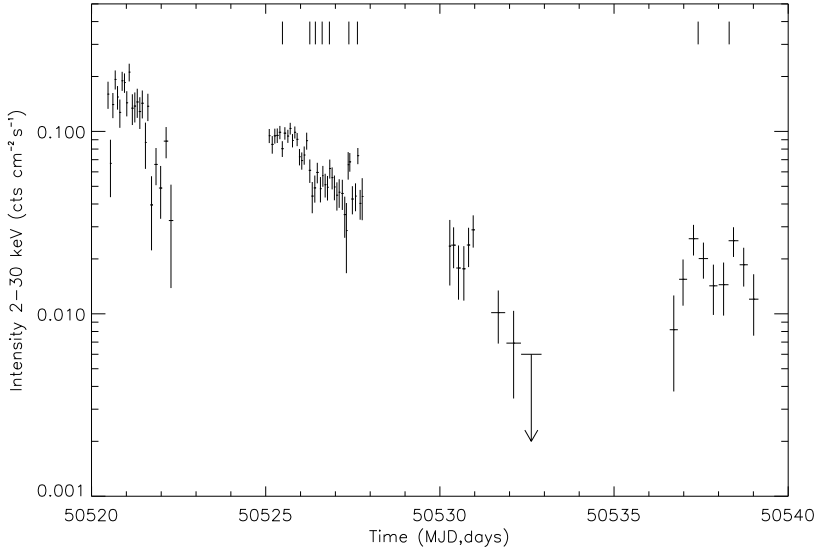
Figure 3.2: Light curve of the persistent emission from SAX J1750.8-2900 in the 2-30 keV band. The markers indicate the epoch of the observed bursts.

transient behaviour is supported by WFC later detections as previously reported by in 't Zand et al. (1997).

The X-ray persistent emission of SAX J1750.8-2900 (i.e., the emission detected during time intervals excluding bursts) was measured by the WFC starting from March 13th, 1997. The source flux was initially at a level of ≈ 70 mCrab in the energy band 2-30 keV. The light curve detected in the 2-30 keV range is shown in Fig. 3.2, along with the burst occurrence time. The outburst profile decay is close to exponential, with intensity changes on the time scale of hours. The first two days measurements (when the source was more luminous) are affected by relatively large errors caused by the off-axis position of the source. The average luminosity in the 2-30 keV band, calculated for 10 kpc distance is $\approx 3 \times 10^{37}$ erg s^{-1} on March 13th. The flux was about ~ 1.5 times weaker five days later, when the source was seen bursting for the first time, and dropped to less than ~ 3 mCrab ($\approx 10^{36}$ erg s^{-1} at 10 kpc) on March 25th. The source was again visible at ~ 10 mCrab on March 30-31, when two more

27

Table 3.1: Summary of spectral fitting for persistent emission

Period MJD	Model	Model Parameter	Flux[a]	χ^2_ν [b]
50520.52-50521.68	Power Law	$\Gamma = 2.40\pm0.17$	15.6±0.9	0.6
	Bremsstrahlung	kT (keV) $= 9.2\pm1.1$		0.5
50521.68-50522.35	Power Law	$\Gamma = 2.42\pm0.25$	14.1±1.2	1.0
	Bremsstrahlung	kT (keV) $= 9.1\pm1.6$		1.0
50525.04-50526.19	Power Law	$\Gamma = 2.70\pm0.08$	8.46±0.4	1.5
	Bremsstrahlung	kT (keV) $= 6.1\pm0.3$		1.0
50526.19-50527.35	Power Law	$\Gamma = 2.76\pm0.14$	5.12±0.3	1.1
	Bremsstrahlung	kT (keV) $= 4.3\pm0.4$		0.9
50527.35-50527.77	Power Law	$\Gamma = 2.78\pm0.23$	4.69±0.2	1.0
	Bremsstrahlung	kT (keV) $= 6.0\pm0.7$		1.0
50530.21-50531.04	Power Law	$\Gamma = 3.59\pm0.50$	1.79±0.2	0.6
	Bremsstrahlung	kT (keV) $= 3.4\pm0.5$		0.5

[a] units of 10^{-10} erg cm^{-2}s^{-1} (2-30keV); [b] reduced χ^2 for 24 d.o.f.

bursts were detected.

We fitted the emission spectra detected in the 2-30 keV band during six ob-serving periods between MJD 50520 and MJD 50531 using a few spectral models. The results obtained for power law and thermal bremssthralung (both with low energy absorption) are shown in Table 3.1. The spectra can be described either by a power law shape having a photon index $\Gamma \approx 2.5$ and extinction parameter $N_H \approx 6 \times 10^{22}$ cm^{-2}, or by bremssthralung emission with kT in the 3 to 10 keV range and $N_H \approx 2.5 \times 10^{22}$ cm^{-2}. The spectra cannot be fitted satisfactorily with single component blackbody emission.

The fit results give indication that the source has experienced spectral soft-ening during the outburst decay. By performing an F-test on the two spectra taken at MJD 50520 and MJD 50527 we find that the probability that there is no softening is less than 1%. If the X-ray emission mechanism is thermal (as observed in many X-ray bursters) the softening could be ascribed to a tem-perature variation of the electron plasma, possibly due to the decrease in the accretion flow.
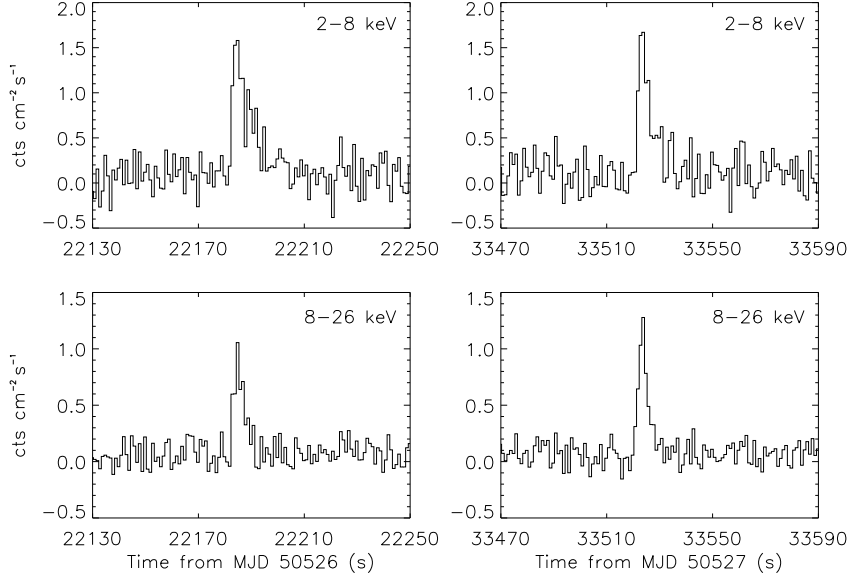
Figure 3.3: Time profiles of two X-ray bursts from SAX J1750.8−2900 detected on 1997 March 19th and March 20th (from left to right).

3.4   The X-ray bursts

A total of 9 X-ray bursts were detected from SAX J1750.8-2900 during an overall time span of 14 days in spring 1997. The first one (the faintest observed) occurred on MJD 50525.48150, with a peak flux of ≈0.4 Crab. 7 out of 9 bursts were detected during three days from March 18th (see Table 3.2 for burst occurrence times), having similar bolometric fluences in the range ≈ 2 to 3×10^{-7} erg cm^{-2}. In Fig. 3.3 burst profiles in two energy bands are plotted for two of these events.

The study of the burst frequency is limited by the fact that during observation the effective exposure time is only a fraction (≈60%) of the total pointing time, due to earth occultations and other shorter non-coverage periods. The observed values of time intervals are in fact an upper limit to the real burst interval time. It is then possible that SAX J1750.8-2900 made bursts during the

first observation period when its persistent flux was above $\sim$50 mCrab. In spite of this, there is evidence that the burst frequency decreased when the source flux dropped below $\sim$20 mCrab, i.e. in observations performed after MJD 50530 (see Fig. 3.2).

The primary question concerning the bursts is whether they are type I X-ray bursts. All burst profiles detected from SAX J1750.8-2900 show a fast rise ($\approx$ 1 s), exponential decay shape, with e-folding time in the range $\approx$ 5-10 s (see Fig. 3.3). The decay times in the energy band 8-26 keV are systematically shorter than those observed in the band 2-8 keV. However, the spectral softening cannot be proven by examining the individual bursts, due to the large statistical error (see Table 3.2). In order to increase significance we summed up the profiles of the last 7 bursts in the energy bands 2-8 and 8-26 keV, with a time resolution of 0.1 s. The first two bursts were excluded because their detection was affected by the earth atmosphere. The start channel of each burst was determined as the first point in the time profile which differed more than $\sim$4σ from the mean persistent emission. The fit of the two profiles obtained with an exponential function gives an e-folding decay time $\tau = 5.3 \pm 0.7$ s in the low energy band and $\tau = 2.8 \pm 0.2$ s in the high energy band, and proves that spectral softening is occurring during burst decay. Together with a consistency of the burst spectrum with that of a few keV blackbody emission (see Table 3.2) this identifies the bursts as type I.

Among the bursts detected, there is no clear evidence of an X-ray burst with double peaked or flat profile, which might have suggested saturation of the luminosity to near-Eddington level and resulting photospheric radius expansion (Lewin et al. 1995). However we can derive an upper limit on the source distance assuming that the maximum burst luminosity was below Eddington. The maximum observed peak flux (burst F, see Table 3.2) is consistent with a 3 σ upper limit of $\approx$ 7 kpc.

Burst spectra are rather soft and generally compatible with blackbody emission having colour temperatures between 2 and 3 keV (see Table 3.2). Under given assumptions (Lewin et al. 1993) the effective temperature $T_{\rm eff}$ and the bolometric flux of a burst can determine the ratio between the blackbody radius $R_{\rm bb}$ (that is, the radius of the emitting sphere) and the distance d of the neutron star. Assuming d=10 kpc and the observed colour temperatures as $T_{\rm eff}$, and not correcting for gravitational redshift the measured blackbody radius is $\approx$ 8 km. For the above upper limit of 7 kpc, this value of $R_{\rm bb}$ scales to a corresponding upper limit of $\approx$ 6 km. This value could be underestimated, due to the uncertainties in the relationship between colour and effective temperature. If, as suggested by Ebisuzaki (1987) the colour temperature exceeds $T_{\rm eff}$ by a factor

30

Table 3.2: Parameter fit results of bursts

Burst id.	Time^a	Peak flux^b	kT_{col}(keV)	$R_{\mathrm{bb}}{}^c$	$\chi_\nu^{2\,d}$	τ_{2-8}	τ_{8-26}
A^e	0.48151	1.2 ± 0.2	1.6 ± 0.3	10.4±3.2	1.3	10.1 ± 5.6	2.5 ± 1.4
B^e	1.25676	3.9 ± 0.5	2.3 ± 0.2	8.3±1.2	0.8	7.5 ± 2.6	2.4 ± 0.6
C	1.42773	3.8 ± 0.6	2.4 ± 0.2	8.0±1.1	0.9	5.0 ± 1.6	3.0 ± 1.0
D	1.62039	2.2 ± 0.3	2.2 ± 0.2	10.7±2.1	1.2	5.2 ± 2.4	2.5 ± 0.7
E	1.82726	4.5 ± 0.7	2.1 ± 0.2	9.2±1.4	0.5	4.1 ± 1.7	1.4 ± 0.4
F	2.38799	5.4 ± 0.8	2.2 ± 0.1	9.3±1.2	1.5	4.5 ± 1.2	1.5 ± 0.4
G	2.63415	2.7 ± 0.4	2.4 ± 0.2	7.4±1.1	1.3	11.2 ± 6.1	4.4 ± 1.0
H	12.41515	4.7 ± 0.6	2.4 ± 0.2	8.4±1.2	1.0	5.4 ± 2.1	2.2 ± 0.6
I	13.30355	4.2 ± 0.5	2.4 ± 0.2	7.8±1.2	1.0	6.7 ± 2.1	3.1 ± 0.9

^{a} time of burst rise in days (MJD-50525); ^{b} in units of 10^{-8} erg cm^{-2} s^{-1} , 2-26 keV.

^{c} for source at 10 kpc distance; ^{d} reduced χ^2 for 23 d.o.f.

^{e} burst detection affected by the earth atmosphere.

$\approx$1.5, then the neutron star radius should be at least two times the measured blackbody radius. These values are therefore consistent with a neutron star nature of the compact object.

3.5 Discussion

3.5.1 Burst emission properties

In the simplest interpretation of the thermonuclear flash model which successfully explains type I X-ray bursts (Lewin et al. 1995 for review) the matter accreted onto a neutron star surface prior to an observed type I burst is converted into nuclear fuel and the fraction of the total accreted energy available for burning depends on the actual reaction process and fuel composition. If the thermonuclear flash is isotropic and the accreted material is totally converted into fuel, the ratio between the mass and radius of the NS is given by $M_*/R_{10km} = (0.01\text{-}0.04)^*\alpha$, where 0.01 and 0.04 hold for helium and hydrogen burning respectively. Here M_* is the mass of the compact object in units of solar masses, R_{10km} is the NS radius in units of 10 km and α is the ratio between the bolometric flux of the persistent emission (integrated over the burst interval) and the bolometric fluence of the burst. A 1.4 $M_\odot$ neutron star would then result in a value of $\alpha \approx 100$ for pure helium burning. For the four shortest observed burst times intervals B-C,C-D,D-E and F-G (see Table 3.2) we estimated the α parameter and found values of 85$\pm$20, 120$\pm$30, 170$\pm$30 and 210$\pm$40 respectively. These intervals are monotonically increasing from 4.1 to 5.9 h on a time scale of 1.5 days, and all the related bursts show similar profiles and fluences. This suggests that perhaps no bursts were missed in between. The fast rise time of the bursts (< 2 s) and the measured values of α seem to favour a pure helium flash respect to combined hydrogen-helium shell burning. (Lewin et al. 1993).

3.5.2 SAX J1750.8-2900 and the transients of the Galactic Bulge

Most X-ray burst sources known so far are type I bursters associated with low-mass X-ray binaries (LMXBs) containing old, weakly magnetized neutron stars, and show concentration in the direction of the Galactic Centre (van Paradijs, 1995). They can be persistent (though variable) or transient, and may have recurrence periods with nearly constant burst activity, like the recently studied

GS 1826-338 (Ubertini et al. 1999b), or conversely show only episodic burst emission, like for example SLX 1735-26 (Bazzano et al. 1997b) and XTE J1709-267 (Cocchi et al. 1998a). Correlation between burst frequency and persistent emission is not an uncommon feature. In general, type I bursts are observed when the source persistent luminosity is comprised between $\sim 10^{-2}$ and ~ 0.3 of the Eddington limit. For the bursting soft X-ray transients (White et al. 1984; see Campana et al. 1998 for recent review) the burst activity is usually detected during the occurrence of outburst episodes, which show peak luminosity of up to $\sim 10^{38}$ erg s^{-1} and often recur on time scales of ~ 1 to ~ 10 years.

SAX J1750.8-2900 shows this type of transient phenomenology. The outburst light curve has a rather clear fast rise and exponential decay shape. In spite of the incomplete sampling it evidently shows variable decay behaviour, as observed in other LMXB transients (Chen et al. 1997). So there is no real evidence that the source had a secondary outburst after MJD 50535 as it could appear at a first glance. The X-ray flux decreased of a factor ≈ 20 in a period of ~ 3 weeks in spring 1997, after which the source remained undetected (the RXTE/ASM and BeppoSAX data do not show any other evident outburst in the period 1996 to 1999 May). We provide evidence that SAX J1750.8-2900 has been observed bursting only whenever the intensity was above ~ 10 mCrab, and that the burst frequency was positively correlated with the persistent emission (at least when the persistent flux was in the range ~ 10 to ~ 50 mCrab). The spectral softening seen by analysis of burst profiles is an evidence that SAX J1750.8-2900 is a type I burster, and hence that the compact object is a neutron star. The observed peak luminosity of bursts suggests an upper limit of 7 kpc on the source distance. Due to the lack of optical identification and/or visible X-ray modulation it is not possible to classify with certainty the binary source as a low mass system. Nevertheless, the detection of type I bursts is sufficient to firmly set SAX J1750.8-2900 as a candidate member of the LMXB class.

The current sample of known LMXB could be biased towards bright X-ray transients, due to instrument selection effects and the established occurrence of weak, short lasting transients with long recurrence time (like e.g., 2S 1803-245, Muller et al. 1998; and SAX J1748.9-2021, in 't Zand et al. 1999). In fact, the recent observations by BeppoSAX and RXTE are significantly growing the number of weak LMXB. Among them, most are NS transients which are also burst sources and often show high energy tails. For this reason, these have been suggested as a possible new subclass of low mass binaries (Heise et al. 1999). Indeed these systems could be NS soft X-ray transients (of the type of Cen X-4 or Aql X-1), which are harboured within the Galactic Bulge at quite

large distances. This is what should be expected, as increasing the sensitivity and coverage will push the limit of observable distances up to a range in which many more sources are available, due to their concentration towards the Galactic Centre.

references

Bazzano, A., et al. 1997a, IAUC 6597.

Bazzano, A., et al. 1997b, IAUC 6668.

Campana, S., et al. 1998, araa, 8, 279.

Caroli, E., et al. 1987, Space .Sci. Rev., 45, 349.

Chakrabarty, D. & Morgan, E. 1998, Nature, 394, 346.

Chen, W., Shrader, C.R. & Livio, M. 1997, ApJ, 491, 312.

Cocchi, M., et al. 1998a, Nucl. Phys. B (Proc.Suppl.), 69, 1

Cocchi, M., et al. 1998b, ApJ, 508, L163.

Ebisuzaki, E. 1987, pasj, 39, 287.

Heise, J., et al. 1997, IAUC 6606.

Heise, J., et al. 1999, in A. Bazzano, Astrophys. Lett. Comm., Vol. 38, p. 297

in 't Zand, J.J.M., et al. 1997, IAUC 6618.

in 't Zand, J.J.M. et al. 1998, aap, 331, L25.

in 't Zand, J.J.M. et al. 1999, aap, 345, L100.

Jager, R., et al. 1997, aap, 125, 557.

Levine, A.M., et al. 1996, ApJ, 469, L33.

Lewin, W.H.G., van Paradijs, J., & Taam, R.E. 1993, Space Sci. Rev., 62, 223.

Lewin, W., van Paradijs, J., & Taam, R. 1995, in W. Lewin, J. van Paradijs,
  E. van den Heuvel (eds.), X-ray binaries, Cambridge U.P., Cambridge, p. 175

Muller, H., et al. 1998, IAUC 6867.

Skinner, G.K., et al. 1993, aap, 97, 143.

Ubertini, P., et al. 1999a, in A. Bazzano, Astrophys. Lett. Comm., Vol. 38,
  p.301

Ubertini, P., et al. 1999b, ApJ, 514, L30.

van Paradijs, J., 1995, in W. Lewin, J. van Paradijs,
    E. van den Heuvel (eds.), X-ray binaries, Cambridge U.P., Cambridge, p. 536
Vargas, M., et al. 1997, in Proc. 2nd INTEGRAL Workshop, The Transparent
    Universe, ESA SP-382, p.129.
White, N.E, Kaluziensky, J.L. & Swank, J.H., 1984, in AIP Conf. Proc. 115,
    High Energy Transients in Astrophysics, ed. S.Woosley (New York: AIP), 31
Wijnands, R. & van der Klis, M., 1998, Nature, 394, 344.

Chapter 4

The longest thermonuclear X-ray burst ever observed?

A BeppoSAX Wide Field Camera observation of
4U 1735−44

R. Cornelisse, J. Heise, E. Kuulkers, F. Verbunt and J.J.M. in 't Zand

Abstract– A long flux enhancement, with an exponential decay time of 86 min, is detected in 4U 1735−44 with the BeppoSAX Wide Field Cameras. We argue that this is a type I X-ray burst, making it the longest such burst ever observed. Current theories for thermonuclear bursts predict shorter and more frequent bursts for the observed persistent accretion rate.

4.1 Introduction

Of the $\simeq$150 low-mass X-ray binaries known in our galaxy, about 40% show occasional bursts of X-rays, in which a rapid rise, lasting from less than a second to $\simeq$10 s, is followed by a slower decay, lasting between $\simeq$10 s to minutes. During the decay the characteristic temperature of the X-ray spectrum decreases. An X-ray burst is explained as energy release by rapid nuclear fusion of material on the surface of a neutron star and thus an X-ray burst is thought to identify the compact object emitting it unambiguously as a neutron star. If the burst

is very luminous, reaching the Eddington limit L_{Edd}, the energy release may temporarily lift the neutron star atmosphere to radii of order $100\,\mathrm{km}$. Reviews of observations of X-ray bursts are given by Lewin et al. (1993, 1995).

The properties of a burst depend, according to theory, on the mass and radius of the neutron star, on the rate with which material is accreted onto the neutron star, and on the composition of the accreted material. It is hoped that a detailed study of X-ray bursts can be used to determine the mass and radius of the neutron star, via the relation between luminosity, effective temperature and flux, and via the changes in the general relativistic correction to this relation when the atmosphere expands from the neutron star surface to a larger radius. However, the physics of the X-ray burst is complex. There is evidence that the emitting area does not cover the whole neutron star and changes with the accretion rate. Reviews of the theory of X-ray bursts are given by Bildsten (1998, 2000).

In this paper we describe a long flux enhancement that we observed with the Wide Field Cameras of BeppoSAX in the X-ray burst source 4U 1735−44, and argue that this event is the longest type I X-ray burst ever observed. In Sect. 2 we describe the observations and data extraction, in Sect. 3 the properties of the flux enhancement. A discussion and comparison with earlier long bursts is given in Sect. 4. In the remaining part of this section we briefly describe earlier observations of 4U 1735−44.

4U 1735−44 is a relatively bright low-mass X-ray binary. Smale et al. (1986) fit EXOSAT data in the 1.4-11 keV range with a power law of photon index 1.8 with an exponential cutoff above $7\,\mathrm{keV}$, absorbed by an interstellar column $N_{\mathrm{H}} \simeq 5 \times 10^{20} \mathrm{atoms\,cm}^{-2}$. The flux in the 1.4-11 keV range is $\simeq 4 \times 10^{-9} \mathrm{erg\,cm}^{-2}\mathrm{s}^{-1}$. Van Paradijs et al. (1988) show that a sum of thermal bremsstrahlung of $\simeq 10\,\mathrm{keV}$ and black body radiation of $\simeq 2\,\mathrm{keV}$, absorbed by an interstellar column $N_{\mathrm{H}} < 8 \times 10^{20} \mathrm{atoms\,cm}^{-2}$, adequately describes EXOSAT data in the same energy range and at a similar flux level, obtained one year later. A similar spectrum, with a higher absorption column $N_{\mathrm{H}} \simeq 3.4 \times 10^{21} \mathrm{atoms\,cm}^{-2}$, fits the Einstein solid-state spectrometer and monitor proportional counter data (Christian & Swank 1997). During GINGA observations, the source was somewhat brighter, at $\simeq 9 \times 10^{-9} \mathrm{erg\,cm}^{-2}\mathrm{s}^{-1}$ in the 1-37 keV range (Seon et al. 1997).

Bursts were detected at irregular time intervals during each of the five occasions in 1977 and 1978 that SAS-3 observed 4U 1735−44, leading to a total of 53 detected bursts (Lewin et al. 1980). EXOSAT detected one burst in 1984 (Smale et al. 1986) and five bursts during a continous 80 hr observation in 1985 (Van Paradijs et al. 1988), one rather bright burst was detected with GINGA

in 1991 (Seon et al. 1997), and five X-ray bursts with RXTE in 1998 (Ford et al. 1998). Burst intervals range from about 30 minutes to more than 50 hrs. Three of the bursts observed with EXOSAT and the single burst observed with GINGA were radius expansion bursts (Damen et al. 1990, Seon et al. 1997), and have been used to determine the distance to 4U 1735−44 at about 9.2 kpc (Van Paradijs and White 1995).

4U 1735−44 was the first X-ray burster for which an optical counterpart was found: V926 Sco (McClintock et al. 1977). From optical photometry an orbital period of 4.65 hrs was derived (Corbet et al. 1986).

4.2   Observations and data extraction

The Wide Field Camera experiment (Jager et al. 1997) is located on the Bep-poSAX platform which was launched early 1996 (Boella et al. 1997). It comprises two identically designed coded-aperture multi-wire Xenon proportional counter detectors. The field of view of each camera is 40×40 degrees full width to zero response, which makes it the largest of any flown X-ray imaging device with good angular resolution. The angular resolution is $5'$ full width at half maximum, and the accuracy of the source location is upward of $0.7'$, depending mainly on the signal-to-noise ratio. The photon energy range is 2-28 keV, and the time resolution is 0.5 ms. Due to the coded mask aperture the detector data consist of a superposition of the background and shadowgrams of multiple sources. To reconstruct the sky image an algorithm is employed which is based on cross correlation of the detector image with the coded mask (Jager et al. 1997).

Since the fall of 1996, the Wide Field Cameras observe the field around the Galactic Center on a regular basis during each fall and spring. The first campaign was a nine-day near-continuous observation from August 21 until August 30, 1996. About 30% of the time, viz. $\simeq$35 minutes per orbit, is lost due to earth occultation and due to passage through the South Atlantic Anomaly.

4.3   A long flux enhancement of 4U 1735−44

In Fig. 4.1 we show the lightcurve of 4U 1735−44 as observed with the WFC between 21 and 30 August 1996. The persistent countrate varies between 0.2 and 0.3 counts cm^{-2}s^{-1}. Immediately after the earth occultation on MJD 50318.1 a strong enhancement (factor $\simeq$3) in the X-ray intensity was seen which sub-

sequently decayed exponentially. An expanded lightcurve of this event is also shown in Fig. 4.1. The position derived for this event is $3''.2 \pm 3''.4$ from the position of 4U 1735−44 as derived from its persistent emission. (Both positions share the same systematic error, and thus their relative position is much more accurate than their absolute positions, which have errors of $\simeq 1'$.) We conclude that the event is from 4U 1735−44.

To the persistent flux we fit the two models discussed in the introduction, i.e. a power law with high energy cutoff, and a sum of bremsstrahlung and black body spectra, in the 2-24 keV range. The spectrum before and after the event are for the intervals MJD 50317.8-50318.1 and MJD 50319.7-50320.8, respectively. The results are given in Table 4.1. We note that the values of the fit parameters are similar to those for earlier observations. Notwithstanding the different flux levels before and after the flux enhancement, the hardness of the spectrum (also shown in Fig. 4.1) is similar. The persistent flux corresponds to an X-ray luminosity at 9.2 kpc of 4.4×10^{37} erg s^{-1} in the 2-28 keV band. In our fits we set the interstellar absorption at a fixed value of $N_{\mathrm{H}} = 3.4 \times 10^{21}$ atoms cm^{-2}; the hard energy range of the WFC is not much affected by absorption, and fits for different assumed absorption values give results similar to those listed in Table 4.1.

To describe the flux decline we first fit an exponential $C = C(0)e^{-t/\tau}$ to the observed countrate in the 2-28 keV range. The fit is acceptable (at $\chi^2_\nu = 1.6$ for 33 d.o.f.) and $\tau = 86 \pm 5$ min. Fits to the counts in the 2-5 keV and 5-20 keV ranges give decay times of 129 ± 15 and 67 ± 5 min, respectively, in accordance with the observed softening of the flux during decline (see Fig. 4.1). We fit the spectrum during the flux enhancement as follows. First we add all the counts obtained between MJD 50318.10 and 50318.25. We then fit the total spectrum with the sum of a black body and either a cutoff power law spectrum or a thermal bremsstrahlung spectrum. In these fits, the parameters of the power law and bremsstrahlung component are fixed at the values obtained for the fit to the persistent spectrum after the event. The resulting parameters for the black body are also listed in Table 4.1. At the observed maximum the bolometric flux was $(1.5 \pm 0.1) \times 10^{-8}$ erg cm^{-2}s^{-1} which for a source at 9.2 kpc corresponds to a luminosity of 1.5×10^{38} erg s^{-1}. The start of the flux enhancement is not observed, but if we assume that its maximum is at the Eddington limit of 1.8×10^{38} erg s^{-1} (for a neutron star mass of $1.4 M_\odot$) and that the decay time is constant, then maximum was reached 23.6 min before the source emerged from earth occultation, leaving at most 12.4 min for the rise to maximum (since the start of the data gap). The decay from maximum was therefore much longer, by a factor >8, than the rise. The fluence in the observed part of the burst is
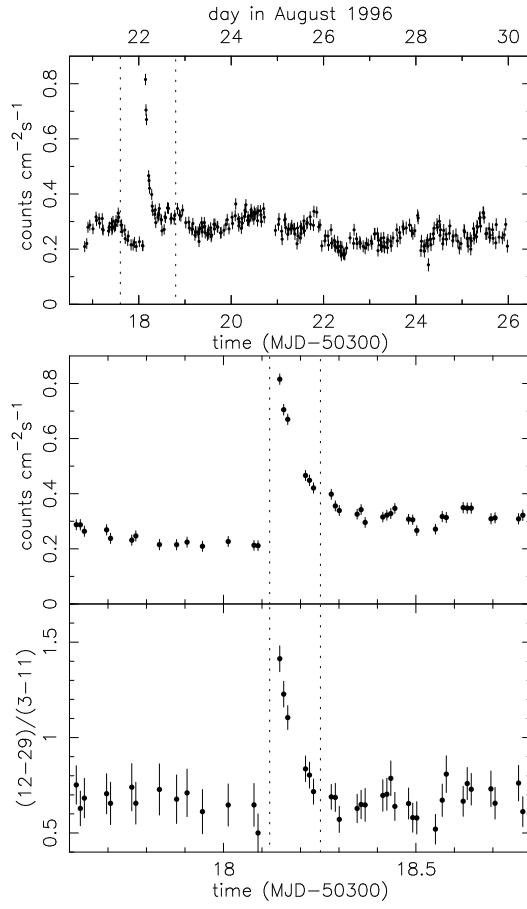
Figure 4.1: Top: The nine day lightcurve of 4U 1735−44 as observed with the WFC in August 1996. Countrates are for channels 1-31 (energy range 2-28 keV). Each time bin corresponds to 15 minutes. A large enhancement in intensity starts near MJD 50318.1 and ends about ≃4.0 hours later. The vertical dotted lines indicate the time interval for which the countrate and hardness ratio are shown in the expanded view of the lower frames. The hardness ratio shown is the ratio of the countrate in channels 12-29 (5-20 keV) to that in channels 3-11 (2-5 keV). During the flux enhancement the exponential softening expected for a type-I X-ray burst is clearly visible. The vertical dotted lines indicate the time interval for which we add the data to obtain the burst spectrum.

41

Table 4.1: Results of the modeling of the X-ray spectrum. We fit a cutoff photon powerlaw spectrum $N(E) = N_{\mathrm{o}}E^{-\Gamma}e^{-(E-E_{\mathrm{o}})/E_{\mathrm{w}}}$ and a sum of a bremsstrahlung of temperature T_{br} and black body spectrum of temperature T_{bb} and radius R to the data before and after the burst. For the burst, we fix the parameters of either the cutoff power law or the bremsstrahlung component to the values found after the burst, and fit for a blackbody added to these. The absorption column is fixed at the value of $N_{\mathrm{H}} = 3.4 \times 10^{21}\,\mathrm{atoms\,cm}^{-2}$ found by Christian & Swank (1997). For each model we give the total flux in the range observed with the WFC, i.e. 2-28 keV, as well as, for comparison with earlier observations, in the range of 1.4-11 keV.

cutoff power law	before	after
χ^2_ν (dof)	0.9 (23)	0.9 (23)
Γ	1.84±0.07	1.55±0.06
E_{o} (keV)	9.4±1.1	6.2±0.4
E_{w} (keV)	3.6±1.7	6.9±0.7
F_{2-28} ($10^{-9}\mathrm{erg\,cm}^{-2}\mathrm{s}^{-1}$)	3.44±0.10	4.31±0.08
$F_{1.4-11}$ ($10^{-9}\mathrm{erg\,cm}^{-2}\mathrm{s}^{-1}$)	3.53±0.06	3.91±0.04
brems plus black body	before	after
χ^2_ν (dof)	1.1 (23)	1.0 (23)
kT_{br} (keV)	7.8±0.6	8.0±1.3
kT_{bb} (keV)	0.	1.6±0.2
R (km)	0.	3.8±0.9
F_{2-28} ($10^{-9}\mathrm{erg\,cm}^{-2}\mathrm{s}^{-1}$)	3.80±0.09	4.32±0.10
$F_{1.4-11}$ ($10^{-9}\mathrm{erg\,cm}^{-2}\mathrm{s}^{-1}$)	3.40±0.05	3.87±0.04
added blackbody for burst	+cutoff	+brems
χ^2_ν (dof)	1.3 (25)	1.3 (25)
kT_{bb} (keV)	1.70±0.05	1.69±0.04
R (km)	6.1±0.3	7.2±0.3
F_{2-28} ($10^{-9}\mathrm{erg\,cm}^{-2}\mathrm{s}^{-1}$)	7.42±0.05	7.43±0.05
$F_{1.4-11}$ ($10^{-9}\mathrm{erg\,cm}^{-2}\mathrm{s}^{-1}$)	6.76±0.04	6.71±0.04

$5.1 \times 10^{-5}\,\mathrm{erg\,cm^{-2}}$, corresponding to $5.2 \times 10^{41}\,\mathrm{erg}$; this is a lower limit to the energy released during the full event.

We have also made fits to the first and second half of the event separately, and find temperatures for the blackbody component of 2.1-2.2 keV and 1.3-1.4 keV for the first and second half respectively, confirming the softening. For the blackbody radius we find 5.7-6.5 km and 8.5-8.8 km, for the first and second half, respectively. This apparent increase in radius is probably due to the difference between the observed colour temperature and the actual effective temperature of the black body; when we apply corrections to the colour temperature as given by van Paradijs et al. (1986) the value for the radius in the first part of the burst increases to 14 km, whereas that for the second half is unchanged.

4.4   Discussion

In addition to the thermonuclear X-ray bursts, also called type I bursts, low-mass X-ray binaries show other sudden enhancements in X-ray flux. Type II bursts are different from type I bursts in that type II bursts do not show cooling of the characteristic temperature of the X-ray spectrum during the decline. X-ray flares have an irregular flux evolution. Type II bursts are thought to be accretion events; the nature of flares is unknown.

The flux enhancement of 4U 1735−44 shows a smooth exponential decay of the countrate and of the characteristic temperature. Its rise must have been shorter than the decline. A black body gives a good fit to the observed spectrum, for a radius as expected from a neutron star, similar to earlier, ordinary bursts of 4U 1735−44. All these properties indicate a type I burst. The only special property of the new burst is its duration, which when expressed as the ratio of fluence E_{b} and peak flux $F_{\max}$: $E_{\mathrm{b}}/F_{\max} > 3400\,\mathrm{s}$, is more than 300 times longer than the longest burst observed previously from this source (see Lewin et al. 1980). This duration also translates in a fluence which is several orders of magnitude larger than the previous record holder for 4U 1735−44, because the peak flux is similar to those of normal type I bursts. The fluence of a type I burst which burns all matter deposited onto a neutron star since the previous burst must be $\simeq 1\%$ of the accretion energy released by deposition of this matter. We do not have a measurement to the previous burst, but in seven days following the burst no other burst was observed. Multiplying this time by the persistent luminosity we obtain $\simeq 2.7 \times 10^{43}\,\mathrm{erg}$, or about 50 times the energy of the burst, well in the range of previously observed ratios for type I bursts.

The presence of clear cooling argues against a type II burst; this and the

smooth decay argues against a flare. If the flux enhancement were due to an accretion event, the amount of matter dropped extra onto the neutron star (assuming a mass of $1.4 M_\odot$ and a radius of $10\,\mathrm{km}$) must have been $> 3 \times 10^{21}\,\mathrm{g}$, which may be compared to the average accretion rate of $2.3 \times 10^{17}\,\mathrm{g\,s^{-1}}$ derived for the persistent flux. If the inner part of the accretion disk would have depleted itself onto the neutron star during the flux enhancement, one would expect the accretion rate immediately after to be lower than before. The observations suggest the opposite.

We conclude that a type I X-ray burst is the best explanation for the enhanced flux event. We consider it significant that the occurrence of this burst is accompanied by the absence of any ordinary – i.e. short – burst throughout our 9-day observation, whereas all previous observations of 4U 1735−44 did detect ordinary bursts (see Introduction).

Searching the literature for long bursts we find that the longest type I burst published previously is a radius expansion burst observed with SAS-3, probably in 4U 1708−23 (Hoffman et al. 1978; see also Lewin et al. 1995). The ratio of fluence and peak flux for that burst was $\simeq 500\,\mathrm{s}$, so that the BeppoSAX WFC burst of 4U 1735−44 lasted at least six times longer. Other events published as long bursts from Aql X-1 (Czerny et al. 1987) and from X 1905+000 (Chevalier and Ilovaisky 1990) are in fact relatively short bursts followed by an enhanced constant flux level which persisted for several hours: in both cases the flux declined to $1/e$ of the peak level within $20\,\mathrm{s}$. These events are clearly different from the long exponential bursts seen in 4U 1708−23 and 4U 1735−44.

From the theoretical point of view, a long interval between bursts would allow hydrogen to burn completely before the onset of the burst, so that the energetics of the burst is dominated by pure helium burning. If matter accreted at a rate of $2.3 \times 10^{17}\,\mathrm{g\,s^{-1}}$ during one week, the energy released by helium burning is compatible with the energy of the observed burst. The problem with this model is that theory predicts for this accretion rate that the burst initiates well before hydrogen burning is completed, i.e. that bursts are more frequent and less energetic, in accordance with those previously observed of 4U 1735−44. Indeed, Fujimoto et al. (1987) find that a burst of $10^4\,\mathrm{s}$ duration occurs only for accretion rates $\dot{M} < 0.01 \dot{M}_{\mathrm{Edd}}$. The persistent flux during the BeppoSAX observation is a factor $\simeq 20$ higher than this limit; observations previous to ours have consistently found 4U 1735−44 at a similar luminosity.

An alternative model for bursts with a duration of $10^4\,\mathrm{s}$ is accretion of pure helium at an accretion rate in excess of the Eddington limit ($\dot{M} > 5 \times \dot{M}_{\mathrm{Edd}}$, Brown & Bildsten 1998). The orbital period and optical spectrum indicate a main-sequence, i.e. hydrogen-rich, donor star (Augusteijn et al. 1998).

Perhaps the main challenge for any theoretical explanation is that the properties of the persistent flux during our nine day long observation, during which a single very long X-ray burst was observed, are not different from those during earlier observations with EXOSAT when more frequent ordinary bursts were found.

references

Augusteijn, T., van der Hooft, F., de Jong, J., van Kerkwijk, M.H., & van Paradijs,
    J. 1998, A&A, 332, 561

Bildsten, L. 1998, in A. Alpar, L. Buccheri, J. van Paradijs (eds.), The many
    faces of neutron stars, NATO ASI, Kluwer, Dordrecht, 419

Bildsten, L. 2000, in S. Holt, W. Zhang (eds.), Cosmic explosions, AIP, p. E65

Boella, G., Butler, R., Perola, G., et al. 1997, A&AS, 122, 299

Brown, E., & Bildsten, L. 1998, ApJ, 496, 915

Chevalier, C., & Ilovaisky, S. 1990, A&A, 228, 115

Christian, D., & Swank, J. 1997, ApJS, 109, 117

Corbet, R., Thorstensen, J., Charles, P., et al. 1986, MNRAS, 222, 15

Czerny, M., Czerny, B., & Grindlay, J. 1987, ApJ, 312, 122

Damen, E., Magnier, E., Lewin, W., et al. 1990, A&A, 237, 103

Ford, E., van der Klis, M., van Paradijs, J., et al. 1998, ApJ 508, L155

Fujimoto, M., Hanawa, T., Iben, I., & Richardson, M. 1987, ApJ, 315, 198

Hoffman, J., Lewin, W., Doty, J., et al. 1978, ApJ, 221, L57

Jager, R., Mels, W., Brinkman, A., et al. 1997, A&AS, 125, 557

Lewin, W., van Paradijs, J., Cominsky, L., & Holzner, S. 1980, MNRAS, 193,
    15

Lewin, W., van Paradijs, J., & Taam, R. 1993, Space Sci. Rev., 62, 223

Lewin, W., van Paradijs, J., & Taam, R. 1995, in W. Lewin, J. van Paradijs,
    E. van den Heuvel (eds.), X-ray binaries, Cambridge U.P., Cambridge, p. 175

McClintock, J., Bradt, H., Doxsey, R., et al. 1977, Nat, 270, 320

Seon, K., Min, K., Yoshida, K., et al. 1997, ApJ, 479, 398

Smale, A., Corbet, R., Charles, P., Menzies, J., & Mack, P. 1986, MNRAS, 223,
    207

van Paradijs, J., Penninx, W., Lewin, W., Sztajno, M., & Trümper, J. 1988,
    A&A, 192, 147

van Paradijs, J., Sztajno, M., Lewin, W., et al. 1986, MNRAS, 221, 617

van Paradijs, J., & White, N. 1995, ApJ, 447, L33

Chapter 5

A four-hours long burst from Serpens X-1

R. Cornelisse, E. Kuulkers, J.J.M. in 't Zand, F. Verbunt and J. Heise

Astronomy & Astrophysics 2002, 382, 174

Abstract– During a serendipitous observation of the BeppoSAX Wide Field Cameras, a very long Type I X-ray burst was observed from the low mass X-ray binary Serpens X$-$1. The burst lasted for approximately 4 hours and had an exponential decay time of 69 ± 2 min (2-28 keV). The bolometric peak-luminosity is $(1.6 \pm 0.2) \times 10^{38}$ erg s^{-1} and the fluence $(7.3 \pm 1.4) \times 10^{41}$ erg. The first 'normal' Type I burst was observed 34 days after the superburst. This is in rough agreement with recent predictions for unstable carbon burning in a heavy element ocean.

5.1   Introduction

Since the first report of a very long thermo-nuclear X-ray burst in 4U 1735$-$44 (Cornelisse et al. 2000), six more of these so-called 'superbursts' have been noted (Strohmayer 2000; Heise et al. 2000; Wijnands 2001; Kuulkers 2001). The superbursts have the following common properties: a long duration of a few hours, a large burst energy ($\sim 10^{42}$ erg) and a persistent pre-burst luminosity between 0.1 an 0.3 times the Eddington limit L_{Edd} (Wijnands 2001). In addition, all superbursts are known Type I X-ray bursters.

Apart from its duration, a superburst shows all the characteristics of a Type I X-ray burst, namely: the lightcurve has a fast rise and exponential decay; spectral softening occurs during the decay; black-body radiation describes the burst X-ray spectrum best. Normal Type I bursts can be explained very well by unstable He and/or H fusion on a neutron star surface (for reviews see e.g. Lewin et al. 1993, 1995; Bildsten 1998). In contrast, the superbursts are possibly due to unstable carbon fusion in layers at larger depths than where a typical Type I burst occurs (Cumming & Bildsten 2001; Strohmayer & Brown 2001).

In this paper we report the detection of one of the seven superbursts, namely from the X-ray source Serpens X$-$1 (Ser X$-$1), as observed with one of the Wide Field Cameras (WFC) onboard BeppoSAX. Ser X$-$1 is a relatively bright persistent X-ray source discovered in 1965 (Friedmann et al. 1967). Over 100 'normal' Type I bursts have been reported from Ser X$-$1 (e.g. Swank et al. 1975, Sztajno et al. 1983, Balucińska 1985). The proposed optical counterpart is MM Ser (Thorstensen et al. 1980). Wachter (1997) showed that the object is a superposition of two stars, and that no clear period could be derived from a photometric study. A distance of 8.4 kpc derived from Type I bursts is given by Christian & Swank (1997).

In this paper we describe the observation and properties of the Ser X$-$1 superburst, and discuss this in context to the other superbursts reported so far. (The occurrence of this burst was first mentioned in Heise et al. 2000.)

5.2   Observations

The Wide Field Cameras are two identical coded mask cameras onboard the Italian-Dutch satellite BeppoSAX (Jager et al. 1997, Boella et al. 1997). An overview of the characteristics of the WFC is given in Jager et al. (1997).

Most WFC observations are done in secondary mode. These are arbitrary sky-pointings except that they are perpendicular to the direction of the target to which the Narrow Field Instruments onboard BeppoSAX are pointed, and dictated by solar constraints. During the first half of 1997, the WFC observed Ser X$-$1 for a total of 411 ks (corrected for earth occultation and south Atlantic anomaly passages), distributed over 12 observations. In Table 5.1 an overview of all these observations is given.

During this period, there were also two RXTE Proportional Counter Array (RXTE/PCA) observations. The RXTE/PCA is an array of 5 co-aligned Proportional Counter Units (PCU). In Jahoda et al. (1996) a detailed description is given of the instrument. All PCU's were on during the observations. We

Table 5.1: Overview of the WFC and PCA observations of Ser X−1 between February 23 and May 13 1997. The exposure time is corrected for earth occultation, South Atlantic Anomaly passages and other data gaps. The WFC observation of Ser X−1 prior to this period was on November 6 1996 (MJD 50393) and the one following on August 22 1997 (MJD 50682).

	start (MJD)	end (MJD)	net exposure (s)
WFC	50502.29	50503.37	43437
	50506.82	50508.02	32237
	50508.61	50509.29	31180
	50513.16	50513.86	29020
	50517.70	50518.00	15306
	50518.26	50519.36	33699
	50529.63	50530.20	15496
	50541.26	50542.08	36302
	50542.63	50543.37	33310
	50554.62	50555.77	60707
	50563.69	50565.86	75693
	50581.47	50581.63	4652
PCA	50535.5	50539.9	34560
	50554.4	50554.7	25920

use standard 1 data for our analysis. Also on-board RXTE are three Scanning Shadow Cameras with a $6° \times 90°$ field of view forming the All-Sky Monitor (ASM; Levine 1996). We use the data products provided by the RXTE/ASM team at the MIT web-pages.

5.3 Data analysis & Results

On February 28, 1997 a flare-like event was observed which lasted for almost 4 hours. In Fig. 5.1 we show the RXTE/ASM lightcurve of Ser X−1 over a period of 5 years (a), and an expanded lightcurve during spring 1997 (b). The flare was observed after BeppoSAX came out of earth occultation on MJD 50507.075. In Fig. 5.1c and d a detailed view of the flare is shown. The rise to maximum was missed. After the satellite came out of earth occultation a flat top is observed before the decay starts, so it appears that the peak is covered. The flare shows an exponential decay. In Fig. 5.1 we see that spectral softening occurs during

the decay. This is indicative for Type I bursts. In Table 5.2 we summarize the exponential decay times from fits in different energy bands.

We divided the observation in which we discovered the superburst (see Fig. 5.1c and d) in three different intervals before, during and after the superburst, as indicated by dashed lines in Fig. 5.1c. In the first and last interval we fit the persistent flux with solely an absorbed bremsstrahlung spectrum. During the superburst we used a sum of the (persistent) bremsstrahlung and black-body radiation to describe the flux, taking the persistent bremsstrahlung emission as fixed at the average level of the spectral fits before and after the burst. We tried several other spectral models for the persistent emission, like a cut-off power-law and a disk black-body. The derived fluxes did not change significantly for the different models, and the best fit during the superburst is given by the bremsstrahlung model. In all our fits we fixed the absorption column at $N_{\rm H} = 0.5 \times 10^{22}$ atoms cm^{-2} (Christian & Swank 1997). We also added a black-body component to model the emission after the burst. However, an F-test showed that this extra component did not improve the fit significantly ($\simeq 2.5\sigma$ probability).

In Fig. 5.2 the results of the time-resolved spectral fits are shown. It is seen that both the black-body flux and the temperature drop exponentially, while the radius stays nearly constant. This is typical for normal Type I bursts.

An increase in the RXTE/ASM count-rate is observed on MJD 52120.15. This increase lasted for several dwells, having a total duration of at least 8.6 minutes and less then 2.3 hrs. Spectral softening can not be proven. This flare-like event may be another superburst.

5.4   Discussion

The flare-like event from Ser X−1 shows, except for its duration, all characteristics of a Type I burst. There are now six sources showing superbursts lasting for hours up to half a day. This superburst occurred at a persistent flux level of $0.21L_{\rm Edd}$, for $L_{\rm Edd} = 2 \times 10^{38}$ erg s^{-1}. This is comparable to that for the other superbursts. The fact that the persistent luminosity before the superburst is similar in the 6 sources may be an observational selection effect. As suggested by Cumming & Bildsten (2001), superbursts can occur at higher luminosities, where they are more difficult to detect due to the smaller contrast with the persistent flux. The total energy emitted during the burst, $E_{\rm b} = (7.3 \pm 1.4) \times 10^{41}$ erg, and the exponential decay time, are also comparable to those of the other superbursts.
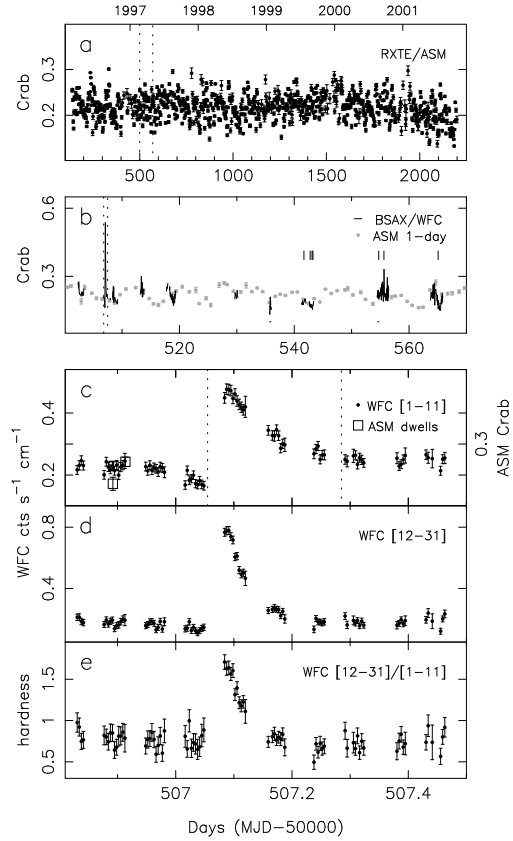
Figure 5.1: **a)** RXTE/ASM lightcurve of Ser X−1. Each bin is a 2 day average, and normalized to that of the Crab; only data with more than one dwell per day were included. The time span between the dashed lines has been blown up in **b)**, where we also show the data of the WFC (2-28 keV), and RXTE/PCA (indicated by small horizontal bars underneath). The WFC bins are one orbit averages and the PCA bins are 5 min averages; data points are connected to guide the eye when less than 0.2 days apart. The ASM points are one day averages (with more than one dwell per day). All observations are normalized to the Crab. A sharp increase can be seen at MJD 50507. The vertical tick-marks at the middle-right indicate the occurrence of 'normal' Type I bursts. Panels **c-e** show again a blow-up, indicated by the dashed line in **b)**, of the superburst in two different energy-bands, i.e. 2-5 keV **(c)** and 5-28 keV **(d)**, and their ratio in **(e)**. Each bin is 5 min. In panel **c)** individual ASM dwells are also over-plotted.

51

Table 5.2: Fit results of the superburst. The top panel shows the decay times for exponential decay fits in different passbands. The next panels shows the spectral fit results for the persistent emission before, after and during the burst, respectively. A bremsstrahlung model is employed to describe the persistent emission. The burst-emission is described by a sum of the bremsstrahlung and black-body spectrum, taking the bremsstrahlung emission fixed at the average of the spectral fits before and after the burst. For all spectral fits we fixed the absorption column at the value of $N_{\mathrm{H}} = 0.5 \times 10^{22}$ atoms cm^{-2} (from Christian & Swank (1997)).

exponential decay	
$\tau_{2-28\,\mathrm{keV}}$ (min) (χ^2_ν, d.o.f.)	69±3 (1.2, 53)
$\tau_{2-5\,\mathrm{keV}}$ (min) (χ^2_ν, d.o.f.)	108±12 (1.2, 51)
$\tau_{5-28\,\mathrm{keV}}$ (min) (χ^2_ν, d.o.f.)	52±2 (1.4, 56)
brems before	
kT_{br} (keV)	7.3±0.4
$F_{2-28\,\mathrm{keV}}$ (10^{-9}erg cm^{-2}s^{-1})	5.0±0.2
F_{bol} (10^{-9}erg cm^{-2}s^{-1})	8.3±0.2
χ^2_ν (d.o.f.)	0.8 (27)
brems after	
kT_{br}(keV)	6.2±0.4
$F_{2-28\,\mathrm{keV}}$ (10^{-9}erg cm^{-2}s^{-1})	5.7±0.3
F_{bol} (10^{-9}erg cm^{-2}s^{-1})	10.1±0.4
χ^2_ν (d.o.f.)	1.0 (27)
brems & black-body during	
kT_{bb} (keV)	2.4±0.1
R (km at 8.4 kpc distance)	3.6±0.3
$F_{2-28\,\mathrm{keV}}$ (10^{-9}erg cm^{-2}s^{-1})	6.1±1.1
F_{bol} (10^{-9}erg cm^{-2}s^{-1})	6.3±1.1
L_{peak} (10^{38}erg s^{-1})	1.6±0.2
E_{b} (10^{41} erg)	7.8±1.4
χ^2_ν (d.o.f.)	1.7 (26)
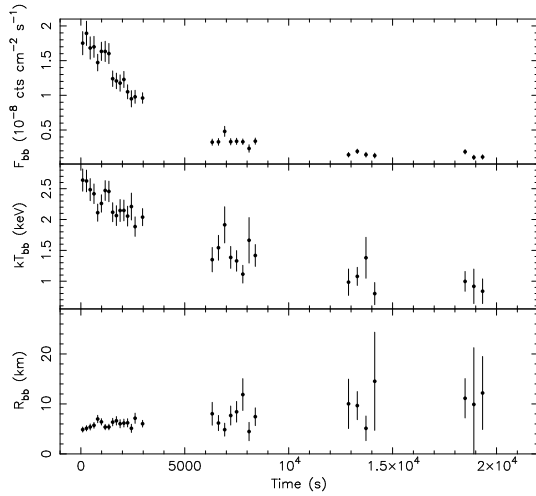
Figure 5.2: Results from time resolved spectroscopy from the beginning of the burst back to the persistent emission level. We show the black-body flux (F_{bb}), black-body temperature (kT_{bb}) and black-body radius (R_{bb}) of the burst, respectively. We have taken the persistent emission level, modeled by a bremsstrahlung spectrum, as fixed at the same values as used with the spectral fit of the total burst (see Table 5.2). Also the absorption column is fixed at $N_H = 0.5 \times 10^{22}$ atoms cm^{-2} (Christian & Swank 1997). During the first part of the burst each bin is 180 s. After the first gap due to earth occultation the bin size becomes 300 s and the last two intervals have bin sizes of 420 s. The black body radius is for a source at 8.4 kpc distance.

Cornelisse et al. (2000) noticed the absence of normal Type I bursts in the regular burster 4U 1735−44 throughout the 9-day observation. In the case of KS 1731−260, no Type I bursts were seen after the superburst, whereas they were present beforehand (Kuulkers et al. 2001). From Fig. 5.1 we see a similar effect in Ser X−1. The first normal burst is observed about 34 days after the superburst, at MJD 50541.32. After that, Ser X−1 is seen to burst rather regularly, having a total of seven bursts in 210.7 ks (about 3 bursts per day). For this burst-rate the Poisson distribution predicts a probability of 24% that no bursts are detected in the 55 ks WFC observations before the superburst, so it is possible that the lack of observed bursts before the superburst is due to chance. The probability that the absence of ordinary bursts in the 34 days after

the superburst is due to chance is 1.2%.

We also performed Monte Carlo simulations to verify in more detail the significance of finding no bursts around the superburst. We randomly varied the burst waiting time in an interval symmetric around 0.38 day (i.e. the average waiting time), and taking as the lower limit 0.04 day (the lowest waiting time observed by Sztajno et al. 1983). We then determined the number of bursts in: 1) the observing window before the superburst, and 2) the observing windows between the superburst and the occurrence of the first normal Type I burst. By doing 10^6 simulations for each window we found that the expected number of bursts for window 1) is 1.5 ± 1.1 and the chance of observing no bursts is 14%. For window 2) the expected number of bursts is 4.9 ± 1.9 and the chance of observing no bursts is only 0.4%. We conclude that the absence of bursts after the superburst is significant.

Fig. 5.1 shows that after the superburst the persistent flux-level in the low energy passband is higher then before the burst, while in the high energy passband no significant increase is observed. This is also visible in the burst from 4U 1735−44 (Cornelisse et al. 2000), but less obvious in KS 1731−260 (Kuulkers et al. 2001). This offset could be due to the heating of the neutron star atmosphere after the superburst, and could be present in the spectrum as a black-body component. However, for both Ser X−1 and KS 1731−260 no significant black-body contribution can be proven. We re-analyzed the off-set emission after the superburst of 4U 1735−44 (interval MJD 50318.55-50319.0). Here, $\chi^2 = 38.2$ (27 d.o.f.) for the absorbed bremsstrahlung model, which improves to $\chi^2 = 17.2$ (25 d.o.f.) when a black-body component was added. Performing an F-test shows that this is a significant ($\simeq 4\sigma$ probability) improvement. This may indicate that, at least for 4U 1735−44, the neutron star atmosphere is still cooling $\simeq 0.5$ day after the superburst.

Cumming & Bildsten (2001) propose that these bursts are due to unstable carbon burning in an ocean of heavy elements, e.g. ^{104}Ru. This can explain the observed durations and fluences for these superbursts. Also, the recurrence time is roughly consistent with that found for 4U 1636−53 (Wijnands 2001). A waiting time is predicted before the normal Type I bursts start again; $t_{\mathrm{wait}} \simeq 5t_{\mathrm{cool}}$, where the cooling time is a function of mass accretion rate (Cumming & Bildsten 2001). In the case of Ser X−1, for which the persistent flux is roughly $0.2L_{\mathrm{Edd}}$, a waiting time of $\sim$15 days is predicted. Given the rough estimates above, and the small observational coverage between 15 days and 34 days after the burst, the predicted waiting time is consistent with the observation.

If the increase in the RXTE/ASM data is due to a superburst, an upper limit of 4.4 years on the recurrence time of superbursts in Ser X−1 can be estimated.

This timescale is comparable to the 4.7 years found for 4U 1636−53 (Wijnands 2001).

References

Balucińska, M., & Czerny, M. 1985, AcA, 35, 291

Bildsten, L. 1998, in Bucheri, J., van Paradijs, J., Alpar, M.A. (eds.), The many faces of neutron stars, Kluwer, Dordrecht, p. 419

Boella, G., Butler, R., Perola, G., et al. 1997, A&AS, 122, 299

Christian, D.J., & Swank, J.H. 1997, ApJS, 109, 177

Cornelisse, R., Heise, J., Kuulkers, E., Verbunt, F., & in 't Zand, J.J.M. 2000, A&A, 357, L21

Cumming, A., & Bildsten, L. 2001, ApJ, 559, L127

Friedmann, H., Byram, E., & Chubb, T. 1967, Science, 156, 374

Heise, J., In 't Zand, J.J.M., & Kuulkers, E., 2000, HEAD 32, 28.03

in 't Zand, J.J.M. 2001, in A. Gimenez, V. Reglero, & C. Winkler (eds.), Exploring the gamma-ray universe, ESA Pub. Div., p. 463

Jager, R., Mels, W., Brinkman, A., et al. 1997, A&AS, 125, 557

Jahoda, K., Swank, J.H., Giles, A.B. et al. 1996, Proc. SPIE 2808, 59

Kuulkers, E. 2001, ATEL #68

Kuulkers, E., In 't Zand, J.J.M., Kerkwijk, M.H., et al. 2001, A&A 382, 503

Levine, A.M., Bradt, H., Cui, W., et al. 1996, ApJ, 469, L33

Lewin, W., van Paradijs, J., & Taam, R. 1993, Space Sci. Rev., 62, 223

Lewin, W., van Paradijs, J., & Taam, R. 1995, in W. Lewin, J. van Paradijs, E. van den Heuvel (eds.), X-ray binaries, Cambridge U.P., Cambridge, p. 175

Strohmayer, T.E. 2000, HEAD 32, 24.10

Strohmayer, T.E., & Brown, E.F. 2001, ApJ 566, 1045

Swank, J., Becker, R., Pravdo, S., & Serlemitsos, P.J. 1976, IAUC 2963

Sztajno, M., Basinska, E.M., Cominsky, L.R., Marshall, F.J., & Lewin, W.H.G. 1983, ApJ, 267, 713

Thorstensen, J.R., Charles, P.A., & Bowyer, S. 1980, ApJ, 238, 964

Wachter, S. 1997, ApJ, 490, 401

Wijnands, R. 2001, ApJ, 554, L59

Chapter 6

BeppoSAX Wide Field Cameras observations of six type I X-ray bursters

R. Cornelisse, F. Verbunt, J.J.M. in 't Zand, E. Kuulkers, J. Heise,
R.A. Remillard, M. Cocchi, L. Natalucci, A. Bazzano and P. Ubertini

Abstract− We have discovered three certain (SAX J1324.5−6313, 2S 1711−339 and SAX J1828.5−1037) and two likely (SAX J1818.7+1424 and SAX J2224.9+ 5421) new thermonuclear X-ray burst sources with the BeppoSAX Wide Field Cameras, and observed a second burst ever from a sixth one (2S 0918−549). Four of them (excluding 2S 1711−339 and 2S 0918−549) are newly detected X-ray sources from which we observed single bursts, but no persistent emission. We observe the first 11 bursts ever from 2S 1711−339; persistent flux was detected during the first ten bursts, but not around the last burst. A single burst was recently detected from 2S 0918−549 by Jonker et al. (2001); we observe a second burst showing radius expansion, from which a distance of 4.2 kpc is derived. According to theory, bursts from very low flux levels should last $\gtrsim 100$ s. Such is indeed the case for the last burst from 2S 1711−339, the single burst from SAX J1828.5−1037 and the two bursts from 2S 0918−549, but not for the bursts from SAX J1324.5−6313, SAX J1818.7+1424 and SAX J2224.9+5421. The bursts from the latter sources all last ∼20 s. We suggest that SAX J1324.5−

6313, SAX J1818.7+1424, SAX J1828.5−1037 and SAX J2224.9+5421 are members of the recently proposed class of bursters with distinctively low persistent flux levels, and show that the galactic distribution of this class is compatible with that of the standard low-mass X-ray binaries.

6.1   Introduction

About 40% of the low mass X-ray binaries in our Galaxy occasionally show (so-called Type I) X-ray bursts, which are thermonuclear flashes due to unstable helium and/or hydrogen burning of matter accreted on a neutron star surface (for a review see e.g. Lewin et al. 1993). A typical burst shows a fast rise ($\simeq 1\,$s) and exponential decay, softening during the decay (interpreted as cooling of the neutron star photosphere), and a spectrum which can be well described with black-body radiation. At the moment, about 70 X-ray bursters are known, approximately 20 of which have been discovered with BeppoSAX (e.g., in 't Zand 2001).

Most X-ray bursters are detected with persistent X-ray flux observed before and after bursts. But some sources have been detected during bursts only, with upper-limits on the persistent emission. These limits vary widely, as they depend on the sensitivity of the instrument used. For example, the X-ray sources in the globular clusters Terzan 1 and Terzan 5 were detected with the Hakucho satellite during bursts only, but EXOSAT and ROSAT also detected the persistent emission (Makishima et al. 1981, Warwick et al. 1988, Verbunt et al. 1995).

The study of X-ray bursts serves various purposes. First, applying the theory of X-ray bursts to observations provides information about the neutron star (e.g., its radius when the distance is known) and about its companion (e.g., whether the matter transferred from the companion is hydrogen-rich or not). Second, the bursts unambiguously decide which of the low-mass X-ray binaries contain a neutron star as opposed to a black hole, and provide (an upper limit to) the distance of the binary, from the condition that its luminosity should be less than the Eddington luminosity. Third, new low-mass X-ray binaries may be discovered by the detection of bursts, in cases where the persistent flux is too low. The last two points help in forming a more accurate view of the total number and distribution of low mass X-ray binaries in our Galaxy, and of the fraction that contains a neutron star.

In this paper we describe the observation with the BeppoSAX Wide Field Cameras of six type I burst sources. Four of these are new X-ray sources with

a persistent flux below the detection threshold of the Wide Field Cameras of $\simeq 10^{-10}$ erg cm^{-2}s^{-1}. The fifth source is a known X-ray source, from which we detect bursts for the first time. The sixth source is also a previously known X-ray source, the first burst of which was recently discovered by Jonker et al. (2001); we describe a second burst from this source and use it to determine its distance. In Sect. 2 we describe the observations and data reduction; the results are described in Sect. 3. Because of their diversity, the sources are discussed in separate subsections, each of which is accompanied by a sub-subsection in which comparison with other observations are made. Finally, in Sect. 4 we discuss some implications of our results for the theory of bursts (Sect. 4.1) and for various sub-populations of the low-mass X-ray binaries with neutron stars (Sect. 4.2).

6.2   Observations and data analysis

Our observations were obtained from mid 1996 to the end of 2001 with the Wide Field Cameras (Jager et al. 1997) on board of the BeppoSAX satellite (Boella et al. 1997). The Wide Field Cameras are two identical coded mask aperture cameras with a $40° \times 40°$ (full width to zero response) field of view and $\sim 5'$ angular resolution. The source location accuracy is between $0.\!'7$ and $5'$, and the passband is 2 to 28 keV. Data are collected with a time resolution of 0.5 ms. The sensitivity depends on the off-axis angle, but is on average a few mCrab in a 10^5 s exposure.

The large sky coverage together with the good angular and time resolution make the Wide Field Cameras an excellent experiment to detect fast transient X-ray phenomena at unexpected sky positions and simultaneously study the behavior of a large fraction of the low mass X-ray binary population in our Galaxy.

Roughly 90% of all observations of the Wide Field Cameras are carried out in the so-called 'secondary mode', in which the pointing of the satellite is set for the Narrow Field Instruments. The pointing of the Wide Field Cameras is arbitrary, except for solar angle constraints and the constraint that the two Wide Field Cameras point in opposite directions, perpendicular to the direction of the Narrow Field Instruments. The remaining 10% of the Wide Field Camera observations are 'primary mode' observations, in which one of the two cameras is pointed at the Galactic Center (and the other, thus, at the anti-center).

We search for X-ray bursts in the lightcurve of the total detector (i.e., a superposition of all the sources in the field of view). With this method we detect

Table 6.1: Results of the BeppoSAX Wide Field Cameras observations. For each burst source the table gives the time of the burst, the position with error δ, the total exposure time on the source between August 1996 and December 2001 $t_{\rm tot}$, the exposure time $t_{\rm exp}$ of the pointing in which the burst was detected, and the hydrogen absorption column $N_{\rm H}$, persistent flux $F_{\rm pers}$ between 2-28 keV, and the distance d derived from the burst peak flux. For the bursts the table gives the e-folding times τ for the total flux, and for the hard and soft energies, where we choose bands 2-x and x-28 keV such that both bands have similar countrates. Spectral fits have been made for counts integrated over $t_{\rm fit}$; we give the black body temperature $kT_{\rm bb}$, radius R at distance (limit) d, the average flux F in two bands, the bolometric peak flux $F_{\rm peak}$, and the total burst fluence $E_{\rm b}$; and the temperature $kT_{\rm brems}$ and photon index Γ for bremsstrahlung and power law fits, respectively. All fluxes are corrected for absorption.

	SAX J1324.5−6313	SAX J1818.7+1424	SAX J1828.5-1037	SAX J2224.9+5421	2S 1711−339	2S 0918−549
Source parameters						
Burst time (MJD)	50672.151	50683.770	51988.863	51488.454	b1-11, Table 6.2	51335.049
RA (J2000)	$13^{\rm h}24^{\rm m}27^{\rm s}$	$18^{\rm h}18^{\rm m}44^{\rm s}$	$18^{\rm h}28^{\rm m}33^{\rm s}$	$22^{\rm h}24^{\rm m}52^{\rm s}$	$17^{\rm h}14^{\rm m}17^{\rm s}$	$09^{\rm h}20^{\rm m}37^{\rm s}$
Dec (J2000)	$-63°13.'4$	$14°24.'2$	$-10°37.'8$	$+54°21.'9$	$-34°3.'3$	$-55°13.'9$
δ (99% confidence.)	$1.'8$	$2.'9$	$2.'8$	$3.'2$	$1.'5$	$0.'7$
l_{II}, b_{II}	$306°.6, -0°.6$	$42°.2, +13°.7$	$20°.9, 0°.2$	$102°.6, -2°.6$	$352°.1, +2°.8$	$275°.9, -3°.8$
$t_{\rm tot}$ (day)	58	31	25	65	66	62
$t_{\rm exp}$ (ks)	18.5	16.2	12.7	40.2	314	36
$N_{\rm H}$ (10^{22} atoms cm^{-2})	1.5^a	0.1^a	1.9^a	0.5^a	1.5^b	0.24^c
$F_{\rm pers}$ (10^{-10} erg cm^{-2}s^{-1})	$< 0.80\,(3\sigma)$	$< 1.7\,(3\sigma)$	$< 1.9\,(3\sigma)$	$< 0.35\,(3\sigma)$	6.3 ± 0.6	3.8 ± 0.6
d (kpc)	< 6.2	< 9.4	< 6.2	< 7.1	< 7.5	4.2
Burst parameters						
$\tau_{2-28{\rm keV}}$ (s)	6.0 ± 0.1	4.5 ± 0.1	11.2 ± 0.6	2.6 ± 0.2	7.1 ± 0.2	48.5 ± 0.2
x	8	4	7	6	6	5
$\tau_{2-x{\rm keV}}$ (s)	9.7 ± 0.4	5.7 ± 0.2	21.5 ± 1.3	3.9 ± 0.7	7.6 ± 0.3	80.6 ± 0.7
$\tau_{x-28{\rm keV}}$ (s)	2.6 ± 0.2	1.17 ± 0.04	4.7 ± 0.6	1.8 ± 0.3	5.9 ± 0.3	36.5 ± 0.2
black-body fit						
$t_{\rm fit}$ (s)	9.3	6.0	25.1	4.0	-	86.4
$kT_{\rm bb}$ (kev)	2.5 ± 0.2	1.1 ± 0.14	2.3 ± 0.2	2.5 ± 0.3	1.6 ± 0.1	2.26 ± 0.05
R (km) at d	4.5 ± 0.5	$24.^{+5}_{-8}$	4.7 ± 0.9	4.7 ± 0.5	$5.5-11.9$	6.3 ± 0.2
$F_{2-10{\rm keV}}$ (10^{-8} erg cm^{-2}s^{-1})	1.23 ± 0.10	1.02 ± 0.03	1.08 ± 0.40	1.00 ± 0.42	0.4 ± 0.1^d	4.05 ± 0.27
$F_{2-28{\rm keV}}$ (10^{-8} erg cm^{-2}s^{-1})	2.17 ± 0.07	1.07 ± 0.05	1.65 ± 0.73	1.66 ± 0.89	0.5 ± 0.1^d	6.1 ± 0.5
$F_{\rm peak}$ (10^{-8} erg cm^{-2}s^{-1})	4.3 ± 0.2	1.9 ± 0.1	4.3 ± 1.6	3.3 ± 1.5	3.0 ± 1.0^d	9.4 ± 1.7
$E_{\rm b}$ (10^{-7} erg cm^{-2})	$\simeq2.6$	$\simeq0.86$	$\simeq4.3$	$\simeq0.67$	-	$\simeq52$
χ^2_ν (d.o.f.)	1.0 (26)	0.6 (26)	0.7(26)	1.0(26)	0.9 (270)	1.6 (26)
bremsstrahlung fit						
$kT_{\rm brems}$ (keV)	56^{+47}_{-34}	5.9 ± 1.7	$44.^{+146}_{-22}$	$50.^{+149}_{-25}$	-	64 ± 14
χ^2_ν (d.o.f.)	1.4 (26)	0.5 (26)	1.1(26)	1.1(26)	-	9.7 (26)
power law fit						
Γ	1.4 ± 0.1	2.3 ± 0.21	1.4 ± 0.2	1.4 ± 0.2	-	1.31 ± 0.04
χ^2_ν (d.o.f.)	1.5 (26)	0.5 (26)	1.1(26)	1.1(26)	-	10 (26)

^{a} Interpolated from Dickey & Lockman (1990); ^{b} From NFI, see Sect. 3.2.1; ^{c} From Christian & Swank (1997); ^{d} Values for b8.

a burst if the fast fluctuations in the overall count-rate are small ($< 10\%$), and if the burst lasts 10 to 100 seconds and reaches a peak count-rate of at least a few times 10^{-8} erg cm^{-2}s^{-1}. If a burst-like event is observed, a sky image is reconstructed by cross-correlating the detector image with the coded mask (Jager et al. 1997). During this reconstruction the background is subtracted automatically. By comparing the sky image with a catalogue of X-ray sources the burst event can be attributed to a known, or previously unknown, X-ray burster. In this way we discovered bursts from SAX J1324.5$-$6313, SAX J1828.5$-$1037, SAX J1818.7+1424, SAX J2224.9+5421 and 2S 0918$-$549. The burst positions of the newly discovered sources are then used to search for persistent emission and other, possibly somewhat fainter, X-ray bursts in all Wide Field Cameras observations of these sources.

During primary mode, lightcurves for individual sources are created and are searched for bursts. In these data we discovered bursts from 2S 1711$-$339.

The SAX positions for new X-ray sources are also used to generate studies with the RXTE All-Sky Monitor (ASM; Levine et al. 1997), which has smaller cameras than the WFC but typically provides many measurements per day for every X-ray source. Retrospective ASM light curves are obtained by refitting the coded mask data as a superposition of the mask shadows for all of the sources in a particular camera exposure (90 s), including the new target of interest. This reprocessing effort yields light curves that track the behavior of X-ray sources with substantially greater sensitivity compared to the threshold for generic identifications of new transients at random sky positions.

6.3   Results

6.3.1   New sources

A single burst was detected at four locations where no X-ray source is known from previous observations, including the ROSAT All Sky Survey (Voges et al. 1999). We conclude that we have detected four new sources and designated them with SAX names in Table 6.1.

All new sources are detected only during the burst: the Wide Field Cameras show no persistent emission or other burst between August 1996 and December 2001 in any of the four cases. To compute the upper limits listed in Table 6.1, we employ absorption columns interpolated from HI maps by Dickey & Lockman (1990), and a power law spectrum with photon index Γ=1.0. (This value is typical for burst sources at low luminosities; see for example Sect. 3.3 below.)

61
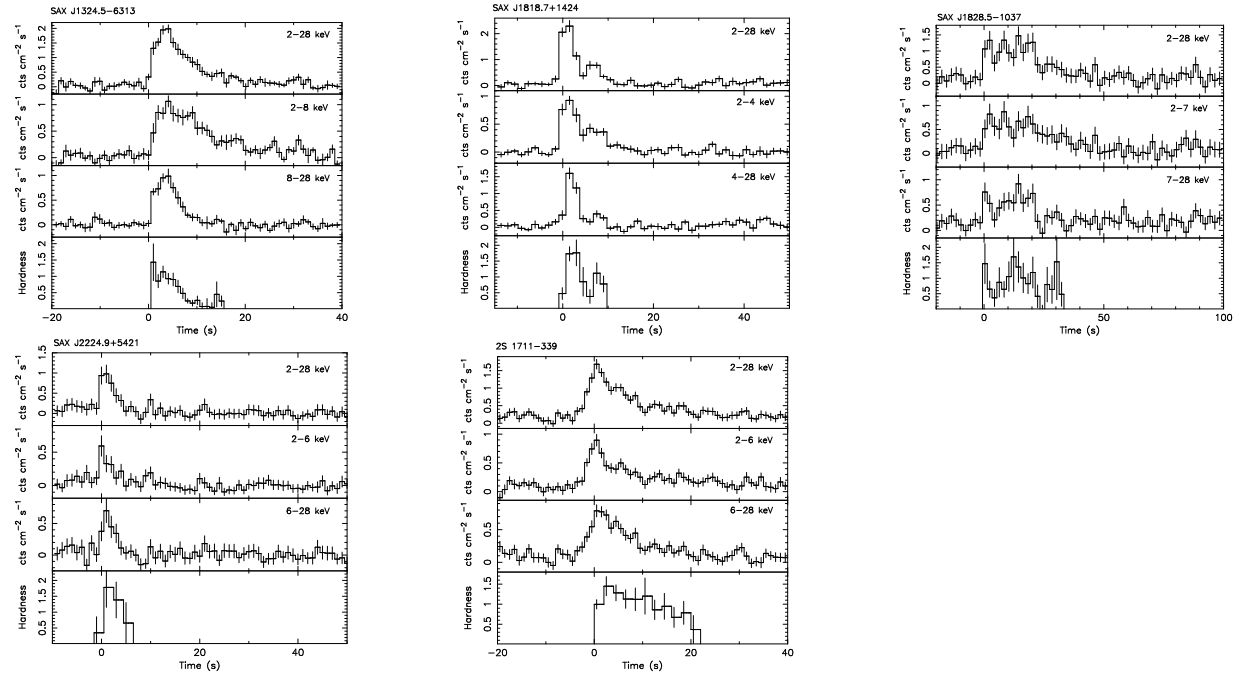
Figure 6.1: Lightcurves of bursts from SAX J1324.5−6313, SAX J1818.7+1424, SAX J1828.5−1037, SAX J2224.9+5421, and 2S 1711−339, respectively. For 2S 1711−339 the profile is the average of bursts b1-b10. Three different energy passbands are shown; the total Wide Field Cameras passband (2-28 keV), a low energy passband, and a high energy passband. The high and low energy passbands are chosen in such a way that the count rate was roughly comparable, giving the same statistical quality. Also, the hardness, i.e. the ratio of the high to the low energy count rate, is shown. For each source the binsizes are 1 s, 1.5 s, 2 s, 1 s, and 1 s, respectively; except for the hardness of SAX J2224.9+5421 and 2S 1711−339, which have binsizes of 2 s.

For a photon index of Γ=2.0 the flux values would be 70% lower.

The All-sky Monitor onboard RXTE satellite (RXTE/ASM) scanned the positions of the four new sources. During the course of our analysis the lightcurves of these sources became available. These lightcurves rather uniformly cover a five year period with, most of the time, several 90 s observations per day and actual exposure times of 1.7×10^6 s and 1.8×10^6 s, respectively. None of the four lightcurves show a clear detection during this period at an upper-limit of $\simeq 2 \times 10^{-10}$ erg cm^{-2}s^{-1} (2-10 keV) in 7 days of observation.

The lightcurves of the bursts in various passbands are shown in Fig. 6.1. They have a fast-rise ($\sim 1-3$ s) and exponential-like decay (for SAX J1828.5$-$1037 this is evident mainly at the lower energies). The decay is faster at higher energies, indicative of spectral softening; decay times are listed in Table 6.1 together with the spectral fits for the bursts.

The burst profile of SAX J1828.5$-$1037, as shown in Fig. 6.1, looks rather strange even considering the low statistical quality. But it is precedented by profiles from at least one well established burster (4U 1636$-$536; van Paradijs et al. 1986). Thus, it would be interesting to observe more bursts from SAX J1828.5$-$1037 with better sensitivity.

To obtain a spectrum we integrate the spectrum over the burst duration; the exact integration times are given in Table 6.1. We fit the spectra with a black-body, power law, and bremsstrahlung model. The black-body gives the best description for three of the four bursts and is acceptable for SAX J1818.7+1424, as expected for type I bursts.

If they are indeed type I bursts, their peak flux must be less than or equal to the Eddington limit of 2×10^{38} erg s^{-1} (for canonical neutron star values), and we can use the observed peak flux to obtain an upper limit to the distance (e.g. Lewin et al. 1993); these upper limits are also listed in Table 6.1. We note that due to systematic uncertainties the errors on the distance are $\sim 30\%$ (e.g. Kuulkers et al. 2002).

To prove that the above-discussed bursts are genuine type I X-ray bursts it must be shown that a black body gives the only acceptable description of their spectrum. From Table 6.1 we see that this is the case only for SAX J1324.5$-$6313; for the other three bursts bremsstrahlung or power-law spectra are still acceptable. That is why we consider the two alternative explanations for these three bursts, i.e. that they are stellar X-ray flares or X-ray flashes.

Stellar X-ray flares are generally much longer ($\sim$hours) and have much lower peak fluxes than the bursts that we have observed (e.g. Greiner et al. 1994, Haisch & Strong 1991). We therefore consider it unlikely that any of the three bursts is a stellar flare.

X-ray flashes are related to gamma-ray bursts in the sense that they look like the prompt X-ray counterparts to Gamma ray bursts but lack the γ-ray emission: they have similar time scales, have the same variety of time profiles (including fast-rise exponential-decay shapes), and have spectra that are best described by a power law rather than black body radiation (Heise et al. 2001). X-ray flashes are non-repetitive, and if they are related to gamma-ray bursts no detectable X-ray emission is expected before or lang after the flash. The Wide Field Cameras have observed about 25 of these (in 't Zand et al., in prep.).

SAX J1828.5−1037 was previously observed during a ROSAT observation (see Sect. 3.1.1), leaving only doubts on the nature of SAX J1818.7+1424 and SAX J2224.9+5421. If these two bursts were X-ray flashes with fast-rise exponential-decay time profiles, they would be the shortest two of all, and they would be the only ones for which the black body model for the spectrum can not be unambiguously ruled out. Together with the fact that the bursts were at positions near the Galactic plane where type I bursters are likely to occur we think that the most probable explanation for all four bursts is therefore that they are type I X-ray bursts.

Other observations

HD 168344, a V=7.6 magnitude K2-type star is within the error-radius at a distance of $2\rlap{.}'1$ from the centroid of SAX J1818.7+1424. There are 18 stars of magnitude 8 or brighter within a $4° \times 4°$ field around SAX J1818.7+1424 (ESA 1997). This makes the chance probability of having an 8th magnitude or brighter star within the error radius 0.8%. This probability is so small that we consider the possibility that the event was an X-ray flare from HD 168344.

According to the Tycho Catalogue (ESA 1997) it is a K2 star with V=7.59 and $B-V$=1.047, a parallax of $0\rlap{.}''0068\pm0\rlap{.}''0055$ and a proper motion of about $0.029''$/yr. A main sequence K2 star with this apparent magnitude would have a distance of only ~ 16 pc, incompatible with the small observed parallax. In contrast, a K2 III star of the observed magnitude would be at a distance of 230-270 pc, compatible with the observed parallax, and its velocity perpendicular to the line of sight would be comparable with the observed radial velocity.

The too short burst time scale of 10 s and the high peak luminosity of 1.2×10^{35} erg s^{-1} at a distance of 230 pc, both exclude that the burst observed by us was a stellar flare on HD 168344. (No stellar flare this short and bright has ever been observed to our knowledge; e.g. Haisch & Strong 1991.) If a neutron star were a companion of HD 168344, the peak flux of its burst would be $\simeq 6 \times 10^{-4}$ of the Eddington flux. This also is unlikely We conclude that HD 168344 is not
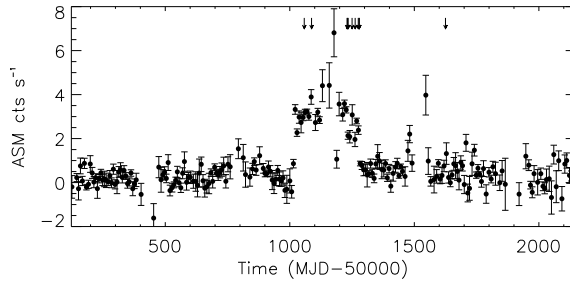
Figure 6.2: Long-term lightcurve of 2S 1711−339 obtained with the RXTE All-sky monitor, which shows an outburst between July 1998 and May 1999. Each point represents a one-week average. The vertical arrows indicate the times at which bursts were detected with the BeppoSAX Wide Field Cameras.

the optical counterpart of SAX J1818.7+1424.

Whereas none of the four burst positions coincides with a catalogued ROSAT source, we find that SAX J1828.5−1037 is in the field of view of a 9.4 ks ROSAT/PSPC pointed observation obtained on April 4 1993. We have analyzed this observation and detect seven sources (in channels 50-240), one of which is in the Wide Field Cameras error-circle. With a radius for the ROSAT field of view of $\sim 50'$ the chance probability that one of seven sources falls in the SAX J1828.5−1037 error-circle of $2.'8$ is about 2%. Thus the ROSAT source is probably the counterpart of SAX J1828.5−1037, confirming that SAX J1828.5−1037 was not an X-ray flasher. The position of the ROSAT source is RA=18^h28^m 25.7^s, Dec=$-10°37'51''$ (J2000) with an error of $39''$ (1σ). The source is not detected in channels 11-50, as expected for a highly absorbed source. The count-rate of 0.011 ± 0.002 cts s^{-1} corresponds to an unabsorbed flux between 0.5-2.5 keV of 1.9×10^{-12} erg cm^{-2}s^{-1} for a power law with photon index $\Gamma = 1$. At a distance of 6.2 kpc this corresponds to a luminosity of 8.7×10^{33} erg s^{-1}.

6.3.2   2S 1711−339

2S 1711−339 is an X-ray source that was bright between July 1998 and May 1999. The Wide Field Cameras covered this outburst in August-October 1998 and February-April 1999. Ten short bursts were detected which we designate b1, b2,...,b10. All these bursts appear to have a similar shape. In the left panel
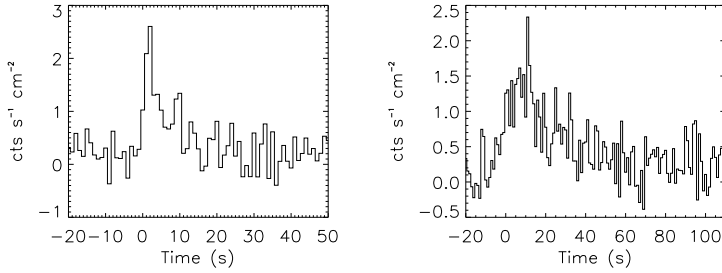
Figure 6.3: Bursts b5 (left panel) and b11 (right panel) of 2S 1711−339 in the 2-28 keV passband. The first 10 bursts show similar shapes and are represented by b5. The persistent emission was detected during the observations before/after all these bursts. Before and after b11 the persistent emission was below the detection limit of the Wide Field Cameras.

of Fig. 6.3 we show the best example (b5) of these bursts. To fit the average persistent emission before and after the bursts, we employ the absorption column derived in Sect. 3.2.1. A cut-off power law with a photon-index of 0.7±0.5 and a high-energy cut off of 2.8±0.8 keV provides a satisfactory fit; the flux of the persistent emission is given in Table 6.1.

During a 40 ks observation on March 22 2000 an eleventh burst (b11) was detected while the persistent emission level before and after the burst was below the detection limit. Assuming that the spectral parameters of the persistent flux observed with bursts b1-b10 still apply, we obtain a 3σ upper-limit on the persistent flux of 7.0×10^{-11} erg cm^{-2}s^{-1} (2-28 keV); this is a factor of ten lower than during bursts b1-b10. This burst, which is shown in the right panel of Fig. 6.3, has a different shape than the previous 10 bursts. Both the rise and decay time for burst b11 are longer. In Table 6.2 we summarize the characteristics for the 11 individual bursts. In Fig. 6.2 we show the RXTE/ASM long-term lightcurve of 2S 1711−339 which shows that the first 10 bursts occurred during an outburst.

It is clear from Table 6.2 that none of the exponential fits to the decay is formally acceptable. Also, for none of the individual bursts cooling can be unambiguously shown. Therefore, we decided to combine the light curves of burst b1 to b10. The last burst, b11, is excluded because of its deviating shape. To combine the bursts we created lightcurves with a time resolution of

Table 6.2: Characteristics of the individual bursts of 2S 1711−339. For each burst we give the time of occurrence, the peak count rate in the WFC, and from a fit of an exponential to the decay, the e-folding decay time and the reduced χ^2.

burst	Start time (MJD)	CR_{peak} $(cm^{-2}\,s^{-1})$	τ_{2-28} (s)	χ^2_ν 47 d.o.f.
b1	51058.024301	1.15±0.05	6.9±0.4	1.3
b2	51087.268967	1.73±0.04	7.0±0.3	1.5
b3	51229.857483	1.72±0.04	6.3±0.2	1.3
b4	51232.083607	1.69±0.04	3.6±0.1	1.4
b5	51234.270915	1.63±0.06	5.2±0.2	1.6
b6	51249.958462	0.94±0.03	14.5±0.8	1.4
b7	51262.473439	1.29±0.03	11.5±0.4	1.4
b8	51274.775982	1.88±0.04	6.9±0.2	1.5
b9	51278.327360	1.25±0.07	10.5±0.9	1.5
b10	51278.992006	could not be constrained		
b11	51625.046991	1.18±0.04	15.0±0.7	1.3

1 s. We took the highest bin as the peak for each burst and the corresponding time as t=0 s. Then the bursts were combined, by averaging the count rates and determining the statistical error in the mean. Fig. 6.1 shows the resulting profile.

A black-body spectrum was fit to the burst spectrum of all 11 burst. We assumed a fixed absorption column, $N_H = 1.5 \times 10^{22}$ atoms cm^{-2} (see Sec. 3.2.1). We fitted the 11 burst spectra simultaneously; the black-body temperature was forced to be the same for all bursts, whereas the black-body radius was allowed to vary. In Table 6.1 we have summarized the results for fits to the spectrum and to the exponential decays in different passbands. Instead of giving the radius of each individual burst we indicate the range of radii in Table 6.1. Varying the temperature and forcing the radius to be the same for all bursts simultaneously gives a range of temperatures between 1.2-2.0 keV and a radius of 7.8±0.9 km (at 7.5 kpc). Burst b8 has the highest peak flux. The temperatures and the radii found are typical values for Type I bursts. We conclude that the 11 events are Type I bursts.

From the observed peak flux during the burst and the constraint that this
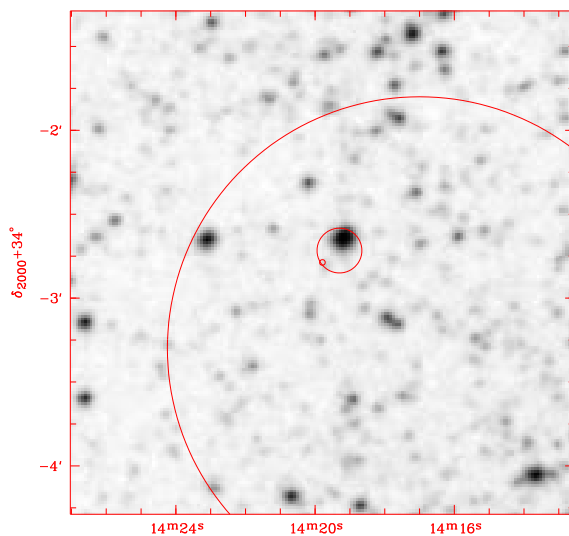
Figure 6.4: Error circles (large to small) from the Wide Field Cameras position (this paper), RXS J171419.3−340243 (Voges et al. 1999), and Chandra position of 2S 1711−339 (this paper) superposed on an image from the Digitized Sky Survey.

must be less than the Eddington limit, we derive from the brightest burst b8 an upper limit to the distance of 2S 1711−339 of 7.5 kpc.

Other observations of 2S 1711−339

A Chandra/ACIS-S observation of 2S 1711−339 was performed on June 9 2000 for a total of 949 s. A single relatively bright source with a countrate of 0.46±0.02 cts s^{-1} is detected at a position RA=17^{h}14^{m}19.8^s, Dec=−34°02′47″ (J2000) with a conservative error-radius of 1″.

Our WFC position for 2S 1711−339 (Table 6.1), the position of the Ariel V source A 1710−34 (Carpenter et al. 1977), and the position of the source RXS J171419.3−340243 from the ROSAT All Sky Survey (Voges et al. 1999) are all compatible with the Chandra position of 2S 1711−339 as illustrated in Fig. 6.4. We conclude that they are all the same source. We note that the nearest source with comparable (ROSAT) brightness in the ROSAT All Sky Survey is at a distance of $\sim 30'$.

The spectrum during a BeppoSAX Narrow Field Instrument (NFI) observation on February 29, 2000 (MJD 51603) of 2S 1711−339 is best described by an absorbed power law model with photon index 2.2 and an absorption column of 1.5×10^{22} atoms cm^{-2} for the persistent emission (Migliari, di Salvo, Belloni, in preparation). Use of this spectrum for the persistent flux measured with the Wide Field Cameras does not significantly change the numbers given in Sect. 3.2 and Table 6.1. The flux between 2 and 6 keV in units of 10^{-11} erg cm^{-2}s^{-1} for 2S 1711−339 varied from < 40 in February 1975 to 200 in September 1976 (Carpenter et al. 1977), to 5 during the EXOSAT Galactic Plane Survey (Warwick et al. 1988). Assuming the spectrum as observed by the NFI we obtain fluxes between 2 and 6 keV in units of 10^{-11} erg cm^{-2}s^{-1} of 2 during the ROSAT All Sky Survey, 2.4 during the NFI observations, and 0.3 during the Chandra/ACIS-S observations. The large range of fluxes shows that 2S 1711−339 is a genuine transient.

6.3.3 2S 0918-549

A single bright burst was detected from the X-ray source 2S 0918-549 on June 6.049, 1999. The burst has a fast rise, a flat top and an exponential decay. In Table 6.1 we summarize exponential-decay fits in different passbands and the results of spectral modeling. We fix the interstellar column at the value found from Einstein X-ray data (Christian & Swank 1997).

The persistent flux is satisfactorily described by a cut-off power law spectrum with a photon index of 0.9±0.6 and a high-energy cut-off of 5.2±3.8 keV, or a bremsstrahlung spectrum with a temperature of 8.9±1.8 keV (the flux is only marginally different between the two models). The black-body model gives the best fit to the burst spectrum. We also performed time-resolved spectral fits for the burst. The values of kT_{bb} and R$_{bb}$ are plotted as a function of time in Fig. 6.5. We notice that the burst shows the characteristics of a radius-expansion burst (an increase in the black-body radius, and a drop in the black-body temperature while the flux stays constant). A distance of 4.2 kpc (with an uncertainty of 30%; see e.g. Kuulkers et al. 2002) and a persistent luminosity of 6.8×10^{35} erg s^{-1} are implied.

Other observations

It turns out that 2S 0918−549 is in the field of view of a 4.8 ks ROSAT PSPC observation of HD 81188, with a countrate (channels 11-240) of 9.83±0.05 cts s^{-1}. We have analyzed its spectrum and tried to model it with the combination of
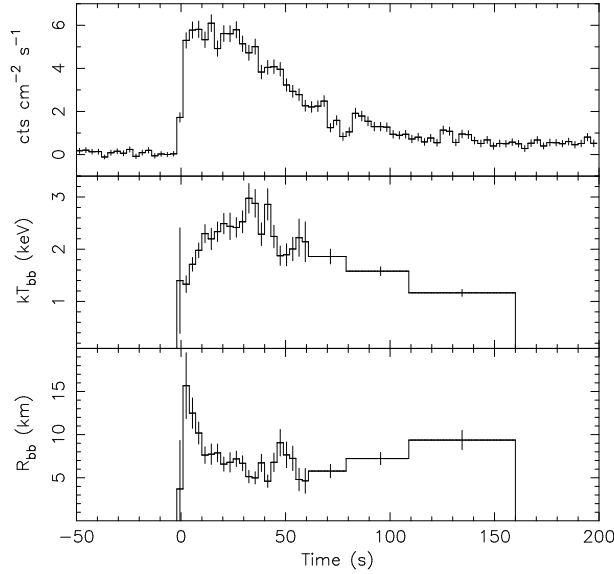
Figure 6.5: The lightcurve and results of the time-resolved spectroscopy of the burst from 2S 0918-549. Each bin is 3 seconds, apart from the last three bins which are 17 s, 30 s and 50 s respectively. The top panel gives the lightcurve, the middle panel the black-body temperature during the burst and the bottom panel the black-body radius for a source at 4.2 kpc. For the spectral fits a fixed column density of $N_{\rm H} = 0.5 \times 10^{22}$ atoms cm^{-2} is assumed.

a 2 keV black body and 2 keV thermal bremsstrahlung spectrum as fitted by Christian & Swank (1997) to Einstein data of this source. This model is not acceptable. An acceptable fit ($\chi^2_\nu = 1.2$, 9 d.o.f.) is obtained for a combination of a 0.1 keV black body and 3.0 keV thermal bremsstrahlung spectrum, absorbed by N_H=5.0 $\times 10^{21}$ atoms cm^{-2}. The ratio of the black-body to the bremsstrahlung flux in the 0.5-2.5 keV band is 1.45. For this fit the 2-10 keV flux is due to the bremsstrahlung only, and is 2×10^{-10}erg cm^{-2}s^{-1}, a factor two below the level observed with the Wide Field Cameras. The flux in the 0.5-20 keV range is 8×10^{-10} erg cm^{-2}s^{-1}, a factor four higher than the level observed with Einstein.

Jonker et al. (2001) were the first to detect a burst of 2S 0918$-$549. The data analyzed by Jonker et al. do not combine good time resolution with spectral

resolution. Therefore Jonker et al. cannot and indeed do not establish that the burst they observed is at the Eddington-limit. However, they estimate a peak luminosity of about $8.8 \times 10^{-8} \mathrm{erg\,cm^{-2}s^{-1}}$ (2-20 keV), close to the peak flux of the burst we observed. Accordingly, their distance upper-limit of 4.9 kpc is comparable to our measurement. We conclude that the burst observed by Jonker et al. must be at, or close to, the Eddington limit as well; indeed, the lightcurve presented Jonker et al. is highly suggestive of a radius-expansion burst. The upper-limit $< 4.2 \times 10^{-10}$ erg cm^{-2}s^{-1} (2-20 keV) for the persistent flux before the burst derived by Jonker et al. is compatible with (and close to) the persistent flux that we detect.

The optical counterpart of 2S 0918−549 was identified by Chevalier & Ilovaisky (1987), as a blue star (V=21.0, $B-V$=0.3) in the error circle of the Einstein position for the X-ray source. The X-ray to optical flux ratio of $\simeq 800$ indicates that the source is a low-mass X-ray binary. Chevalier & Ilovaisky assume a distance of 15 kpc, and note that the X-ray and optical luminosities are low, as compared to those of average low-mass X-ray binaries. Our distance estimate of 4.2 kpc leads to lower luminosities with $M_V \simeq 6.9$ (for $A_V \simeq 1.0$), and $L_x \simeq 8.7 \times 10^{35} \mathrm{erg\,s^{-1}}$.

The visual extinction is estimated by assuming that $(B-V)_\mathrm{o}$=0 − a common value for low-mass X-ray binaries − and is roughly compatible with the value estimated for the X-ray absorption, using the relation between the latter and the visual extinction according to Predehl & Schmitt (1995).

6.4   Discussion

Our observations add at least three and possibly five bursters to the list of X-ray bursters in our Galaxy and provide a distance estimate for a recently discovered burster. In this section we discuss the implications of our results for the theory of bursts (in Sect. 4.1) and make a comparison between the class of bursters with low persistent luminosities – to which we have added four members – with other low-mass X-ray binaries (in Sect. 4.2).

6.4.1   Comparison with burst theory

We compare the properties of the bursts with theory. Fujimoto et al. (1987, see also Bildsten 2000) propose three classes of bursts. At the lowest accretion rates, 10^{-14} M$_\odot$yr^{-1} $\lesssim \dot{M} \lesssim 2 \times 10^{-10}$ M$_\odot$ yr^{-1}, a burst is triggered by thermally unstable hydrogen burning, and can last between 10^2 to 10^4 s.

71

At intermediate accretion rates, $2 \times 10^{-10} \lesssim \dot{M} \lesssim 10^{-9}$ M$_\odot$ yr^{-1}, a pure helium burst occurs with a duration of order 10 s. In the high accretion regime, $10^{-9} \lesssim \dot{M} \lesssim 2.6 \times 10^{-8}M_\odot$ yr^{-1}, a burst with a duration of tens of seconds may occur in a mixed He/H environment. At even higher or lower accretion rates no bursts are expected to occur. To consider our observations, we first converted accretion rates to fractions of the Eddington limit. The pure helium bursts occur when the accretion rate is in the range 0.014 - 0.070 of the Eddington accretion rate. The ratio of (the upper limit to) the persistent flux and the peak flux during the burst, where the latter is (a lower limit to) the Eddington flux, provides an estimate of the fraction of the Eddington limit at which a source is accreting. This assumes that the emission is isotropic and that the persistent flux in the range 2-28 keV is close to the bolometric flux. With the values listed in Table 6.1 we obtain < 0.002 for SAX J1324.5$-$6313, < 0.009 for SAX J1818.7+1424, < 0.004 for SAX J1828.5$-$1037, < 0.001 for SAX J2224.9+5421, 0.02 for 2S 1711$-$339 at bursts b1-b10, and < 0.002 at burst b11, and 0.004 for 2S 0918$-$549.

We thus note that, with the exception of 2S 1711$-$339 during bursts b1-b10, all sources are in the low accretion regime, and thus according to theory should emit bursts lasting longer than about 100 s. Source 2S 1711$-$339 follows this prediction nicely, showing short ($\simeq$10-20 s) bursts b1-b10 when accretion was in the intermediate range, and a longer ($\simeq$60 s) burst b11 when the accretion had dropped to the low regime. Also the burst from SAX J1828.5$-$1037 lasts about 60 s, pointing towards the low accretion regime. Similarly, the bursts observed by Jonker et al. (2001) and by us for 2S 0918$-$549 are long ($\simeq$150 s), as predicted from the low accretion rate.

In remarkable contrast, the bursts from SAX J1324.5$-$6313, SAX J1818.7 +1424 and SAX J2224.9+5421 are all short ($\simeq$10-20 s), even though these systems appear to be in the low accretion regime. Can it be that the true accretion rate is higher than we estimate? One possibility is that the emission is anisotropic. However, to our knowledge no indication has been found for anisotropies in other burst systems. A second possibility would be that most of the persistent flux is outside the observed 2-28 keV range. However, we estimate that more than 50% of the persistent flux is in this range. We therefore consider it unlikely that these effects are sufficient to bring especially SAX J1324.5$-$6313 and SAX J2224.9+5421 to the intermediate accretion regime.

A third possibility is that the accretion is limited to a small area of the neutron star, e.g. a ring connected with the accretion disk (Popham & Sunyaev 2001). This enhances the local accretion rate, which is the parameter determining the properties of the bursts (as discussed by Bildsten 2000). This would

imply that the accreting surfaces in SAX J1324.5−6313 and SAX J2224.9+5421 are less than about 15% and 8% of the surface of the neutron star, respectively. This possibility cannot be excluded *a priori*, but raises the interesting question why the accreting surface areas would be so different between bursters – the rotation period of the neutron star could affect the area over which the accreted matter spreads out, for example.

A fourth possibility is that the persistent flux at the time of the burst is not representative of the time-averaged flux in the months before the burst. In transients like e.g. Aql X-1, Cen X-4, XTE J1709−267 and SAX J1750.8−2900, X-ray bursts were detected during the decline of the outburst, at times when the persistent flux, easily detectable at $L_{\mathrm{x}} \gtrsim 10^{36}$ erg s^{-1}, was at an accretion rate of ordinary burst sources (Matsuoka et al. 1980, Koyama et al. 1981, Cocchi et al. 1998, Natalucci et al. 1999). Also the transient SAX J1808.4−3658 showed a ∼100 s long burst 30 days after the peak of an outburst, when the persistent flux had declined below the detection limit of the Wide Field Cameras, $< 10^{36}$ erg s^{-1} (in 't Zand et al. 2001). However, the RXTE/ASM lightcurves show no detection of SAX J1324.5−6313 and SAX J1818.7+1424, at an upper-limit of $\simeq 10^{36}$ erg s^{-1} making a transient outburst very unlikely.

One might propose the possibility that these systems are old and the companion has only pure helium left. In this case only helium bursts can occur independent of the accretion rate. However, calculations on bursts due to pure helium accretion show that at low accretion rates the burst duration increases to ∼ 100 s (Bildsten 1995).

For pure helium bursts, the energy released during the burst due to nuclear fusion is about 1% of the accretion energy released when the same matter accreted onto the neutron star before the burst (see e.g. Lewin et al. 1993). From the observed burst fluences and the (upper limits to) the persistent flux, we can therefore derive (lower limits to) the interval to the previous burst. The computed waiting time of 16 d is sufficiently long to explain that only one burst was detected for 2S 0918−549, whose WFC exposure times totalled for all observations between August 1996 and December 2001 is about 62 d. For SAX J1324.5−6313, SAX J1818.7+1424, SAX J1828.5−1037 and SAX J2224.9 +5421 the total observation times between August 1996 and December 2001 are about 58 d, 30 d, 25 d and 65 d, respectively. For these sources the waiting times are > 3.7 d, > 0.6 d, > 2.6 d and > 2.2 d. The chance probability of observing at most one burst for these sources is then 0.07% or (much) less. The fact that only one burst was observed for each system suggests that the persistent emission levels are much lower than the upper-limits derived.

73

Table 6.3: Overview of the burst sources at low persistent emission as observed with the Wide Field Cameras.

Name	l_{II}	b_{II}	$F_{\mathrm{peak}}/F_{\mathrm{pers}}$	τ (s)
SAX J1324.5-6313	306°.64	−0°.59	>540	6.0
RX J171824.2-402934[a]	347°.28	−1°.65	>90	47.5
GRS 1741.9-2853[b]	359°.96	0°.12	>130	8.8
			>180	11.0
			>100	16.0
SAX J1752.4-3138[c]	358°.44	−2°.64	>120	21.9
SAX J1753.5-2349[d]	5°.30	1°.10	>180	8.9
SAX J1806.5-2215[d]	8°.15	−0°.71	>200	4.0
			>210	9.0
SAX J1828.5−1037	20°.88	+0°.18	>226	11.2
SAX J1818.7+1424	42°.32	13°.65	>110	4.5
SAX J2224.9+5421	102°.56	−2°.61	>940	2.6

[a] Kaptein et al. (2000); [b] Cocchi et al. (1999).
[c] Cocchi et al. (2001); [d] in 't Zand et al. (1998).

6.4.2   Low persistent emission bursters

Gotthelf & Kulkarni (1997) discovered a burst from a low-luminosity source in the globular cluster M 28, with a peak luminosity that is only 0.02% of the Eddington limit. This low peak flux discriminates it from the bursters discussed by Cocchi et al. (2001) and in this paper, that have fluxes close to the Eddington limit: if their peak fluxes were as low as that of the M 28 source, they would be a local population near the Sun, which is clearly incompatible with their galactic length and latitude distributions.

As discussed by Cocchi et al. (2001), a class of bursters with low persistent emission has emerged in recent years. The four sources discussed in Sect. 3.1 also appear to be member of this class, strenghtening its existence. Whereas most bursters emit their bursts at persistent luminosities $\gtrsim 10^{36}$ erg s^{-1}, most of the members of this new class emit bursts at luminosities below the RXTE/ASM detection-limit of $\simeq 10^{36}$ erg s^{-1}. How much lower is not clear, and we briefly consider three possibilities. One is that the sources are steady in the range 10^{34-35} erg s^{-1}, as suggested for the bursters 1RXS J171824.2−402934 (Kaptein et al. 2000) and SAX J1828.5−1037 (this paper), whose persistent emission lev-
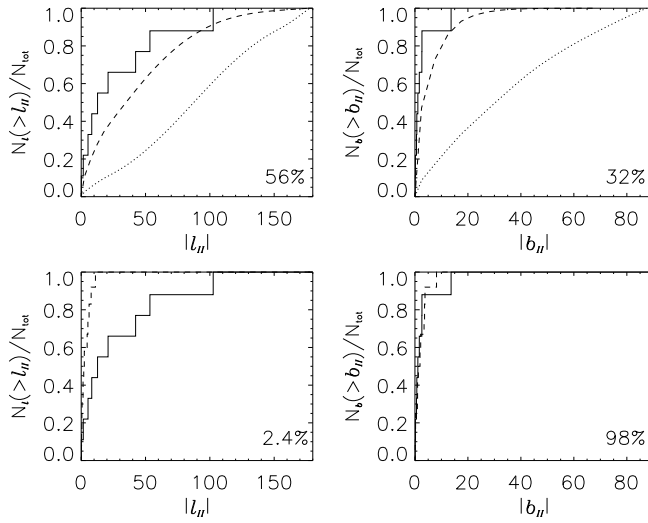
Figure 6.6: The top two panels show the cumulative Galactic longitude l_{II} and latitude b_{II} distributions (solid lines) of the low persistent emission bursters compared to the exponential (Galactic) distribution of the low-mass X-ray binaries weighted with observation times (dashed lines). The probability according to a two-sided Kolmogorov-Smirnov test that they have the same distribution is given in the lower right corners. For comparison we also show an isotropic distribution weighted with observation times (dotted lines). In the bottom two panels the low persistent emission bursters (solid line) are compared to the faint transients (dashed line).

els were detected at this level with ROSAT a few years before the burst. The second possibility is that the sources are steady at the level 10^{32-33} erg s^{-1}, the quiescent level of soft X-ray transients with neutron stars; and the third possibility is that they are usually at this low level, but emit their bursts during or soon after faint ($\lesssim 10^{36}$ erg s^{-1}) outbursts, as suggested by the case of 2S 1711$-$339. More sensitive X-ray observations are required to discriminate between these various possibilities.

However, a first test can be made on the basis of the spatial distributions. In Figure 6.6 we compare the distributions of galactic length and latitude for the bursters with low persistent luminosity – listed in Table 6.3 – with those of

the low-mass X-ray binaries. For the latter we use exponential distributions in galactic longitude and latitude with scale angles of $45°$ and $8°3$, respectively, as determined by van Paradijs & White (1995). Kolmogorov-Smirnov tests indicate that the bursters with low persistent luminosity may indeed be drawn from the distribution of low-mass X-ray binaries.

A new class of faint transients has been discovered with BeppoSAX: transients whose outbursts are rather fainter (peaking below 10^{37} erg s^{-1}) and often also shorter (lasting less than a month) than the outbursts of the ordinary soft X-ray transients which reach the Eddington limit and may last months (Heise et al. 2000). It is tempting to assume that the bursters at low persistent emission are an extension of this class of faint transients. Remarkably, this new class of faint transients is more concentrated towards the galactic center than the ordinary low-mass X-ray binaries (In 't Zand 2001). A Kolmogorov-Smirnov test shows that the galactic longitudes of bursters with low persistent emission cannot be drawn from the longitude distribution of the faint transients, as illustrated in Fig. 6.6.

We conclude that the bursters at low persistent emission are probably not from the same class as the faint transients, which makes the transient explanation even more unlikely.

References

Bildsten, L. 1995, ApJ 438, 852

Bildsten, L. 2000, in S. Holt, W. Zhang (eds.), Cosmic explosions, AIP, p. E65

Boella, G., Butler, R., Perola, G., et al. 1997, A&AS 122, 299

Carpenter, G.F., Eyles, C.J., Skinner, G.K., Wilson, A.M., & Willmore, A.P. 1977, MNRAS 179, 27

Chevalier, C., & Ilovaisky, S.A. 1987, A&A 172, 167

Cocchi, M., Bazzano, A., Natalucci, L., et al. 1998, ApJ 508, L163

Cocchi, M., Bazzano, A., Natalucci, L., et al. 1999, A&A 346, L45

Cocchi, M., Bazzano, A., Natalucci, L., et al. 2001, A&A 378, L71

Christian, D.J., & Swank, J.H. 1997, ApJS 109, 177

Dickey, J.M., & Lockman, F.J. 1990, ARA&A 28, 215

ESA, 1997, The Hipparcos and Tycho Catalogues, ESA SP-1200

Fujimoto, M.Y, Sztajno, M., Lewin, W.H.G., & van Paradijs, J. 1987, ApJ 319, 902

Gotthelf, E., & Kulkarni, S. 1997, ApJ 490, L161

Greiner, J., Duerbeck, H.W., & Gershberg, R.E., eds. 1994, Flares and Flashes (Berlin: Springer)

Haisch, B., & Strong, K.T. 1991, ARA&A 29, 275

Heise, J. in 't Zand, J.J.M., & Kuulkers, E. 2000, HEAD 32, 28.03

Heise, J., In 't Zand, J.J.M., Kippen, R.M., & Woods, P.M., 2001, in E. Costa, F. Frontera, J. Hjorth (eds.), Gamma-Ray Bursts in the Afterglow Era, ESO Astrophys. Symp. Ser., p. 16

in 't Zand, J.J.M., Heise, J., Muller, J.M., et al 1998, Nucl. Phys. B 69/1-3, 228

in 't Zand, J.J.M., 2001, in A. Gimenez, V. Reglero, & C. Winkler (eds.), Exploring the gamma-ray universe, ESA Pub. Div., p. 463

in 't Zand, J.J.M., Cornelisse, R., Kuulkers, K., et al 2001, A&A 372, 916

Jager, R., Mels, W., Brinkman, A., et al. 1997, A&AS 125, 557

Jonker, P. G., van der Klis, M., Homan, J., et al. 2001, ApJ 553, 335

Kaptein, R.G., in 't Zand, J.J.M., Kuulkers, E., et al. 2000, A&A 358, L71

Koyama, K., Inoue, H., Makishima, K., et al. 1981, ApJ 247, L27

Kuulkers, E., Homan, J., van der Klis, M., et al. 2002, A&A 382, 947

Levine, A.M., Bradt, H., Cui, W., et al. 1996, ApJ 469, L33

Lewin, W., van Paradijs, J., & Taam, R. 1993, Space Sci. Rev. 62, 223

Makishima, K., Ohashi, T., Inoue, H., et al. 1981, ApJ 247, L23

Matsuoka, M., Inoue, H., Koyama, K., et al. 1980, ApJ 240, L137

Natalucci, L., Cornelisse, R., Bazzano, A., et al. 1999, ApJ 523, L45

van Paradijs, J., Sztajno, M., Lewin, W.H.G., et al. 1986, MNRAS 221, 617

van Paradijs, J., & White, N. 1995, ApJ 447, 33

Popham, R., & Sunyaev, R. 2001, ApJ 547, 355

Predehl, P., & Schmitt, J.H.M.M. 1995, A&A 293, 889

Verbunt, F., Bunk, W., Hasinger, G., & Johnston, H.M. 1995, A&A 300, 732

Voges, W., Aschenbach, B., Boller, T., et al. 1999, A&A 349, 389

Warwick, R.S., Norton, A.J., Turner, M.J.L., Watson, M.G., & Willingale, R. 1988, MNRAS 232, 551

Chapter 7

Chandra follow-up of bursters with low persistent emission

R. Cornelisse, F. Verbunt, J.J.M. in 't Zand, E. Kuulkers and J. Heise

Abstract– We report on Chandra ACIS-S observations of five type I X-ray bursters with low persistent emission: SAX J1324.5−6313, SAX J1752.3−3128, SAX J1753.5−2349, SAX J1806.5−2215, and SAX J1818.7+1424. We designate candidate persistent sources for four X-ray bursters. All candidates are detected at a persistent luminosity level of $10^{32-33}\,\mathrm{erg\,s^{-1}}$, comparable to soft X-ray transients in quiescence. From the number of bursters with low persistent emission detected so far with the Wide Field Cameras, we estimate a total of such sources in our Galaxy between 30 and 4000.

7.1 Introduction

Many low-mass X-ray binaries show bursts of X-rays which are characterized by a rapid rise and exponential decay, and by a black body spectrum with spectral softening during the decay i.e. the emitter cools. Such type I X-ray bursts are interpreted as thermonuclear flashes on surfaces of neutron stars, and

thus effectively identify the emitting source as a neutron star as opposed to a black hole. The theory of these bursts predicts a relation between the accretion rate onto the neutron star, as measured by the persistent X-ray luminosity, and the properties of the X-ray burst. Briefly, for very low and very high accretion rates, no X-ray bursts are expected, because thermonuclear fusion is steady (Fujimoto et al. 1987). At intermediate accretion rates, hydrogen/helium fusion occurs sporadically in bursts, and the burst frequency is a function of the accretion rate per square meter on the neutron star. Because the effectively accreting area of the neutron star is also a function of the accretion rate, the burst frequency is a non-monotonic function of the persistent X-ray luminosity. Recent reviews of burst theory are given by Bildsten (1998, 2000).

Low-mass X-ray binaries are discovered as either persistent sources or transient sources. The transient sources with neutron stars show outbursts lasting for weeks, sometimes up to years, at luminosities above 10^{36} erg s^{-1}. During their quiescent state their luminosity drops to a level of 10^{32-33} erg s^{-1} (e.g. Campana et al. 1998), and the time averaged luminosities are $\lesssim 10^{36}$ erg s^{-1} (e.g. White et al. 1984). Most bursts are emitted by systems at luminosities $\gtrsim 10^{36}$ erg s^{-1}, e.g. the transients Aql X-1 and Cen X-4 emitted X-ray bursts when they were in outburst (Koyama et al. 1981, Matsuoka et al. 1980).

The Wide Field Cameras (WFC) on board the Italian-Dutch Satellite BeppoSAX discovered sporadic type I bursts from nine previously unknown burst sources, which had persistent X-ray fluxes below the WFC detection limit of a few times 10^{-10} erg cm^{-2}s^{-1} (2-28 keV). At 8 kpc, the distance of the Galactic center, these flux limits correspond to luminosities of $\sim 10^{36}$ erg s^{-1}. Four of the nine previously unknown burst sources were detected with other instruments at fluxes well below the WFC detection limit (see Table 7.1). The five other bursters are listed in Table 7.2. In this article we present Chandra observations which we obtained in order to determine the flux levels of these five burst sources.

The persistent luminosities of the nine previously unknown burst sources are (possibly far) below 10^{36} erg s^{-1}, i.e. below the level X-ray bursts are usually observed. This is the reason why Cocchi et al. (2001) suggested that these sources are members of a new class of bursters with low persistent emission (see also Cornelisse et al. 2002).

The nine sources can be used to explore the low end of the relation between luminosity and burst properties. The long waiting times between type I bursts, compared to brighter burst sources, plus the low persistent emission level make these sources difficult to discover. Its large field of view makes the WFC an efficient instrument for the detection of such rare events.

Table 7.1: Overview of the detection of four of the low persistent emission bursters. For each source we list the instrument which detected the source, the date of observation and the persistent flux in $10^{-11}\,\mathrm{erg\,cm^{-2}s^{-1}}$ plus passband in keV. References: a. Kaptein et al. 2000, b. Cocchi et al. 1999, c. Pavlinsky et al. 1994, d. Cornelisse et al. 2002, f. Antonelli et al. 1999, g. in 't Zand et al. 2002 (in preparation).

source	instrument	date	F	range	ref
1RXS J1718.4−4029	ROSAT/P	1990	1	2-10	a
1RXS J1718.4−4029	ROSAT/H	1994	0.4	2-10	a
GRS 1741.9−2853	GRANAT	1990	19	4-30	b,c
SAX J1828.5−1037	ROSAT/P	1993	0.19	0.5-2.5	d
SAX J2224.9+5421[e]	SAX/NFI	1999	0.013	2-10	f,g

[e] Observation a few hours after burst.

In Sect. 2 we describe the Chandra observations and data analysis and in Sect. 3 we discuss which of the detected sources are the most likely candidates for each burster. In Sect. 4 we briefly present unpublished but relevant observations with other instruments of SAX J1806.5−2215 and GRS 1741.9−2853. In Sect. 5 we discuss the implications for the class of low persistent emission bursters.

7.2 Observations and data analysis

With the Chandra satellite (Weisskopf 1988) we observed the WFC error circles of the five burst sources without persistent emission listed in Table 7.2. For each field we used the ACIS-S3 detector in imaging mode. We analyzed the level 2 FITS data provided with the standard data products using the Chandra Interactive Analysis of Observations Software (CIAO) version 2.1.3. None of the five observations showed periods of high background and we used all data. For source detection we used a wavelet-based algorithm (Freeman et al. 2002), only taking into account the events between 0.5 and 7 keV. We set the significance threshold for the source detection at 10^{-6}, i.e. giving at most one spurious source on the ACIS-S3 detector per observation. In the dithered detector image we checked each source region for the presence of flickering pixels. If a pixel detected more than one photon from a source during the whole observation we

Table 7.2: Observation log of the bursters at low persistent emission. For each source we list the start and exposure time of the Chandra observation, the WFC error radius (99% confidence), the absorption column (N_{H}, in 10^{21} atoms cm^{-2}) as found by interpolating the HI maps of Dickey & Lockman (1990), and the upper limit to the distance (d_{u}, in kpc) derived from the burst peak flux. For comparison with a model spectrum of a neutron star H-atmosphere plus power-law we also list for this model the absorbed flux (F, 0.5-7 keV, in 10^{-12} erg cm^{-2}s^{-1}) corresponding to 1 Chandra count per second, and the absorbed softness-ratio (SR) of the soft count rate (0.5-2 keV) to the total count rate (0.5-7 keV). References: a. Cornelisse et al. (2002), b. Cocchi et al. (2001), c. in 't Zand et al. (1998), d. this paper

source	start date	exp.	δ	N_{H}	d_{u}	F	SR	ref
(SAX J)	(MJD)	(s)	($'$)					
1324.5−6313	52162.39	5101	1.8	15	6.2	1.0	0.69	a
1752.3−3128	52174.20	4717	2.9	5.6	9.2	2.5	0.82	b
1753.5−2349	52187.83	5171	2.5	8.3	8.8	1.6	0.76	c
1806.5−2215	52206.39	4758	2.9	12	8.0	1.5	0.68	d
1818.7+1424	52092.17	4758	2.9	1.0	9.4	5.5	0.94	a

marked this as a flickering pixel; given the small number of photons in each source (see Table 7.3) we think that the chance probability that this happens is too small ($\simeq 10^{-5}$) to be coincidence. In Table 7.3 we have noted the source which is affected by a flickering pixel with an f. The count rate and position are not reliable for this source. The wavelet method also gives an estimate of the background. We consider all sources detected with a significance of more than 3σ. Only for the observation of SAX J1753.5-2349 no sources above 3σ were detected; here we derive an upper limit of 5 counts.

7.3 Selecting candidate burst sources

In Table 7.3 we list the detected sources on the whole S3-chip for each observation, because there is still a 1% possibility that the source is outside the error circle. In all four observations there is more than one source inside or close to the WFC error circles. Based on the photon count rate, there are no extreme examples of sources which would qualify them as particularly likely candidates.

Table 7.3: For each source detected on the S3-chip we list the position, and the counts in the total (0.5-7 keV), and the soft (0.5-2 keV) band as well as the detection significance, σ. A conservative estimate for the error in the positions is $0''.7$. In the second column we indicate – where appropriate – reasons to reject the source as the burster candidate: o. position outside the WFC error circle, *. optical counterpart too bright, s. X-ray spectrum too hard (for discussion see text). In the second column we have also indicated the sources which are disturbed by a flickering pixel with f.

#	note	RA (J2000)	Dec (J2000)	counts	soft	σ
SAX J1324.5−6313						
A		$13^\mathrm{h}24^\mathrm{m}30.2^\mathrm{s}$	$-63°12'41''$	5.9 ± 2.4	5.9 ± 2.4	3.1
B	s	$13^\mathrm{h}24^\mathrm{m}30.3^\mathrm{s}$	$-63°13'50''$	77.9 ± 8.9	21.7 ± 4.7	33
C		$13^\mathrm{h}24^\mathrm{m}38.0^\mathrm{s}$	$-63°12'26''$	6.8 ± 2.6	6.8 ± 2.6	3.4
D		$13^\mathrm{h}24^\mathrm{m}38.3^\mathrm{s}$	$-63°13'28''$	19.5 ± 4.5	19.5 ± 4.5	9.2
E		$13^\mathrm{h}24^\mathrm{m}39.4^\mathrm{s}$	$-63°13'34''$	5.9 ± 2.4	5.9 ± 2.4	3.1
SAX J1752.3−3128						
A		$17^\mathrm{h}52^\mathrm{m}16.7^\mathrm{s}$	$-31°39'46''$	10.7 ± 3.3	10.7 ± 3.3	5.3
B		$17^\mathrm{h}52^\mathrm{m}30.6^\mathrm{s}$	$-31°38'58''$	6.7 ± 2.6	4.8 ± 2.2	3.3
C	o	$17^\mathrm{h}52^\mathrm{m}39.4^\mathrm{s}$	$-31°37'56''$	36.5 ± 6.2	35.9 ± 6.1	13
SAX J1806.5−2215						
A	o	$18^\mathrm{h}06^\mathrm{m}18.1^\mathrm{s}$	$-22°15'39''$	13.7 ± 3.9	2.8 ± 1.7	5.7
B	o	$18^\mathrm{h}06^\mathrm{m}18.5^\mathrm{s}$	$-22°17'24''$	48.4 ± 7.1	43.7 ± 6.7	19
C	o	$18^\mathrm{h}06^\mathrm{m}19.9^\mathrm{s}$	$-22°18'03''$	7.9 ± 2.8	1.9 ± 1.4	4.1
D		$18^\mathrm{h}06^\mathrm{m}31.7^\mathrm{s}$	$-22°13'19''$	9.0 ± 3.2	5.5 ± 2.4	3.9
E	*	$18^\mathrm{h}06^\mathrm{m}35.8^\mathrm{s}$	$-22°15'01''$	10.5 ± 3.3	9.8 ± 3.2	5.0
F	s	$18^\mathrm{h}06^\mathrm{m}36.8^\mathrm{s}$	$-22°15'26''$	14.9 ± 3.9	< 0.66	7.7
G	f	$18^\mathrm{h}06^\mathrm{m}37.4^\mathrm{s}$	$-22°17'22''$	7.9 ± 2.8	6.9 ± 2.6	4.0
H		$18^\mathrm{h}06^\mathrm{m}43.6^\mathrm{s}$	$-22°16'06''$	8.7 ± 3.0	8.7 ± 3.0	4.3
I	o	$18^\mathrm{h}06^\mathrm{m}43.8^\mathrm{s}$	$-22°18'42''$	13.8 ± 3.7	3.0 ± 1.7	6.9
SAX J1818.7+1424						
A	o	$18^\mathrm{h}18^\mathrm{m}32.1^\mathrm{s}$	$+14°22'09''$	45.3 ± 6.9	45.3 ± 6.8	21
B	o	$18^\mathrm{h}18^\mathrm{m}34.3^\mathrm{s}$	$+14°26'29''$	6.8 ± 2.6	4.0 ± 2.0	3.5
C	*	$18^\mathrm{h}18^\mathrm{m}35.6^\mathrm{s}$	$+14°22'32''$	9.9 ± 3.2	9.9 ± 3.2	5.2
D	*	$18^\mathrm{h}18^\mathrm{m}37.6^\mathrm{s}$	$+14°22'44''$	36.6 ± 6.1	36.6 ± 6.1	18
E		$18^\mathrm{h}18^\mathrm{m}37.8^\mathrm{s}$	$+14°22'06''$	7.0 ± 2.6	6.0 ± 2.4	3.7
F		$18^\mathrm{h}18^\mathrm{m}38.6^\mathrm{s}$	$+14°22'59''$	27.8 ± 5.3	21.9 ± 4.7	14
G		$18^\mathrm{h}18^\mathrm{m}48.3^\mathrm{s}$	$+14°22'43''$	9.9 ± 3.2	9.9 ± 3.2	5.1
H	o	$18^\mathrm{h}18^\mathrm{m}55.8^\mathrm{s}$	$+14°27'38''$	10.2 ± 3.5	7.8 ± 3.0	4.0

This could very well mean that all detected sources are spurious and none are the bursters, also given that no source was detected during the observation of SAX J1753.5−2349.

Thus, we resort to several criteria to select viable burster candidates. We start with excluding all sources outside the WFC error circles. In Fig. 7.1 we see that several X-ray sources are close to optical sources from the Sloan Digitized Sky Survey. We have listed the closest star from the USNO catalogue within $4''$ of the X-ray sources in Table 7.4. Given the small number of counts we estimate an error in the X-ray position of 1 pixel, i.e. $0\!''\!.5$, and a systematic error of another pixel. This gives a total error of $0\!''\!.7$. The positional error for the sources in the USNO Digitized Sky Survey is negligible in comparison. For each source in Table 7.4 we count the number of stars from the USNO catalogue inside the WFC error-circle and brighter than the potential counterpart. On the basis of this number we estimate the chance coincidence as in the following example. In the USNO catalogue the star closest to source D of SAX J1324.5−6313 is at $0\!''\!.83$ (see Table 7.4). We find 24 stars in the USNO catalogue inside the WFC error circle of $1\!'\!.8$ that are brighter than B=17.2 and R=15.3. This gives a chance probability of 0.14% that *one* arbitrarily chosen position falls within one of the 24 error circles of $0\!''\!.83$. The five Chandra sources inside the WFC error circle correspond to five trials, i.e. the chance probability that one or more of these sources are close to a star is 0.71%. In Table 7.4 we have listed the chance probabilities P thus computed for all Chandra sources within $4''$ of an optical star.

Although it is difficult to draw firm conclusions from a posteriori statistics, we think that the optical counterparts with $P < 0.1\%$ are secure. The optical sources located at a distance $\Delta \gtrsim 1''$ from the X-ray position are very likely chance coincidences. This leaves only D of the SAX J1324.5−6313 field as a borderline case, which may or may not be the counterpart. We have indicated the optically identified sources in Table 7.3 with an asterisk.

Assuming that the V magnitudes are between the B and R magnitudes given in the USNO Digitized Sky Survey, we find that the X-ray to optical flux ratios of these stars are well within the range of the coronal emission from normal nearby stars found in the ROSAT All Sky Survey (Hünsch et al. 1999; here we use that for coronal sources with interstellar absorption columns up to 10^{21} atoms cm^{-2} the ROSAT/PSPC count rate is typically 1/3 to 1/4 of the Chandra count rate). Soft X-ray transients with neutron stars have X-ray to optical flux ratios in quiescence several orders of magnitude higher than ordinary stars (e.g. Fig. 5 in Pooley et al. 2002a). Thus we conclude that the optically identified Chandra sources indicated in Table 7.3 are too bright in the optical for them to

Table 7.4: USNO Digitized Sky Survey sources close to detected Chandra detections. For each source we give the position, B and R magnitudes, the distance (Δ) from the X-ray source, and the chance probability P that the optical source is in the Chandra error-circle.

#	RA	Dec	B	R	Δ ($''$)	P (%)
D	$13^{\rm h}24^{\rm m}38.284^{\rm s}$	$-63°13'27.16''$	17.2	15.3	0.83	0.7
A	$17^{\rm h}52^{\rm m}16.723^{\rm s}$	$-31°39'44.24''$	19.5	17.3	1.78	5.7
B	$17^{\rm h}52^{\rm m}30.537^{\rm s}$	$-31°38'58.88''$	19.0	17.3	1.19	1.9
D	$18^{\rm h}06^{\rm m}31.589^{\rm s}$	$-22°13'18.94''$	15.7	13.1	3.32	1.1
E	$18^{\rm h}06^{\rm m}35.819^{\rm s}$	$-22°15'00.87''$	16.1	14.8	0.28	0.0
H	$18^{\rm h}06^{\rm m}43.734^{\rm s}$	$-22°16'06.08''$	19.8	17.0	1.86	6.3
C	$18^{\rm h}18^{\rm m}35.593^{\rm s}$	$+14°22'32.67''$	-	11.1	0.66	0.0
D[a]	$18^{\rm h}18^{\rm m}37.634^{\rm s}$	$+14°22'44.44''$	8.6	7.4	0.0	0.0

[a] star HD 168344 with V=7.6

be the bursters.

Due to the small number of counts in each source, it is not possible to constrain the spectral shape of the X-ray emission. The most commonly used models to describe the quiescent emission of neutron star X-ray transients are 0.3 keV black body radiation, 0.3 keV Raymond-Smith emission, power-law emission with a slope of $\Gamma \sim 3$ or emission from a hydrogen atmosphere (e.g Campana et al. 1998). Added to these models is a hard energy tail detected at high energies (e.g. Campana et al. 1998, Asai et al. 1996). Here we assume emission from a hydrogen atmosphere of a neutron star (Zavlin et al. 1996) plus a power-law, as was, for example, found for the quiescent emission of the neutron star X-ray transients Cen X-4 and Aql X-1 (Rutledge et al. 2001a, 2001b). We estimate the number of photons below 2 keV using the average parameters found for Cen X-4 and Aql X-1, i.e. a power-law photon-index Γ=1.0, neutron star radius R_∞=16 km, a neutron star temperature kT=100 eV, and a ratio of the unabsorbed flux (0.1-7 keV) expected from the H-atmosphere to the power-law component of 5:1. For such a spectrum we compute the flux for a source with 1 Chandra count per second, and the ratio of counts at energies between 0.5 and 2 keV to the total count rate. The resulting numbers are listed in Table 7.2. By comparison with the observed soft-to-total count ratios listed in Table 7.3 we can exclude sources which are harder than expected for soft X-ray

transients in quiescence. We do not reject sources with soft spectra, because there is evidence that the photon-index of the power-law component could be higher than we have assumed (Campana et al. 1998). The two sources which are excluded in this way are indicated in Table 7.3 with s. Unacceptably high column densities are needed ($\simeq 10^{23}$ atoms cm^{-2}) to account for the lack of soft photons due to absorption (for source F of SAX J1806.5$-$2215 we do not detect anything below 2 keV). The fluxes do not significantly change if we assume the other spectral models or change the temperature and radius of the neutron star atmosphere model.

For all sources the distribution of the arrival times of the photons is compatible with a constant flux. Given the small number of photons for each source the limits on variability are not very constraining, but we can exclude that the flux measured is due to a flare lasting shorter than the exposure time.

Taking all these criteria into account we conclude that we have four candidate counterparts left for SAX J1324.5$-$6313 (source A, C, D and E), two for SAX J1752.3$-$3128 (A and B), two for SAX J1806.5$-$2215 (D and H), and three for SAX J1818.7+1424 (E, F and G). For SAX J1753.5$-$2349 we have no candidate.

7.4   SAX J1806.5$-$2215 and GRS 1741.9$-$2853

In 't Zand et al. (1998) reported the detection of two X-ray bursts from SAX J1806.5$-$2215, and showed the analysis of the first burst. We take the opportunity of the present paper to report the detection of two additional type I bursts from SAX J1806.5$-$2215 during WFC observations on MJD 50537.91 and MJD 50732.90. No persistent emission is observed for this source in any WFC observation. The first and strongest burst (on MJD 50325.88) has a duration of $\simeq$150 s, all other bursts last $\simeq$20 s. The observed spectra can be well described by an absorbed black body model with temperatures between 1.7 and 2.2 keV. The unabsorbed bolometric peak flux of the strongest burst is $(2.6 \pm 1.2) \times 10^{-8}$ erg cm^{-2}s^{-1}. This gives an upper-limit on the distance of 8.0 kpc and neutron star radii between 4.8 and 7.0 km, assuming that the peak flux is below the Eddington limit of L_{Edd}=2×10^{38} erg s^{-1}. The waiting times between the four bursts are 41, 171 and 195 days, respectively.

Recently the ASM lightcurve of SAX J1806.5$-$2215 became available. It shows a faint but clear detection between March 1996 and October 1997. This coincides with the same period as the occurence of the four X-ray bursts observed with the WFC. The maximum persistent flux was $\simeq 2 \times 10^{-10}$ erg cm^{-2}s^{-1} (2-10
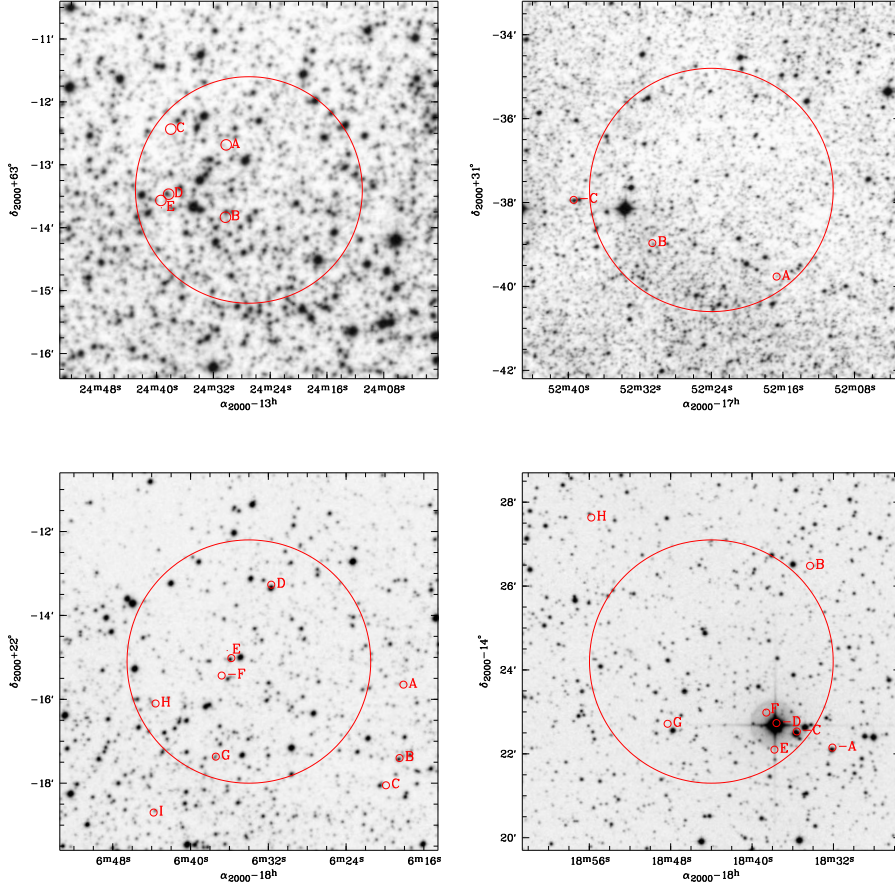
Figure 7.1: Sources detected inside or close to the WFC error circles for SAX J1324.5−6313, SAX J1752.3−3128, SAX J1806.5−2215, and SAX J1818.7+1424, respectively. All detections are superposed on an image from the Digitized Sky Survey. The large circles indicate the WFC error circles. The error circles of all sources are increased to 5″ for easier reference.

keV) , and slowly decreased over time. This is comparable to the upper-limit derived during the WFC observations. Assuming the distance derived above, this corresponds to a luminosity of $\simeq 2 \times 10^{36}$ erg s^{-1}.

GRS 1741.9−2853 was in the field of view of a 47.2 ks ROSAT/PSPC pointed observation of the Galactic center region obtained on March 2–9, 1992. It is not detected, and we determine an upper-limit of 0.0003 cts s^{-1} (channels 50–240), corresponding to an unabsorbed luminosity in the 0.5 to 2.5 keV range of 3×10^{34} erg s^{-1} at the distance of 7.2 kpc, for an assumed power-law spectrum with photon index 1 absorbed by a column $N_H = 10^{23}$ atoms cm^{-2} (see Cocchi et al. 1999). This proves that GRS 1741.9−2853 is a burster with low persistent emission.

7.5 Discussion

Three of the nine burst sources with low persistent emission discovered with the WFC were observed during ROSAT observations at luminosities of $\simeq 10^{34-35}$ erg s^{-1} a few years prior to the X-ray burst (Kaptein et al. 2000; Cornelisse et al. 2002; this paper). If the five burst sources of Table 7.2 had similar luminosities and spectra, their countrate with Chandra would be several orders of magnitude higher than the countrates of the sources listed in Table 7.3. Instead, the luminosities of the burst sources are at $\simeq 10^{33}$ erg s^{-1}, comparable to the BeppoSAX/NFI observations of SAX J2224.9+5421 (Antonelli et al. 1999; in 't Zand 2002, in preparation) and in the range of quiescent soft X-ray transients with neutron stars (e.g. Campana et al. 1998).

With the interstellar hydrogen column and upper limits to the distances listed in Table 7.2 and the spectrum described in Sect. 3, we compute the unabsorbed flux and upper limits to the luminosities between 0.5 and 7.0 keV. For the brightest candidate counterparts of SAX J1324.5−6313, SAX J1752.3−3128, SAX J1806.5−2215 and SAX J1818.7+1424 we obtain upper limits to the unabsorbed persistent luminosity of 4×10^{32}, 3×10^{32}, 2×10^{32} and 4×10^{32} erg s^{-1}, respectively. From the upper-limit derived from the observation of SAX J1753.5 −2349 we get a luminosity of $< 4 \times 10^{32}$ erg s^{-1} (0.5-7 keV). These luminosities are indeed in the range expected for quiescent soft X-transients with a neutron star.

Because our Chandra observations give more than one possible counterpart, several possible counterparts must be chance coincidences. This is in agreement with known $\log N - \log S$ distributions, which predict $\simeq 5$ sources in the field of view (see e.g. Rosati et al. 2002). This raises the question whether *all*

Chandra sources are chance coincidences, i.e. whether we have not detected the actual counterparts for the bursters. Given that these systems are neutron star low mass X-ray binaries, we compare them to known other systems, i.e. the soft X-ray transients in quiescence. The lowest X-ray luminosities detected for quiescent soft X-ray transients are $\sim 10^{32}$ erg s^{-1} (e.g. Cen X-4, Campana et al. 1998). This is around the detection limit for the Chandra observations discussed in this paper. We therefore consider it possible that we actually *have* detected the persistent flux of the bursters, and that they are soft X-ray transients in quiescence, for which no outburst has as yet been detected. If so, this implies that their actual distances are not much less than the upper limits listed in Table 7.2.

The persistent luminosities of the bursters observed with Chandra is well below the limit set with the WFC observations. This means that we cannot exclude that the persistent luminosity during the WFC observations was ~10-100 times higher than detected with Chandra, and that it was this higher flux level which triggered the burst. The detections with ROSAT of 1RXS J171824.2−402934 and SAX J1828.5−1037, and of GRS 1741.9−2853 with GRANAT combined with non-detections at other epochs, show that the persistent flux level of these sources is variable.

The energy released during a burst due to nuclear fusion is about 1% of the accretion energy of the matter accreted onto the neutron star (see e.g. Lewin et al. 1993). Dividing the fluence of the bursts detected with the WFC by 1% of the persistent emission detected by Chandra we estimate burst intervals of ~10 years. If only 1/6th of the persistent flux is due to accretion, the remainder being due to the cooling of the neutron star (i.e. if only the power-law component is due to accretion, see Sect. 3) the estimated burst intervals rise to ~60 years. It is also suggested that the power-law component during quiescence is not due to accretion (see e.g. Campana et al. 1998), and this means that the waiting time derived above is an under-limit. This explains why these events are so rare, and why we have only seen one burst for most of these sources.

This raises the question how many of these burst sources with low persistent emission exist in our Galaxy. With the WFC the Galactic Center region is observed every half year since 1996, for a total observation time of 5.5×10^6 s up to end 2001. If we assume the Galactic distribution of low-mass X-ray binaries derived by van Paradijs & White (1995), $\simeq 50\%$ of the population is in the field of view ($40° \times 40°$) of the WFC. During all Galactic center observations 5 bursters with low persistent emission have been detected, i.e. SAX J1752.3−3128, SAX J1753.5−2349, SAX J1806.5−2215, 1RXS J171824.2−402934, and GRS 1741.9−2853 (the other four are outside the Galactic center

region). This gives an average waiting time between the detection of these bursters of 1.1×10^6 s. If we also assume that the waiting time between burst of one source is 60 years (1.9×10^9 s) we expect $\simeq 2 \times 10^3$ sources in the Galactic center region, giving 4×10^3 sources in the whole Galaxy. If on the other hand these sources are extensive periods of time at a persistent luminosity of 10^{34} erg s^{-1}, as the detections of SAX J1828.5$-$1037, 1RXS J171824,2$-$402934, and GRS 1741.9$-$2853 suggests, the waiting time drops to 0.5 year (see Table 7.1). This gives a number of 30 sources in our Galaxy. We conclude that the estimates for the total number of X-ray bursters with low persistent fluxes range from 0.5 to 60 times the number of known bursters ($\simeq 70$).

In this respect it is interesting to note that the first Chandra observations of globular clusters indicate that these systems harbour more quiescent soft X-ray transients than bursters with high persistent fluxes. For example, Liller 1, NGC 6440 and NGC 6652 all contain such quiescent sources in addition to the bright source (Homer et al. 2001, Pooley et al. 2002b, Heinke et al. 2001); and 47 Tuc, ω Cen, NGC 5139 and NGC 6397 contain quiescent sources but no bright source (Grindlay et al. 2001a, 2001b, Rutledge et al. 2002, Pooley et al. 2002a). The formation mechanism for low-mass X-ray binaries in globular clusters (tidal capture or exchange encounter; see review by Hut et al. 1992) is different from the formation mechanism in the galactic disk (evolution of a primordial binary). If the ratio of quiescent to bright X-ray bursters depends on the formation mechanism, we do not necessarily expect comparable ratios in the cluster and in the Galactic disk.

If bursts can arise from quiescent systems, we must consider the possibility that a burst from a globular cluster is due to a dim source, rather than to the bright source in it. This would undermine the argument that a burst from a cluster proves that the bright source in it is a neutron star. Nonetheless, we think that the argument holds in all eleven cases where it has been applied so far, as bursts from dim sources are extremely rare. For example, we have detected ~ 2200 X-ray bursts in our WFC observations of the Galactic center region; only five of these are from dim sources. Indeed, bursts from the globular cluster NGC 6440 were detected only when the transient in this cluster was active (in 't Zand et al. 2001).

References

Antonelli, L.A., Gandolfi, G., & Feroci, M. 1999, GCN notice, 445

Bildsten, L. 1998, in Bucheri, J., van Paradijs, J., & Alpar, M.A. (eds.),

The many faces of neutron stars, Kluwer, Dordrecht, p. 419

Bildsten, L. 2000, in Holt, S.S., Zhang, W.W. (eds.), Cosmic explosions, AIP, p. E65

Campana, S., Colpi, M., Mereghetti, S., Stella, L., & Tavani, M. 1998, A&AR 8, 279

Cocchi, M., Bazzano, A., Natalucci, L., et al. 1999, A&A 346, L45

Cocchi, M., Bazzano, A., Natalucci, L., et al. 2001, A&A 378, L37

Cornelisse, R., Verbunt, F., in 't Zand, J.J.M., et al. 2002, A&A 392, 885

Dickey, J.M., & Lockman, F.J. 1990, ARA&A 28, 215

Freeman, P.E., Kashyap, V., Rosner, R., & Lamb, D.Q. 2002, ApJS 138, 185

Fujimoto, M.Y, Sztajno, M., Lewin, W.H.G., & van Paradijs, J. 1987, ApJ 319, 902

Grindlay, J., Heinke, C., Edmonds, P., & Murray, S.S. 2001a, Science 292, 2290

Grindlay, J., Heinke, C., Edmonds, P., Murray, S.S., & Cool, A.M. 2001b, ApJ 563, L53

Heinke, C., Edmonds, P., & Grindlay, J., 2001, ApJ 562, 363

Homer, L., Deutsch, E.W., Anderson, S.F., & Margon, B. 2001, AJ 122, 2627

Hünsch, M., Schmitt, J.H.M.M., Sterzik, M.F., & Voges, W. 1999, A&AS 135, 319

Hut, P., McMillan, S., Goodman, J., et al. 1992, PASP 104, 981

in 't Zand, J.J.M., Heise, J., Muller, J.M., et al 1998, Nucl. Phys. B 69/1-3, 228

in 't Zand, J.J.M., van Kerkwijk, M.H., Pooley, D., et al. 2001, ApJ 563, L41

Kaptein, R.G., in 't Zand, J.J.M., Kuulkers, E., et al. 2000, A&A 358, L71

Koyama, K., Inoue, H., & Makishima, K. 1981, ApJ 247, L27

Lewin, W., van Paradijs, J., & Taam, R. 1993, Space Sci. Rev. 62, 223

Matsuoka M., Inoue, H., Koyama, K., et al. 1980 ApJ 240, L137

Pavlinsky, M.N., Grebenev, S.A., & Sunyaev, R.A. 1994, ApJ 425, 110

Pooley, D., Lewin, W., Homer, L., et al. 2002a, ApJ 569, 405

Pooley, D., Lewin, W., Verbunt, F., et al. 2002b, ApJ 573, 184

Rosati, P., Tozzi, P., Giacconi, R., et al. 2002, ApJ, 566, 667

Rutledge, R.E., Bildsten, L., Brown, E.F., Pavlov, G.G., & Zavlin, V.E. 2001a, ApJ 551, 921

Rutledge, R.E., Bildsten, L., Brown, E.F., Pavlov, G.G., & Zavlin, V.E. 2001b, ApJ 559, 1054

Rutledge, R.E., Bildsten, L., Brown, E., et al. 2002, ApJ 578, 405

van Paradijs, J., & White, N. 1995, ApJ 447, 33L

Weisskopf, M.C. 1988, Space Sci. Rev. 47, 47

White, N.E., Kaluzienski, J.L., & Swank, J.H. 1984, in Woosley, S.E., High

energy transients in astrophysics, AIP, p. 31
Zavlin, V.E., Pavlov, G.G., & Shibanov, Y.A. 1996, A&A 315, 141

Chapter 8

Observations of nine type I X-ray bursters

Six years of BeppoSAX Wide Field Cameras observation

R. Cornelisse, J.J.M. in 't Zand, F. Verbunt, E. Kuulkers, J. Heise, M. Cocchi,
L. Natalucci, A. Bazzano and P. Ubertini

Abstract– We present an overview of BeppoSAX Wide Field Cameras observations of the nine most frequent type I X-ray bursters in the Galactic center region. Six years of observations (from 1996 to 2002) have amounted to 7 Ms of Galactic center observations and the detection of 1823 bursts. The 3 most frequent bursters are GX 354−0 (423 bursts), KS 1731−260 (339) and GS 1826−24 (260). These numbers reflect a unique dataset. We show that all sources have the same global burst behavior when they are at the same luminosity. At the lowest luminosities bursts occur quasi-periodically and the burst rate increases linearly with accretion rate. At $L_{\mathrm{pers}}{=}2{\times}10^{37}$ erg s^{-1} the burst rate drops by a factor of five, corresponding to the transition from, on average, a hydrogen-rich to a pure helium environment for the flashes that are responsible for the bursts. At higher luminosities the bursts recur irregularly and no bursts are observed anymore at the highest luminosities. Our central finding is that most of the trends in bursting behavior are driven by the onset of stable hydrogen burning in the neutron star atmosphere. Furthermore, we notice three new observations which are more difficult to explain with current burst theory: the presence of

short pure-helium bursts at the lowest accretion regimes, the bimodal distribution of peak burst rates, and an accretion rate at which the onset of stable hydrogen burning occurs that is ten times higher than predicted. Finally, we note that our investigation is the first to signal quasi-periodic burst recurrence in KS 1731-260, and a clear inverse proportionality between the frequency of the quasi-periodicity and the persistent flux in GS 1826-24 and KS 1731-260.

8.1 Introduction

Since the discovery of type I bursts by Grindlay & Heise (1975) about 65 other X-ray bursters have been discovered (e.g., in 't Zand 2001). Most of these are concentrated towards the Galactic center, which illustrates their Galactic origin. X-ray bursts are characterized by a fast rise and an exponential decay with durations ranging from seconds to tens of minutes. Their spectrum can best be described by black body radiation with cooling during the decay of the burst. These type I X-ray bursts are due to unstable hydrogen/helium burning in a thin shell on a neutron star surface (see, e.g., the review by Lewin et al. 1993).

By far most of the X-ray bursts are emitted by sources, persistent or transient, with luminosities of 10^{36-37} erg s^{-1}. Sources at higher persistent luminosities also show X-ray bursts (e.g., Kuulkers et al. 2002), but such bursts are less common. At lower luminosities bursts have also been sporadically observed (e.g., Gotthelf & Kulkarni 1997, Cocchi et al. 2001a, Cornelisse et al. 2002).

Assuming that the amount of fuel burnt per burst is roughly the same, one expects that the burst rate increases linearly with accretion rate. However, for most X-ray bursters where it is possible to study this the opposite is observed (van Paradijs et al. 1988a). An example is GX 3+1 (den Hartog et al. 2002). Bildsten (2000) noted that the onset of a burst is governed by the local rather than the global accretion rate (see also Marshall 1982). If the area on the neutron star on which accretion takes place increases rapidly with the global accretion rate, the local accretion rate may actually drop, giving rise to a lower burst rate.

Observations of several sources (e.g., 4U 1705−44, Gottwald et al. 1986a; EXO 0748−676, Gottwald et al. 1986b), show different burst properties at different accretions rates. Fujimoto et al. (1981) predicted this behavior by showing that the composition of the unstable burning shell changes with accretion (see also Bildsten 1998 for a recent overview). Briefly, at the highest accretion rates ($\dot{M} \gtrsim 10^{-9}$ M$_\odot$ yr^{-1}) the helium ignites in an unstable fashion

in a mixed He/H environment, causing bursts with durations of minutes. At the intermediate accretion regime ($10^{-9} \gtrsim \dot{M}/(M_\odot \ \mathrm{yr}^{-1}) \gtrsim 2 \times 10^{-10}$) the helium ignites in a hydrogen-poor environment, causing bursts with durations smaller than 10 s. At the lowest accretion regime ($\dot{M} \lesssim 2 \times 10^{-10} \ M_\odot \ \mathrm{yr}^{-1}$) unstable hydrogen burning triggers a helium flash causing bursts with durations larger than 10 s.

If the accretion rate is stable over long periods of time, periodic burst behavior is expected. It should always take the same amount of time to accrete enough matter to start the unstable burning again. This quasi-periodic burst behavior is observed in several burst sources, for example 4U 1820−30 (Haberl et al. 1987) or 4U 1705−44 (Langmeier et al. 1987), but only for limited periods of time. During other periods the occurrence of bursts appear completely a-periodic. An exception is GS 1826−24 whose bursts are always seen to recur quasi periodically (Ubertini et al. 1999; Cocchi et al. 2001b).

In this paper we describe the burst behavior of the nine most frequent X-ray bursters in the Galactic center region observed with the Wide Field Cameras. All are known X-ray bursters and most of them are persistently bright. We compare these bursters with each other and others. The observations and the search for type I bursts are described in Sect. 2. In Sect. 3 we present the results. We start in Sect. 3.1 with the general properties of the nine burst sources. In Sect. 3.2 we discuss the wait time as a function of persistent emission for the bursters where this is possible. In Sect. 3.3 we compare the exponential decay times of the bursts with the theoretical regimes. Finally in Sect. 4.1 we start with a summary of the observations and compare our results with previous studies and in Sect. 4.2 discuss some implications for burst theory. We also derive some general properties of the population of X-ray bursters.

8.2   Observations and data analysis

The BeppoSAX satellite operated from May 1996 until May 2002 (Boella et al. 1997). During this period the Wide Field Cameras (Jager et al. 1997) onboard the satellite observed the Galactic center region each spring and fall with an average schedule of one day per week. This adds up to 12 Galactic center campaigns with a total net observation time of 7 Ms. The Wide Field Cameras (WFC) are two identical coded mask cameras with a $40° \times 40°$ field of view, a $5'$ angular resolution, 2-28 keV bandpass and 20% spectral resolution(full width at half maximum at 6 keV). The large field of view combined with the good angular resolution makes it an excellent instrument to simultaneously observe

Table 8.1: Overview of the nine most frequent burster sources in the Galactic center region. They are ordered in decreasing number of bursts observed with the WFC. For each source a factor (conv.) in erg/count is derived to convert photon flux to energy flux in 2-28 keV . We also show the net exposure for each individual source and the distance as quoted in the literature. For each distance estimate we assume an error of 30%. The distances are derived from: [1] Galloway et al. 2002, [2] Muno et al. 2000, [3] in 't Zand et al. 1999, [4] Lutovinov et al. 2001, [5] Muno et al. 2001, [6] Gottwald et al. 1989, [7] Augusteijn et al. 1998, [8] Kuulkers & van der Klis 2000, [9] Heasley et al. 2000.

Source	#bursts WFC	exp. time (Ms)	conv. (10^{-8})	d (kpc)	ref.
GX 354$-$0	423	7.4	1.9	5.4	[1]
KS 1731$-$260	339	6.7	1.5	7.0	[2]
GS 1826$-$24	260	6.5	1.9	8.0	[3]
A 1742$-$294	178	7.0	2.2	8.5	[4]
4U 1702$-$429	104	8.9	1.7	6.7	[5]
4U 1705$-$44	66	8.7	1.8	8.9	a
4U 1636$-$536	61	4.7	1.5	5.9	[7]
GX 3+1	61	6.9	1.6	4.5	[8]
4U 1820$-$30	49	7.1	1.6	7.6	[9]

a: distance estimated from [6]

a large fraction (50%) of the low mass X-ray binary (LMXB) population in our Galaxy when pointed at the Galactic center.

Each source in the field of view casts a shadow of the mask pattern on the detector. The detector accumulates the sum of differently shifted mask shadows. By cross-correlating this detector image with the mask pattern a sky image is reconstructed (e.g., in 't Zand 1992). This procedure is supplemented with a dedicated iterative cleaning algorithm (Hammersley et al. 1992). When no new sources are detected in the iterative process the background is estimated from the (supposedly) empty sky image. Lightcurves are constructed in the full bandpass for each detected source with a time resolution of 5 s, which is a trade-off between the average duration of a type I burst ($\simeq 10$ s) and the statistical quality of the data.

These lightcurves are employed in the following manner. We estimate the

average flux and the standard deviation (σ) for each orbit (about 60 minutes of net exposure time). If a bin is at least 4σ above the average flux we mark this as a candidate burst. We estimate that we have only one false peak triggered as a burst per average observation. A marked bin is visually approved as a burst if the shape of the lightcurve around the bin can be described by a fast rise and exponential decay. If needed, this is done at 1 s time resolution. Thus, we detect all bursts with e-folding times $\gtrsim 2$ s and peak fluxes in excess of 0.5 Crab. Bursts with lower peak intensities or shorter e-folding times do exist but we think that this is only a minor fraction compared to the bursts detected in this way (e.g. Cocchi et al. 2001b, van Paradijs et al. 1988b).

We also searched the lightcurve of all photons detected on the whole detector ("detector lightcurve") for X-ray bursts from sources whose persistent flux is below the detection limit of the WFC, and note that this limit becomes worse towards the edge of the field of view. Detector lightcurves are created with a resolution of 1 s. A running average of 50 bins is calculated and if at maximum 24 successive bins are >4% above the average the first bin is labeled as a candidate burst. For all potential new bursts we cross-correlate the detector image again with the coded mask but only for the burst time interval. In this way a genuine point source is identified. The sensitivity in this procedure is at most a factor of 2 worse than in the above mentioned procedure.

8.3   Results

8.3.1   Global burst behavior

A total of 1823 bursts have been detected from 37 sources in the Galactic center region, not counting bursts from the Rapid Burster (MXB 1730−333) and the Bursting Pulsar (GRO J1744−29). For each burst we determined the exponential decay time in the total energy band (2-28 keV), the peak flux and average persistent flux over the observation in WFC cts s^{-1} cm^{-2}. In Table 8.1 we give an overview of the nine most frequent bursters in the Galactic center region. All these sources are known X-ray bursters and have been studied in the past. The number of type I bursts detected with the WFC in other burst sources becomes too small for a meaningful statistical analysis.

In Fig. 8.1 we show RXTE All Sky Monitor (RXTE/ASM; Levine et al. 1996) lightcurves of the sources listed in Table 8.1. Most lightcurves show a smooth variation and no large fluctuations on a timescale of weeks. On the timescale of years a variation by a factor of roughly 50% is often present in these sources, and
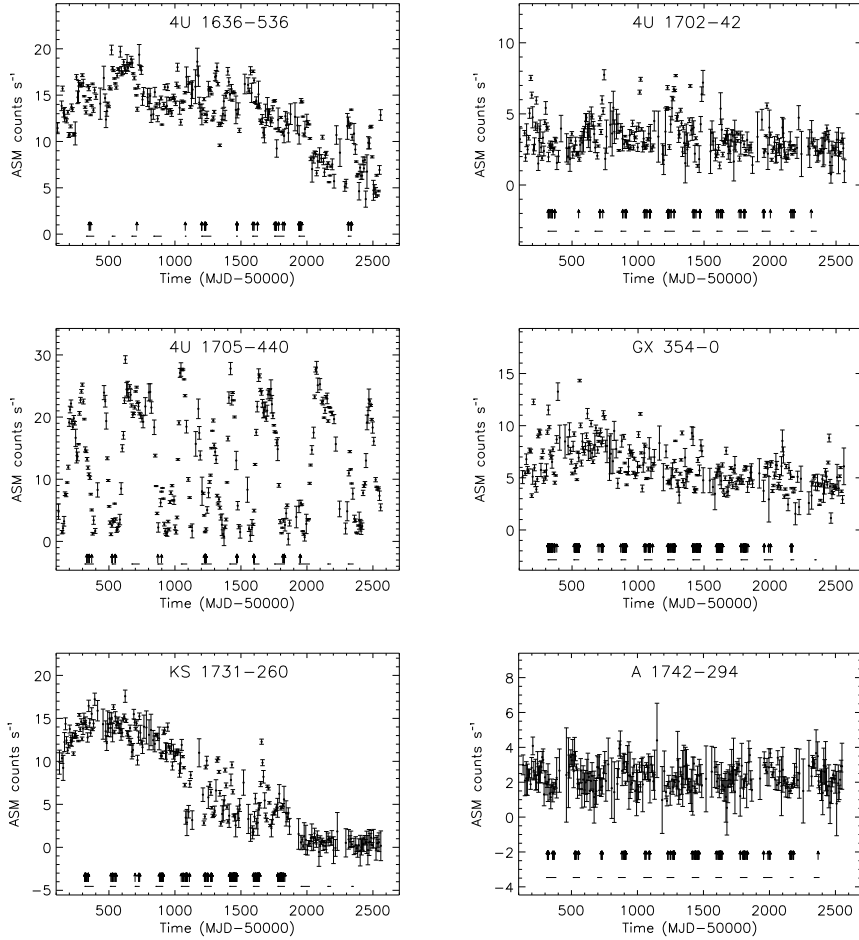
97

Figure 8.1: ASM/RXTE lightcurves of 9 of the most frequent X-ray bursters in the WFC database. Each bin is a one week average. Below the lightcurve the WFC observations on these sources are indicated with horizontal bars. The arrows just above the horizontal bars indicate the times of type I bursts.
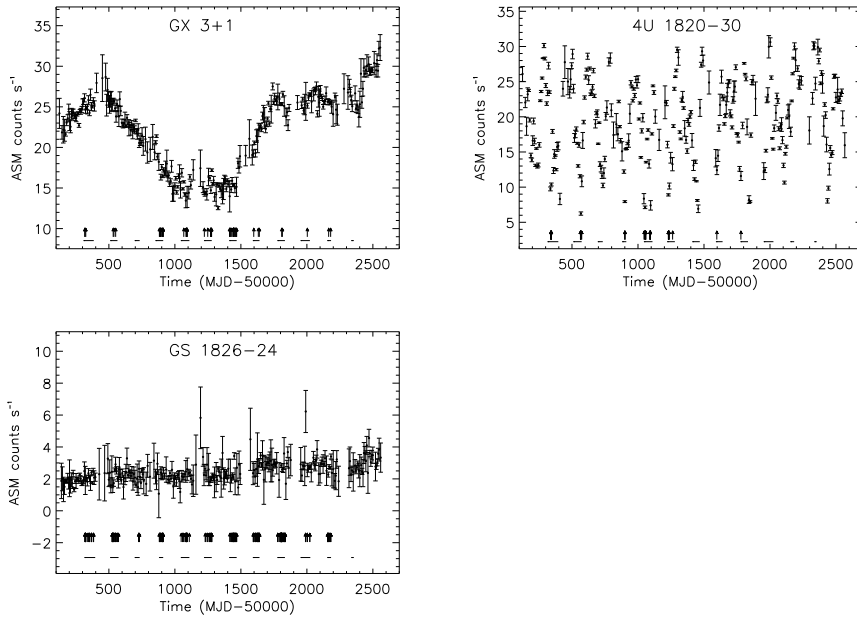
Fig. 8.1 Continued...

an apparent increase in burst rate when the source becomes fainter. In contrast, the lightcurves of 4U 1705−440 and 4U 1820−30 show strong variations, and bursts are observed only when the flux is low. Note that bursts would have been easily detected at the highest observed persistent flux levels of all sources, because those levels are presumed to be still significantly below the Eddington limit.

To study the burst rate as a function of persistent flux we assigned to each burst the average WFC-measured flux over the complete observation in which the burst occurred. We also checked the average persistent flux in a 5-minute time interval prior to each burst, but the difference with the aforementioned flux is negligible (within the errors). We divided the persistent flux range in 5 or 10 intervals of equal size. Only the flux range of KS 1731−260, the sole transient source in our sample, was divided in 10 bins with averaging bin size. For each flux interval we determined the total exposure time and the number of bursts, assigning an error equal to the square root of this number. In Fig. 8.2 we show
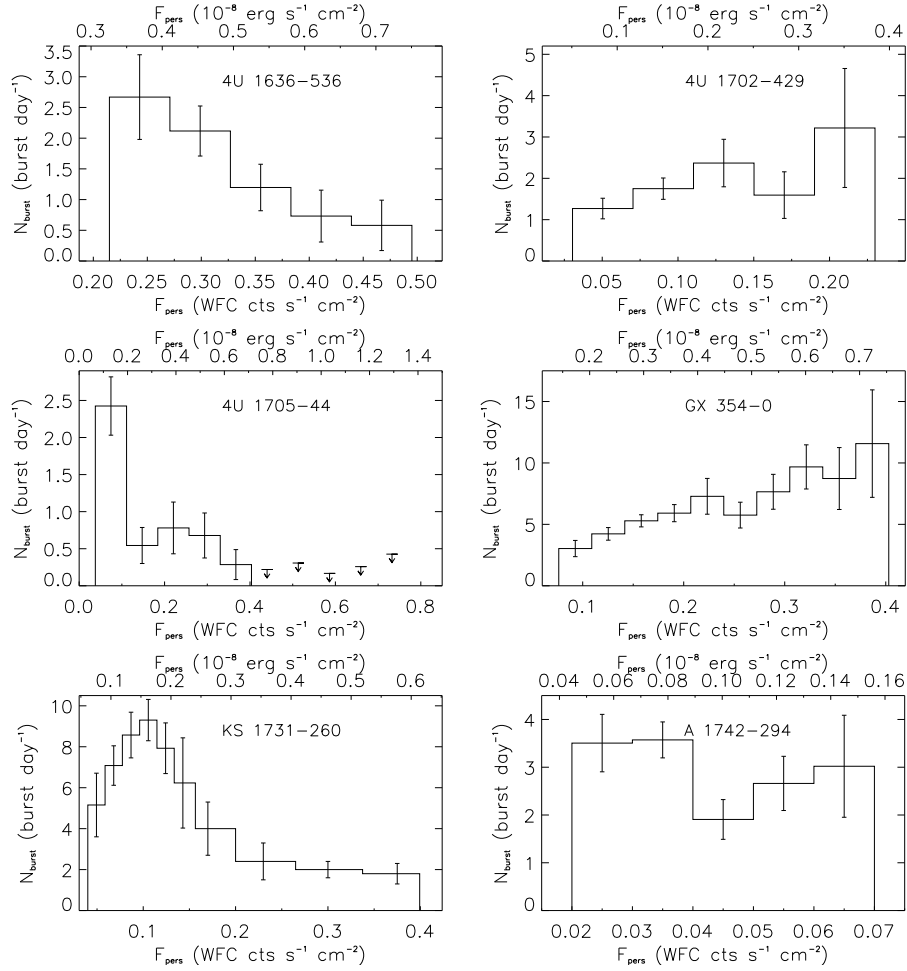
Figure 8.2: Burst rate as a function of the observed count rate (bottom axis) and the persistent flux (top axis) for the nine frequent X-ray bursters in the galactic center region. The photon and energy flux are for a bandpass of 2-28 keV.
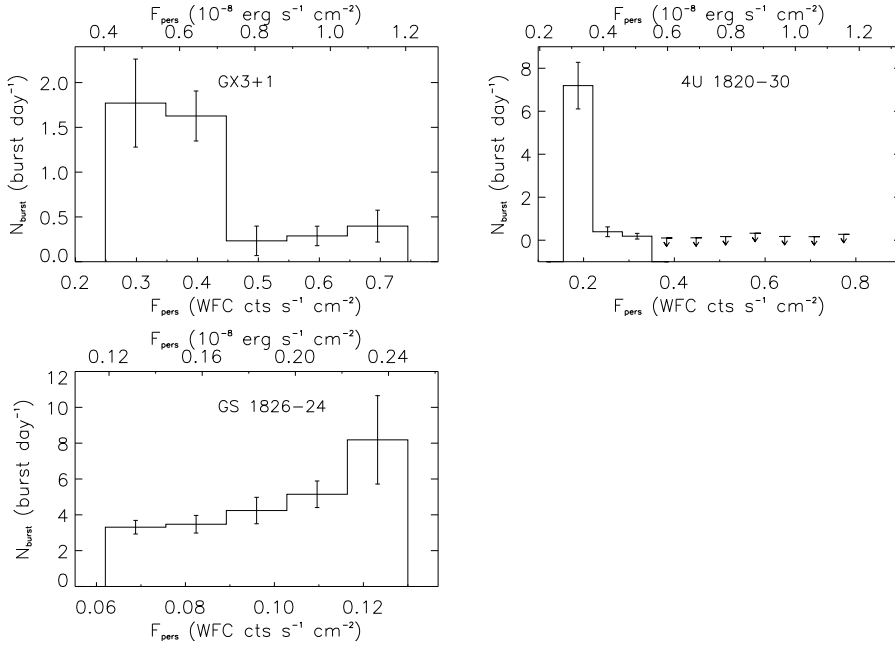
Fig. 8.2 Continued...

for each source the burst rate as a function of observed photon flux (bottom axis) and the derived energy flux (top axis). To convert the photon flux to energy flux we created for each source a spectrum for each campaign. Assuming an absorbed thermal bremsstrahlung model we derived the conversion factors (corrected for absorption), see Table 8.1. The spread in the conversion factors over all campaigns is about 10% for each source.

We notice in Fig. 8.2 that at the lowest flux levels KS 1731−260 shows an increase in burst rate with increasing persistent flux. When KS 1731−26 reaches 1.7×10^{-9} erg cm^{-2}s^{-1}, the burst rate drops by a factor of 5 and at the higher flux levels the burst rate slowly decreases. If we compare the behavior of the other sources it is noticeable that 4U 1702−429, GX 354−0 and GS 1826−24 all show only an increasing burst rate, while 4U 1636−536 is the only source that shows a decreasing burst rate 4U 1705−44, GX 3+1 and 4U 1820−30 show a drop by a factor of $\simeq 5$ in burst rate over a small range of persistent flux. A 1742−294 is the only source for which no trend is visible, and the burst rate

101

stays constant over the total observed flux range. This source traces out the lowest fluxes within our sample.

8.3.2   Wait times

Several sources are known to show quasi-periodic burst recurrence. The best example is GS 1826−24, which exhibited in 1996-1997 a burst every $\simeq$6 hours, and the burst wait times were constant within a few minutes for long periods of time (Ubertini et al. 1999; Cocchi et al. 2001b).

In the left panel of Fig. 8.3 we plotted the wait time as a function of the persistent flux for GS 1826−24. Most wait times appear to follow a straight line, and a second linear trend can clearly be distinguished above this line (and even two more above that). Given the fact that BeppoSAX has a 96-minute low-earth orbit, it is probable that bursts are missed during data gaps and multiples of the burst wait times observed. We checked bursts with long wait times within one observation and find that for all of them the previous burst may very likely have occurred during an earth occultation or South Atlantic Anomaly passage. From Fig. 8.3 we see that the wait time between the bursts decreases linearly with increasing persistent flux. We performed a least-squares fit on the bursts where the previous one is *not* missed to the function: $\Delta t = AF_{\mathrm{pers}} + B$. The results for the parameters are given in Table 8.2. Assuming a wait time that is two times longer (i.e., doubling the numbers derived above) gives a good description of the trend followed by the bursts forming the second line from the bottom. This shows again that for these points the previous burst is missed.

Formally the fit is not acceptable ($\chi^2_\nu = 5.7$, 92 d.o.f.), but the general trend is clearly visible. This means that there are significant fluctuations in the wait time around the average relation.

From theory a linear relation between the burst rate (inverse of the wait time) and the persistent flux is expected, and no bursts are expected anymore when F_{pers}=0 erg cm^{-2}s^{-1}. We therefore tried to fit the relation: $\Delta t = C/F_{\mathrm{pers}}$. The result of the fit of parameter C is given in Table 8.2.

Given the large number of bursts, we have also investigated the relation between the wait time and persistent flux for KS 1731−260 and GX 354−0. In the middle panel of Fig. 8.3 we show the results for KS 1731−260, and notice the strong suggestion of a linear dependency. However, this only applies to persistent flux levels below 0.14 WFC cts cm^{-2} s^{-1}. At higher persistent flux the wait time between bursts becomes apparently random. We fitted the relations as given above for the bursts with a persistent flux below 0.14 WFC cts cm^{-2} s^{-1}
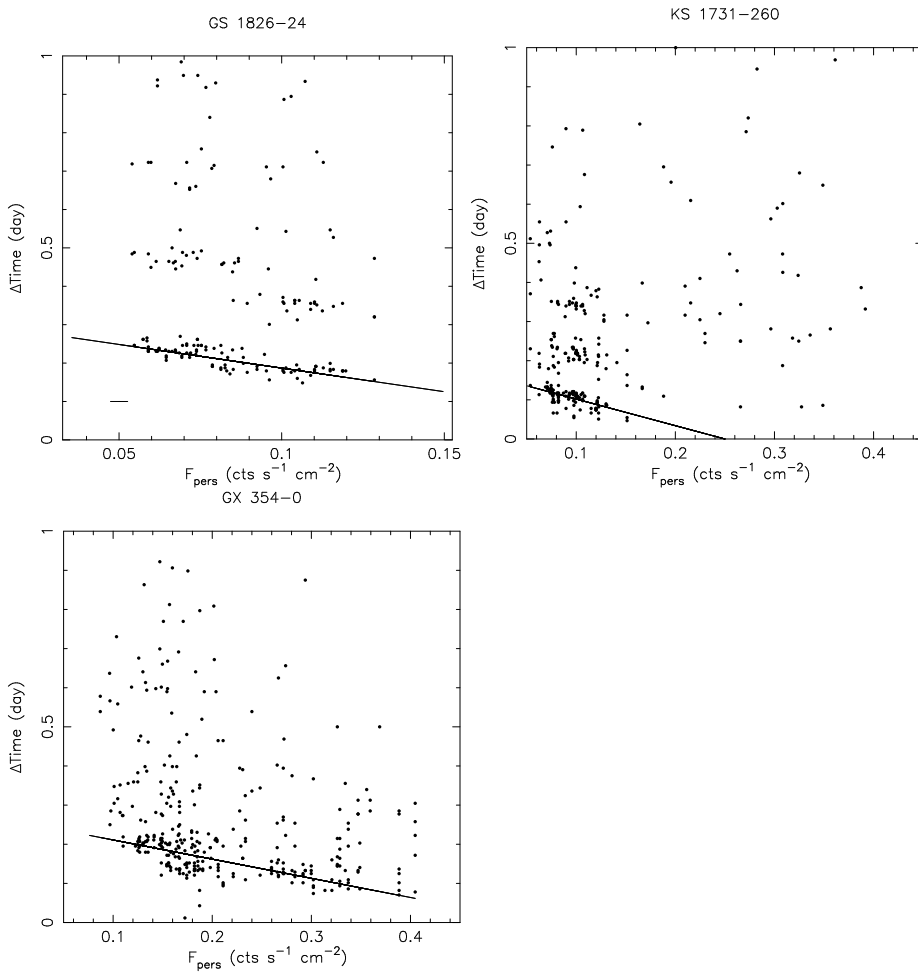
Figure 8.3: The burst rate as a function of persistent flux for the sources GS 1826−24 (left panel) and KS 1731−260 (middle panel) and GX 354−0 (right panel). A typical error in the flux for GS 1826−24 is indicated at the bottom left, while the error in the flux for the other two sources is as large as a dot. The error in the wait time for all sources is much smaller than the size of a dot. A best linear fit is drawn for the bursts for which the previous burst is not missed.

Table 8.2: Best fit parameters for a relation where the wait time is proportional (A and B) or inversely proportional (C) to the persistent flux. Due to the large χ^2_ν the formal errors on the parameters have no meaning.

parameter	GS 1826−24	KS 1731−260	GX 354−0
A	-1.23±0.10	-0.68±0.09	-0.49±0.07
B	0.31±0.01	0.17±0.01	0.26±0.01
χ^2_ν (d.o.f.)	5.7 (92)	20 (100)	266 (202)
C	0.017±0.001	0.009±0.001	0.029±0.001
χ^2_ν (d.o.f.)	6.2 (93)	38 (101)	234 (203)

and where we expect that the previous burst is not missed. The best fit parameters are given in Table 8.2.

Also for GX 354−0 there vaguely appears to be a linear relation between the persistent flux and the wait time (right panel Fig. 8.3). However, the scatter is significantly larger than in the previous two cases, making a clear distinction between the different multiples of the wait time very difficult. Therefore, an iterative process was used to search for bursts where we expect that the previous one is not missed. We simultaneously fitted a straight line (the single wait time line) plus several lines at multiples of the wait time. The bursts closest to the single wait time line were attributed to this line and used for a least-square fit to get a better estimate. This process was continued until a best fit was found. The bursts attributed to the single wait time line were also used to fit the relation: $\Delta t = C/F_{\mathrm{pers}}$. The results are summarized in Table 8.2.

For the other six sources the number of subsequent bursts with a wait time of less than one day becomes very small, and the data does not allow the verification of a linear relation.

We converted the fit parameters as given in Table 8.2 from the observed flux to luminosities using the conversion factors and distances as given in Table 8.1. For the parameter C the values are $(2.5 \pm 1.5) \times 10^{36}$, $(0.8 \pm 0.5) \times 10^{36}$ and $(1.9 \pm 1.1) \times 10^{36}$ for GS 1826−24, KS 1731−260 and GX 354−0, respectively (taking into account an error of 30% in the distance). Although the errors are very large, these slopes are the same within their errors. The burst rate may be a unique function of the persistent flux.
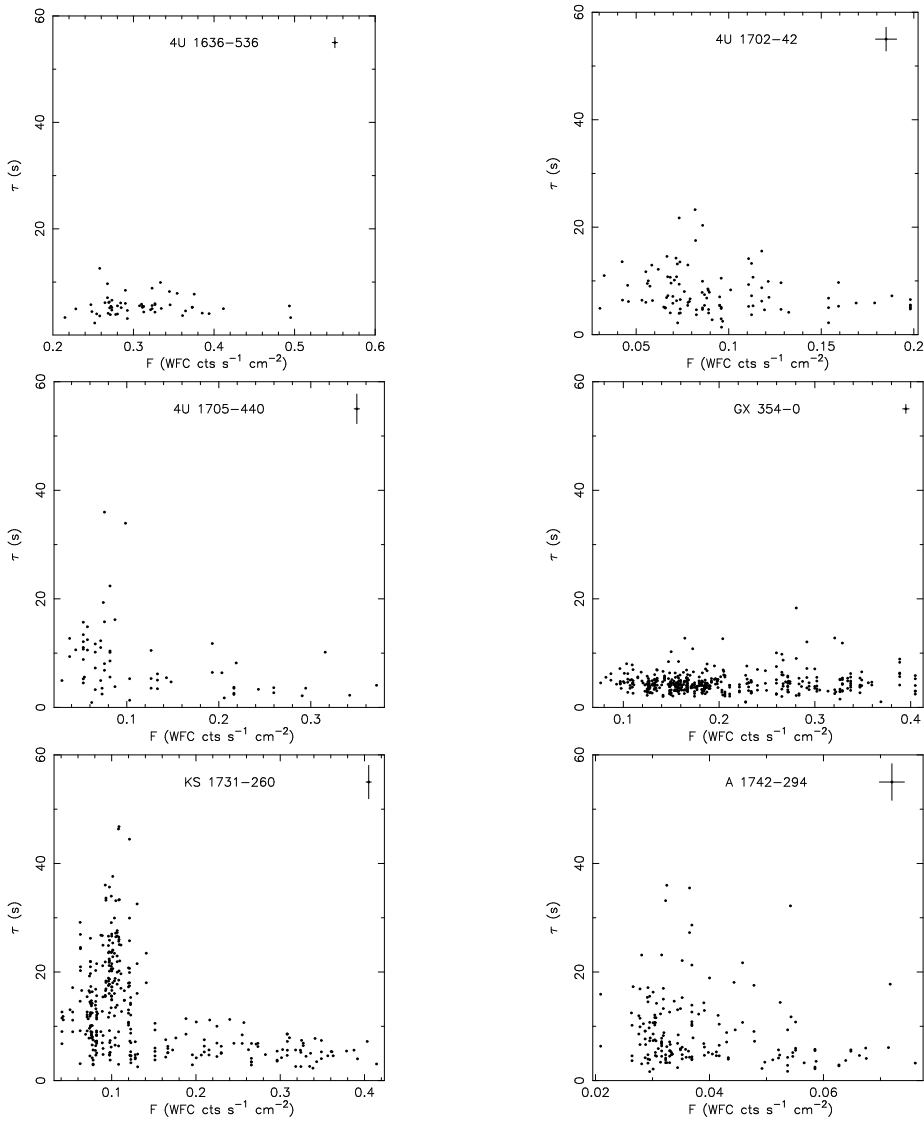
Figure 8.4: The exponential decay time as a function of persistent flux for the nine most frequent burst sources observed with WFC. In the upper-right corner of each panel a typical error-bar is shown.
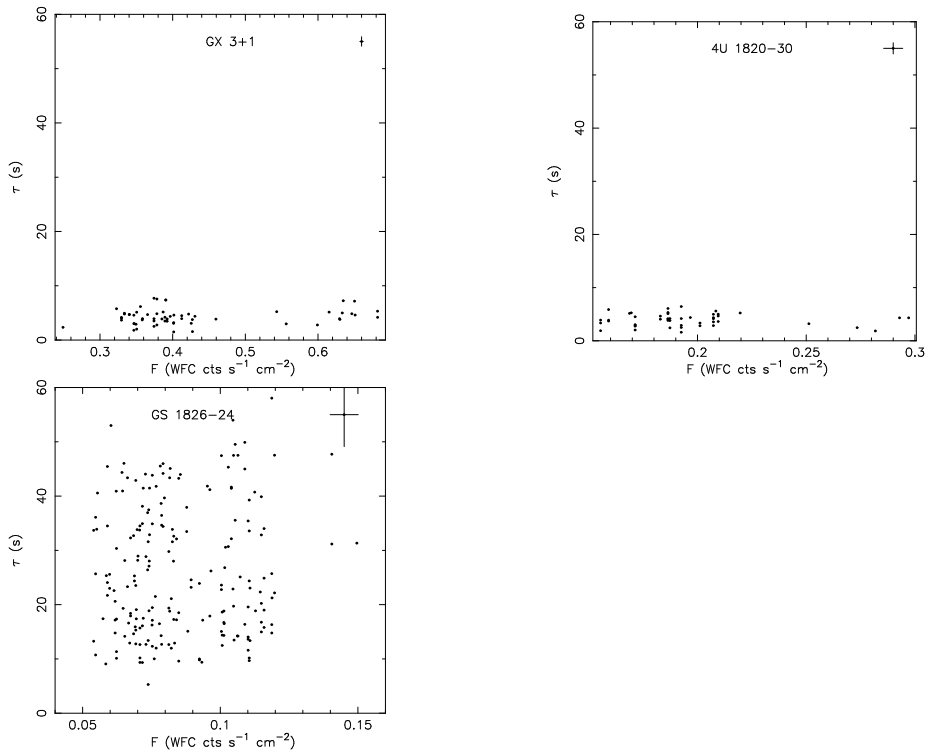
Fig. 8.4 Continued...

8.3.3 Decay times

Another important burst parameter is the e-folding decay time. As discussed in Sect. 1, this diagnoses the composition of the burst fuel. To derive the decay time for each burst we created a lightcurve with a 1 s time resolution. A running average of 5 s was used to determine the moment of the peak flux. The persistent emission level and the decay time are then simultaneously fitted with a constant and exponential, respectively. We took the bin in which the peak flux was reached as the first data point. In Fig. 8.4 we show the decay times as a function of persistent emission for the nine sources. We discuss GX 354−0, KS 1731−260 and GS 1826−24 in more detail and compare them with the other sources.

GX 354−0 only shows bursts with decay times shorter than $\simeq$10 seconds at all flux levels. The same applies to 4U 1636−536, GX 3+1 and 4U 1820−30. GS 1826−24 shows a large range of decay times at all persistent flux levels, but almost no bursts below 10 seconds are observed (less than 5% of all bursts). Of the nine sources, this is the only one that shows this behavior.

Two trends can be observed for the decay times of KS 1731−260. At high persistent flux ($\gtrsim$0.14 WFC cts s^{-1} cm^{-2}) all decay times are below 10 seconds, as for GX 354−0. At lower fluxes the spread in decay times increases rapidly and most bursts have decay times well above 10 s, as for GS 1826−24. However, in contrast to GS 1826−24, still a significant fraction of bursts shows decay times below 10 s (about 30%). The same behavior is also suggested by the figures for 4U 1702−429, 4U 1705−44 and A 1742-294.

A spectral variation of the persistent emission could explain the occurrence of both long and short bursts at low persistent flux. We therefore investigated the low persistent flux levels of KS 1731−260 in a little more detail. At MJD 51799.60 and MJD 51799.72 there were bursts with decay times of 4.7±0.1 s and 20.8±3.5 s, respectively. Due to the low flux level of the source full resolution spectra do not have enough statistics, and we resorted to the study of hardness ratios. The WFC passband was divided in two channels from 2-6 keV and 6-28 keV, and derived hardness ratios of 0.68±0.07 and 0.70±0.08 for the periods prior to the two bursts, respectively. We also note that the average persistent flux stayed constant at 0.111 and 0.115 WFC cts s^{-1} cm^{-2} in these periods The 1σ statistical fluctuations at one minute time resolution are 24% and 30%. We conclude that no significant changes occurred between the two bursts caused by a change in burst fuel composition or accretion flow.

The transition from short bursts to long/short bursts in KS 1731−260 is rapid. Therefore, an observation (at MJD 51637) where the persistent emission is at this transition was analyzed in more detail. A spectrum was derived for this observation, assuming an absorbed bremsstrahlung spectrum with a hydrogen absorption column of 1.3×10^{22} atoms cm^{-2} (Predehl & Schmitt 1995). A temperature of 21.4±3.4 keV and an unabsorbed flux of $(2.4\pm0.3)\times10^{-9}$ erg cm^{-2}s^{-1} (2-28 keV) was estimated. A power law spectrum with a photon index of 1.64±0.06 gives a flux of $(2.6\pm0.2)\times10^{-9}$ erg cm^{-2}s^{-1} (2-28 keV; corrected for absorption). Converting these numbers to a mass accretion rate, assuming standard neutron star parameters and 100% efficiency in converting gravitational energy to radiation, gives 1.3×10^{-9} M$_\odot$ yr^{-1}, similar to the mass accretion rate of GX 3+1 at its transition (den Hartog et al. 2002).
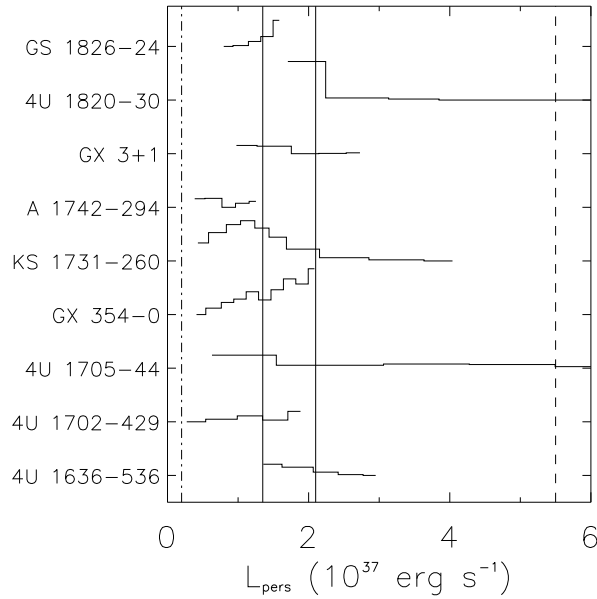
Figure 8.5: A schematic diagram of the burst rate as a function of luminosity for the nine X-ray burst sources (see Fig. 8.2). Between the solid lines the region is indicated where the burst rate drops by a factor of 5. No type I bursts were observed at luminosities above the dashed line. The dotted-dashed line indicates the theoretical predicted transition from hydrogen-rich bursts to pure helium bursts.

8.4 Discussion

8.4.1 Observational summary

Our observations of the burst rate for the nine frequent X-ray bursters are summarized in Fig. 8.5. In order to compare sources we calculated the 2–28 keV luminosity from the flux and the distances as listed in Table 8.1. Given that the distance has an estimated accuracy of 30% and that the 2–28 keV luminosity is only a crude indicator of the accretion rate, we estimate that the luminosity correspondence between sources is accurate to about a factor of 2. The following conclusion can be drawn from Figs. 8.5 and 8.2: the burst rate shows trends with luminosity that are consistent over all sources. At 1 to 2×10^{37} erg s^{-1} the burst

rate peaks. Above that the burst rate drops fast by roughly a factor of 5 (first observed in GX 3+1 by den Hartog et al. 2002, and now also seen for 4U 1820-30, KS 1731-269, and 4U 1705-44). Below that there is a smooth increase. Above 5.5×10^{37} erg s^{-1} no bursts are seen anymore. The latter is confirmed by observations of brighter low-mass X-ray binaries in the same field with presumably similar distances such as GX 9+1, GX 349+2, GX 340+0, GX 17+2, GX 13+1 and GX 5-1. None of these were seen to burst by the WFC. The general trends in burst rate were known previously. The knowledge that our work adds is 1) that there does seem to be a rather consistent burst rate behavior from one burster to another, and 2) that there is a rather discrete transition in this behavior between 1.4 to 2.1×10^{37} erg s^{-1}.

Our searches for (quasi-)periodicity in burst recurrence were meaningful in three sources: GX 354-0, KS 1731-260 and GS 1826-24. The presence of quasi-periodicities is obvious in GS 1826-24 (see also Ubertini et al. 1999 and Cocchi et al. 2001b) and KS 1731-260, but only suggestive in GX 354-0. The quasi-periodicity is only present during times when the persistent flux is below that for the peak burst rate, as is most clearly demonstrated by KS 1731-260 which, thanks to its transient nature, traces a relatively wide range of fluxes. GS 1826-24 never leaves this domain which explains why its bursts *always* recur quasi-periodically. The same appears to apply to GX 354-0. Quasi-periodicity has been seen previously with EXOSAT in a number of other sources: EXO 0748-676 (Gottwald et al. 1986), 4U 1705-44 (Gottwald et al. 1989), Ser X-1 (Sztajno et al. 1983) and 4U 1636-536 (Lewin et al. 1987). Our observations for the first time show empirically that quasi-periodicity is restricted to a very particular luminosity range and shows a narrow relationship between its frequency and the persistent flux.

Our determinations of burst decay times in KS 1731-260 and 4U 1705-44 suggest a clear correspondence between decay time, burst rate behavior and quasi-periodicity, in the sense that there is a clear transition at a luminosity between 1.4 and 2.1×10^{37} erg s^{-1}. However, the decay times observed in GX 3+1 and 4U 1705-44 do not follow this trend despite tracing out similar ranges in luminosity (formally the same applies to 4U 1820-30 but here we know that decay times cannot be long because the mass donor is proven to be a helium white dwarf).

To summarize: the central finding in our study is the likely identification of a single luminosity between 1.4 to 2.1×10^{37} erg s^{-1}, consistent with a single mass accretion rate, where the bursting behavior changes in three basic ways: going to higher luminosities, bursts 1) become a factor of 5 less frequent, 2) stop recurring quasi-periodically, 3) stop being long. To our knowledge, the first two

109

observations are new.

8.4.2   Theoretical interpretation

From theory it is expected that long bursts can only be due to helium flashes in a hydrogen-rich environment, which is predicted to occur at the highest or lowest accretion regimes (Fujimoto et al. 1981; Bildsten 1998; see also introduction). Given the fact that in our sample only short bursts are observed at higher luminosities, we identify the transition in burst behavior with the transition from the lowest to the middle accretion regime.

At the lowest luminosities the helium flash is triggered by unstable hydrogen burning (Fujimoto et al. 1981). Between two bursts no hydrogen is burned, and it is only the accretion of matter that increases the pressure and temperature to high enough values to start this burning. If we assume that the accretion flow is stable then the burst wait time is only dependent on the accretion rate, and a quasi-periodic behavior is not unexpected, as is a narrow relationship between its frequency and the persistent flux.

In the middle accretion regime, bursts take place in a pure helium shell which is fed by stable hydrogen burning in a layer above that. When a critical temperature and pressure are reached the helium ignites. Here the onset of the bursts is determined by the heating of the shell due to the hydrogen burning and the accretion. But more importantly, the onset of helium burning is very sensitive to the temperature (Bildsten 1998), making it highly dependent on local perturbations in the hydrogen burning. This means that local conditions determine the onset (and thus the wait time) of a burst, and quasi-periodic behavior is not readily expected anymore.

Hydrogen starts burning in an unstable fashion at lower column depths than helium (Joss 1977). This means that the conditions for triggering an X-ray burst in the lowest accretion regime are reached sooner than in the middle accretion regime, and a higher burst rate is expected. Given the fact that only the accretion rate can set the condition for the start of unstable hydrogen burning, it is expected that this transition happens in a fairly small range of accretion rates.

We have for the first time shown that the largest decrease in burst rate towards higher fluxes is coincident with the onset of stable hydrogen burning. Thereby, the above-mentioned explanation for the decreasing burst rate may partly resolve a long-standing problem for explaining decreasing burst rates. Van Paradijs et al. (1988) explained this by invoking increased stable helium burning with increasing accretion rate. However, such burning is not expected

to occur at sub-Eddington accretion rates (Fujimoto et al. 1981). Nevertheless, Bildsten (2000) suggested that non-global accretion on the neutron star (Marshall 1982; Inogamov & Sunyaev 1999) may explain that: the accretion area may be smaller than the neutron star surface so that the *local* mass accretion rate is higher than the globally measured one.

It is unclear how the burst rate behaves above this transition. Direct measurements (Fig. 8.2) are ambiguous: it may be constant or slowly decreasing. The rarity of X-ray bursts for more luminous sources suggests that there is a decrease, but observations in this domain are subject to strong selection effects as was already noted by other investigators (i.e., since the persistent emission is already close to Eddington there is hardly any room for flux increases by bursts). If the decrease is real, that does need to be explained, perhaps in a manner as proposed by Van Paradijs et al. (1988) and Bildsten (2000).

So far, we have dealt with observations that are explainable in current burst theory. There are three observations for which this is more difficult. The first is the fact that short bursts seem to be rather common in the low accretion regime. Long bursts would be expected because the flashes occur in a hydrogen-rich layer. This problem was also recently recognized by Den Hartog et al. for the specific case of GX 3+1. Also, short type-I bursts have been detected with extremely low persistent fluxes (e.g., a burst from SAX J2224.9+5421 was quickly and deeply followed up in X-rays and no persistent source was found with a 2–10 keV upper limit of 1.3×10^{-13} erg cm^{-2}s^{-1}; see Cornelisse et al. 2002). Fujimoto et al. (1981) briefly sketch an alternative path to trigger bursts in the lowest regime that could explain this. If the unstable hydrogen burning in the bottom shell does not trigger the helium burning instantaneously it will cause temporary stable hydrogen burning in the higher shells. The unstable hydrogen burning is not observable (Joss et al. 1977). A pure helium layer will be built up by the stable hydrogen burning and it will probably take a number of invisible hydrogen flashes to trigger a helium flash in this layer, very much like in the middle accretion regime, with a short burst as result.

It is unclear what determines the varying mix of short and long bursts (100% short bursts for GX 3+1 and GX 354-0, less than 5% for GS 1826-24, and in-between percentages for other sources). We suspect that variability of the persistent flux may be an issue. If we compare the ASM lightcurves in Fig. 8.1 of KS 1731−260 and GS 1826−24 we notice that KS 1731−260 is more variable at comparable luminosities (between MJD 51000 and MJD 51700). During the last WFC campaign (around MJD 51800) only long bursts are observed for KS 1731−260 and the variability becomes comparable to GS 1826−24. This would indicate that low variability, (i.e., a smooth accretion rate) gives rise to

solely long X-ray bursts, while a more inhomogeneous accretion rate gives rise to incidental pure helium flashes.

Another issue unexplainable by current burst theory is the inconsistent peak burst rate between different sources. A bi-modal distribution appears to be present. GX 354−0, KS 1731−260, 4U 1820−30 and GS 1826−24 all have a peak burst rate of about 9 bursts day^{-1}, while the other sources have a peak burst rate of about 2.5 bursts day^{-1}. EXOSAT observations of 4U 1636−536 showed a burst rate of 8 bursts day^{-1}, more in line with the first group (Lewin et al. 1987). Given the large uncertainty in the distance it could well be possible that during the WFC observations the luminosity of 4U 1636−536 is not low enough for such high burst rates, and this might be the case for the other sources. We have no good explanation for the bi-modality.

A large discrepancy between theory and observations is the accretion rate at which the transition from the middle accretion regime to the lowest regime takes place. Bildsten (1998) gives a value of 2×10^{-10} $M_{\odot}$ yr^{-1} (indicated in Fig. 8.5 with a dashed dotted line), while we find $(1.4\text{-}2.1) \times 10^{-9}$ $\dot{M}$ yr^{-1}. The values Bildsten derived are for certain assumptions on the conditions in the neutron star (abundances of CNO elements, opacity etc.). This easily gives a uncertainty of a factor of two, but this is not enough. A non-global accretion on the neutron star does not help, because that would imply an even larger local mass accretion rate.

8.5   Summary

Thanks to the wide (50%) and long (7 Ms) coverage of the population of low-mass X-ray binaries we detected an unprecedented large number of type-I X-ray bursts for nine sources which enabled us to perform a comparative study of bursting behavior which was hitherto not possible. We were able to accurately detect systematic trends in burst rate, burst duration and burst recurrence periodicity and to put them under the common denominator provided by current burst theory. Our central finding is that most of the trends in bursting behavior are driven by the onset of stable hydrogen burning in the neutron star atmosphere. Furthermore, we notice three new observations which are more difficult to explain with current burst theory: the presence of short pure-helium bursts at the lowest accretion regimes, the bimodal distribution of peak burst rates, and an accretion rate at which the onset of stable hydrogen burning occurs that is ten times higher than predicted. Finally, we note that our investigation is the first to signal quasi-periodic burst recurrence in KS 1731-260, and a clear

inverse proportionality between the frequency of the quasi-periodicity and the persistent flux in GS 1826-24 and KS 1731-260.

References

Augusteijn, T.J., van der Hooft, F., de Jong, J.A., van Kerkwijk, M.H., & van Paradijs, J. 1998, A&A 332, 561

Bildsten, L. 1998, in Bucheri, J., van Paradijs, J., Alpar, M.A. (eds.), The many faces of neutron stars, Kluwer, Dordrecht, p. 419

Bildsten, L. 2000, in S. Holt, W. Zhang (eds.), Cosmic explosions, AIP, p. E65

Boella, G., Butler, R., Perola, G., et al. 1997, A&AS 122, 299

Cocchi, M., Bazzano, A., Natalucci, L., et al. 2001a, A&A 378, L37

Cocchi, M., Bazzano, A., Natalucci, L., et al. 2001b, in Advances of Space Research Vol. 28, Elsevier, p. 275

Cornelisse, R., Verbunt, F., in 't Zand, J.J.M., et al. 2002, A&A 392, 885

den Hartog, P.R., in 't Zand, J.J.M., Kuulkers, E., et al. 2002, submitted to A&A

Fujimoto, M.Y., Hanawa, T., & Miyaji, S. 1981, ApJ 247, 267

Galloway, D.K., Psaltis, D., Chakrabarty, D., & Muno, M.P. 2002, submitted to ApJ (astro-ph/0208464)

Gotthelf, E., & Kulkarni, S. 1997, ApJ 490, L161

Gottwald, M., Haberl, F., Parmar, A.N., & White, N.E. 1986a, ApJ 308, 213

Gottwald, M., Haberl, F., Parmar, A.N., & White, N.E. 1986b, ApJ 308, 199

Gottwald, M., Haberl, F., Langmeier, A. 1989, ApJ 339, 1044

Grindlay, J., Heise, J. 1975, IAUC 2879

Haberl, F., Stella, L., White, N.E., Gottwald, M., & Priedhorsky, W.C. 1987, ApJ 314, 266

Hammersley, A., Ponman, T., Skinner, G.K. 1992, Nuc. Instr. Meth. Phys. Res. A311, 585

Heasley, J.N., Janes, K.A., Zinn, R., et al. 2000, AJ 120, 879

Inogamov, N.A., & Sunyaev, R.A. 1999, AstL 25, 269

Jager, R., Mels, W., Brinkman, A., et al. 1997, A&AS 125, 557

Joss, P.C. 1977, Nature 270, 211

Kuulkers, E., & van der Klis, M. 2000, A&A 356, L45

Kuulkers, E., Homan, J., van der Klis, M., Lewin, W.H.G., & Mendez, M. 2002, A&A 382, 947

Langmeier, A., Sztajno, M., Hasinger, G., & Trümper, J. 1987, ApJ 323, 288

Levine, A.M., Bradt, H., Cui, W., et al. 1996, ApJ 469, L33

Lewin, W.H.G., Penninx, W., van Paradijs, J., et al. 1987, ApJ 319, 893

Lewin, W.H.G., van Paradijs, J., & Taam, R. 1993, Space Sci. Rev. 62, 223

Lutovinov, A.A., Grebenev, S.A., Pavlinsky, M.N., & Sunyaev, R.A. 2001, AstL 27, 501

Marshall, H.L. 1982, ApJ 260, 815

Muno, M.P., Fox, D.W., Morgan, E.H., & Bildsten, L. 2000, ApJ 542, 1016

Muno, M.P., Chakrabarty, D., Galloway, D.K., & Savov, P. 2001, ApJ 553, L157

van Paradijs, J., Penninx, W., & Lewin, W.H.G. 1988a, MNRAS 233, 437

van Paradijs, J., Penninx, W., Lewin, W.H.G, Sztajno, M., & Truemper, J. 1988b, A&A 192, 147

Predehl, P., & Schmitt, J.H.M.M. 1995, A&A 293, 889

Sztajno, M., Basinska, E.M., Cominsky, L.R., Marshall, F.J., & Lewin, W.H.G. 1983, ApJ 267, 713

Ubertini, P., Bazzano, A., Cocchi, M., et al. 1999, ApJ, 514, L27

in 't Zand, J.J.M. 1992, A coded-mask imager as monitor of galactic X-ray sources, Ph.D. thesis, Utrecht University

in 't Zand, J.J.M., Heise, J., Kuulkers, E., et al. 1999, A&A 347, 89

in 't Zand, J.J.M. 2001, in Exploring the gamma-ray universe, ed. A. Gimenez, V. Reglero, & C. Winkler, ESA Pub. Div., 463

Hoofdstuk 9

Nederlandse samenvatting

9.1 De hemel

Wanneer 's nachts naar een onbewolkte hemel wordt gekeken is het eerste wat opvalt de vele fonkelende sterren. Met wat geluk kan ook de melkweg worden gezien als een oplichtende band. Als met een telescoop naar deze band wordt gekeken blijkt die te bestaan uit vele miljoenen individuele sterren. Samen vormen al deze sterren het melkwegstelsel waar onze zon, ook een ster, onderdeel van uit maakt.

Alle sterren die op deze manier worden waargenomen, hebben gemeen dat ze ongeveer dezelfde temperatuur hebben als de zon, zo rond de 6000 graden Celsius. Het is niet vreemd dat we alleen deze sterren zien, want bij deze temperatuur zendt een ster voornamelijk straling uit waar onze ogen het meest gevoelig voor zijn. Deze straling wordt licht genoemd, maar ook wel optische straling.

Zouden we een fictieve ster zoals de zon steeds koeler kunnen maken, dan zou het licht dat wordt uitgezonden steeds roder worden. Als de ster nog maar een temperatuur van ongeveer 600° C heeft, kan deze niet meer worden gezien met onze ogen. We moeten dan een infra-rood bril opzetten om die ster te kunnen waarnemen.

Uiteraard kan deze fictieve ster ook heter worden gemaakt. Hij zal dan langzaam maar zeker steeds blauwer licht gaan uitstralen. Als een temperatuur van 10.000° C wordt bereikt is de meeste straling niet meer zichtbaar met het blote oog. Hij zendt dan voornamelijk ultra-violette straling uit. Indien de

115

temperatuur van deze ster verder wordt verhoogd tot ongeveer 100.000° C zou hij röntgenstraling gaan uitzenden.

Onze ogen zijn dus eigenlijk heel beperkte instrumenten om het heelal te bestuderen. We zien alleen maar de objecten met een bepaalde temperatuur, terwijl vele objecten onzichtbaar blijven voor ons oog. Als we het heelal ooit willen begrijpen zullen dus we dus ook de koude en warme objecten moeten bestuderen die geen optische straling uitzenden. Vandaar dat er instrumenten zijn ontwikkeld die andere straling dan het optische kunnen waarnemen.

9.2 Een stukje sterevolutie

Er bestaan geen sterren die zo heet zijn dat ze voornamelijk röntgenstraling uitzenden. Om toch een beetje te begrijpen wat voor objecten röntgenstraling uitzenden, is een stukje sterevolutie nodig.

Sterren zijn grote gasbollen die voornamelijk bestaan uit waterstof en helium. Aan de buitenkant hebben ze een temperatuur van ongeveer 6000° C, maar in het centrum kan dit oplopen tot vele miljoenen graden. Deze hoge temperaturen en de hoge druk in het centrum van de zon maakt kernfusie mogelijk, ofwel de waterstof verbrandt tot helium. Bij deze verbranding komt energie vrij die wij uiteindelijk zien als het licht dat een ster uitstraalt.

Pas na enkele miljarden jaren is voor de meeste sterren het waterstof verbrand tot helium. Een ster is dan aan het eind van zijn leven gekomen. Sterren zoals onze zon zullen dan de buitenste lagen verliezen, en de kern zal krimpen tot een zogenaamde witte dwerg. Een witte dwerg is ongeveer zo groot als de aarde, maar heeft nog steeds een massa vergelijkbaar met die van de zon. Zwaardere sterren, tot ongeveer 10 keer de massa van de zon, zullen aan het eind van hun leven exploderen, dit wordt ook wel een supernova explosie genoemd. Tijdens deze explosie zal de kern van deze zware sterren tot een zogenaamde neutronenster in elkaar storten. Neutronensterren zijn net zo groot als de stad Utrecht maar zijn net zo zwaar als de zon. Ofwel, een kruiwagen vol met neutronenster materie is net zo zwaar als onze aarde! Bij nog zwaardere sterren zal de kern in elkaar storten tot een zwart gat. Daar is alle materie samengepakt in een punt, iets wat niet meer is voor te stellen.

Het zijn voornamelijk deze restanten van sterren die röntgenstraling kunnen uitzenden. Zo'n restant, dat compact object wordt genoemd, kan verbonden zijn met een 'normale' ster waardoor ze om elkaar heen draaien. Dit wordt ook wel een dubbelster genoemd. In de melkweg zijn veel van dit soort dubbelsterren. Het overgrote deel van deze systemen bestaan uit twee 'normale' sterren,

116
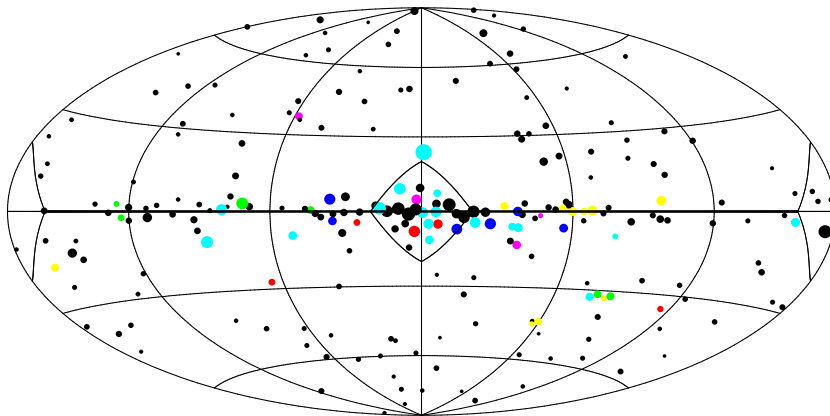
Ariel V 3rd Catalogue

Figuur 9.1: De röntgenhemel zoals deze met de satelliet Ariel V is waargenomen. De horizontale lijn in het midden van het figuur geeft de melkweg aan, met het centrum van de melkweg in het midden. Elke stip geeft de plek van een röntgenbron in de hemel aan, met de grootte van de stip een maat voor de relatieve helderheid. Het vierkant dat om het centrum van de melkweg is getekend geeft het deel van de hemel aan dat de groothoekcameras in één keer kunnen waarnemen.

maar een heel kleine fractie heeft een compact object plus 'normale' ster. De begeleidende ster van zo'n compact object zal tegen het eind van zijn evolutie de buitenste gaslagen afstoten (zie boven). Dit gas (voornamelijk bestaande uit waterstof) zal op het compacte object 'vallen' waarbij het wordt verhit tot 100.000° C zodat het voornamelijk röntgenstraling gaat uitzenden.

Nu blijkt dat vele van deze dubbelsterren zich richting het centrum van de melkweg bevinden. Dit is geïllustreerd in Figuur 9.1. Dit was een reden om in Utrecht de röntgen groothoekcameras te ontwerpen. Deze kunnen een groot deel van de hemel in één keer bekijken, zodat vele van deze systemen tegelijk kunnen worden waargenomen als richting het melkwegcentrum wordt gekeken. Dit proefschrift gaat over waarnemingen aan deze dubbelsterren die met de groothoekcameras zijn gedaan, en dan met name de bronnen die röntgenflitsen vertonen.

117

9.3 Röntgenflitsen

De meeste heldere bronnen in Figuur 9.1 hebben als compact object een neutronenster. De afgestoten gaslaag van de begeleidende normale ster zal op het oppervlak van de neutronenster worden verzameld. Maar de temperatuur en druk aan het oppervlak van een neutronenster zijn al extreem hoog zodat de verbranding van waterstof tot helium direct optreedt. Er zal een steeds dikkere laag van helium ontstaan op het oppervlak van de neutronenster, en de onderkant van die groeiende helium laag zal een nog hogere temperatuur en druk krijgen. Deze laag blijft groeien totdat aan de onderkant een temperatuur en druk wordt bereikt waarbij helium kan verbranden tot koolstof. Dit gaat op zeer explosieve wijze, en er komt in enkele seconden net zo veel energie vrij als de zon in ongeveer een dag produceert. Dit is voldoende energie om ook het koolstof direct te verbranden tot nog zwaardere elementen (zoals ijzer).

Deze explosies worden waargenomen als zogenaamde röntgenflitsen. Een voorbeeld van een röntgenflits is te zien in Figuur 9.2. Hier is te zien hoe de röntgenstraling van een neutronenster varieert in de tijd. Voor het grootste deel van de tijd is de bron constant aan het stralen (dit is het gas dat op de neutronenster valt), maar soms is er een ploseling een grote toename van röntgenstraling te zien. Dit is het moment waarop de helium verbrand tot koolstof, en het begin van de flits. Deze uitbarsting verwarmt de atmosfeer van de neutronenster, en zodra alle helium is verbrand en er geen energie meer vrij komt (het moment dat de piek van de flits wordt bereikt) kan de atmosfeer weer gaan afkoelen tot de temperatuur is bereikt van voor de flits. Deze afkoeling is te zien als een "afvallende staart", die in dit geval ongeveer 100 seconden duurt. Gemiddeld duurt een röntgenflits (vooral het afkoelen) ergens tussen de paar seconden en een tiental minuten. De duur van een röntgenflits is voornamelijk afhankelijk van de snelheid waarmee de neutronenster de buitenste gaslaag van de begeleider ontvangt.

De groothoekcameras hebben in totaal ongeveer 1823 van deze röntgenflitsen waargenomen, en die kwamen voor het overgrote deel van bronnen waarvan al bekend was dat ze röntgenflitsen vertonen. De regelmaat waarmee een bron röntgenflitsen produceert varieert sterk, van maar een keer per maand (of nog minder) tot eens in de twee uur. De tijdsduur tussen twee flitsen hangt van een aantal omstandigheden af. In de eerste plaats de snelheid waarmee de neutronenster het gas ontvangt van zijn begeleider, maar ook welke fractie van het oppervlak wordt bedekt door die waterstof en de snelheid waarmee het waterstof kan verbranden.
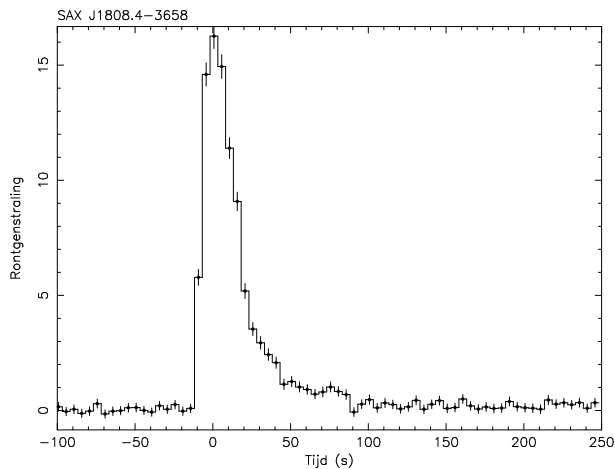
Figuur 9.2: Een typische röntgenflits zoals die werd waargenomen door de groothoekcameras.

9.4 Dit proefschrift

De röntgenflitsen zijn in de jaren 70 van de vorige eeuw ontdekt (door John Heise en medewerkers) en het hierboven geschetste model is niet lang daarna ontwikkeld. In de jaren daarna zijn vele waarnemingen aan röntgenflitsen gedaan die dit model bevestigen. Dus wat is nu de bijdrage van dit proefschrift aan dit veld?

De afgelopen jaren is men zich gaan realiseren dat er een sub-klasse bestaat van de dubbelsterren met compact object. De bronnen in deze klasse zijn maar voor een paar weken actief. In die periode wordt er röntgenstraling van zo'n bron waargenomen, terwijl de rest van de tijd (dit kan jaren maar misschien zelfs wel decennia zijn) er niets is waar te nemen van zo'n bron. Blijkbaar kan de begeleider elke keer maar korte periodes zijn buitenste gaslagen afstoten. Hoofdstuk 3 van dit proefschrift beschrijft de actieve periode (in dit geval 2 weken) van zo'n bron. Tijdens die actieve periode werden er 7 röntgenflitsen waargenomen van die bron, wat aantoont dat het compacte object een neutronenster is.

Hoofdstuk 4 gaat over de ontdekking van een nieuw verschijnsel, de zogenaamde superflits, en hoofdstuk 5 over een tweede waargenomen superflits. Deze superflitsen werden beide waargenomen in heldere röntgenbron die bekend stonden als röntgenflitser. Superflitsen zijn verwant aan de 'normale' röntgenflits,

119

maar duren veel langer (uren in plaats van minuten) en er komt veel meer energie vrij (wat de zon ongeveer in een half jaar produceert). Tijdens de ontdekking was er geen enkele theorie die zo'n soort flits kon verklaren. Het is namelijk onmogelijk om voldoende helium (en waterstof) te verzamelen voordat het verbrandt tot koolstof (en verder) om de totale waargenomen energie te verklaren.

Men kwam toen met een aangepaste theorie die voorspelt dat een klein beetje koolstof als één van de eindproducten overblijft na een 'normale' röntgenflits. De hoeveelheid koolstof zal langzaam opbouwen over vele flitsen. Zodra er voldoende koolstof is verzameld kan dit ook op explosieve wijze verbranden. Dit wordt dan waargenomen als een superflits.

Een sub-klasse van röntgenflitser wordt behandeld in hoofdstukken 6 en 7. De meeste röntgenflitsers zijn altijd zeer heldere röntgenbronnen, zeker in de periode als ze ook röntgenflitsen vertonen. Maar de afgelopen paar jaar zijn, voornamelijk door de groothoekcameras, een aantal nieuwe bronnen ontdekt die erg zwak zijn maar wel een röntgenflits vertonen (de meeste hebben tot nog toe maar één flits vertoond). Het is alleen dankzij de flits dat ze konden worden ontdekt. In hoofdstuk 6 wordt de ontdekking van vier van deze bronnen (ongeveer de helft van de bronnen in deze sub-klasse) besproken. In hoofdstuk 7 wordt geprobeerd een aantal van deze bronnen met de röntgensatelliet Chandra waar te nemen, deze satelliet is veel gevoeliger in het detecteren röntgenstraling dan de groothoekcameras, om zo na te gaan hoe zwak deze bronnen nu precies zijn.

Tot slot worden in hoofdstuk 8 de negen bronnen waar de groothoekcameras de meeste flitsen van hebben waargenomen besproken. Door de grote aantallen flitsen kunnen de verschillende bronnen op statistische wijze met elkaar worden vergeleken en de huidige theorie worden getest. Daarmee kon voor het eerst worden aangetoond dat alle bronnen eigenlijk hetzelfde gedrag vertonen wanneer ze de zelfde hoeveelheid gas van hun begeleider ontvangen per seconde. Ook kon bij een aantal bronnen worden aangetoond dat als de hoeveelheid gas dat wordt ontvangen per seconde toeneemt ook het aantal flitsen toeneemt. En tot slot werd aangetoond dat de theorie niet altijd de juiste duur van een flits kon voorspellen. In dit hoofdstuk wordt dan ook een suggestie gedaan hoe de theorie moet worden aangepast.

Dit proefschrift laat hopelijk zien dat we nog lang niet alles begrijpen van de röntgenflitsen, en dat er na 30 jaar nog steeds nieuwe verschijnselen zijn te ontdekken in dit veld.

Other publications

- The orbital period of the recurrent X-ray transient in Terzan 6
  in 't Zand, J.J.M., Bazzano, A., Cocchi, M., Cornelisse, R., et al. 2000,
  A&A 355, 145

- BeppoSAX observations of the nearby low-mass X-ray binary and fast
transient SAX J1819.3−2525
  in 't Zand, J.J.M., Kuulkers, E., Bazzano, A., Cornelisse, R., et al. 2000,
  A&A 357, 520

- Turmoil on the accretion disk of GRO J1655−40
  Kuulkers, E., in 't Zand, J.J.M., Cornelisse, R., et al. 2000, A&A 358, 993

- Discovery of 1RXS J171824.2−402934 as an X-ray burster
  Kaptein, R.G., in 't Zand, J.J.M., Kuulkers, E., Verbunt, F., Heise, J.
  & Cornelisse, R. 2000, A&A 358, L71

- The first outburst of SAX J1808.4−3658 revisited
  in 't Zand, Cornelisse, R., Kuulkers, E., et al. 2001, A&A 372, 916

- Discovery of the X-ray burster SAX J1752.3−3138
  Cocchi, M., Bazzano, A., Natalucci, L., Ubertini, P., Heise, J., Kuulkers, E.,
  Cornelisse, R., in 't Zand, J.J.M. 2001, A&A 378, L37

- A half-a-day long thermonuclear X-ray burst from KS 1731−260
  Kuulkers, E., in 't Zand, J.J.M., van Kerkwijk, M.H., Cornelisse, R., et al.
  2002, A&A 382, 503

- Discovery of the neutron star nature of SLX 1737−282
  in 't Zand, J.J.M., Verbunt, F., Kuulkers, E., Markwardt, C.B., Bazzano,
  A., Cocchi, M., Cornelisse, R., et al. 2002, A&A 389, L43

- The nature of the X-ray transient SAX J1711.6-3808
  in 't Zand, J.J.M., Markwardt, C.B., Bazzano, A., Cocchi, M., Cornelisse,
  R., et al. 2002, A&A 390, 597

Curriculum vitae

Op 15 augustus 1974 ben ik geboren te Vlaardingen, waar ik de eerste 19 jaar van mijn leven heb doorgebracht. Na het behalen van mijn VWO diploma in 1992 aan de Vlaardingse Openbare Scholengemeenschap ben ik Sterrenkunde gaan studeren in Leiden. Mijn afstudeeronderzoek bestond uit de analyse van waarnemingen van de Deep Near Infrared Southern Sky Survey onder supervisie van Harm Habing en Erik Deul. Met name was ik geinteresseerd in de populatie van Mira variabelen richting het centrum van de melkweg.

Na het behalen van mijn doctoraal examen in September 1998 ben ik Assistent In Opleiding geworden in Utrecht onder leiding van Frank Verbunt. Hoewel ik in dienst was van de sterrenwacht, was mijn dagelijkse werkplek op het SRON. Hier bevond zich namelijk het archief van de groothoekcameras aan boord van de BeppoSAX satelliet, maar vooral ook de kennis over het onderwerp van mijn promotie in de vorm van Jean in 't Zand, Erik Kuulkers en John Heise. Het resultaat van dit onderzoek ligt nu voor u.

Tijdens mijn promotie onderzoek heb ik conferenties bezocht in Warschau, Amsterdam en Albuquerque (VS). Maar ook ben ik naar een zomerschool te Kreta geweest, en heb een maand waargenomen op de Dutch telescope te La Silla (Chili). Dit alles heeft er toe bijgedragen dat mijn interesse in sterrenkunde alleen nog maar groter is geworden. Vandaar dat ik heb besloten om na mijn promotie het sterrenkundig onderzoek voort te zetten als post-doctoral fellow aan het astronomisch instituut te Southampton.

Nawoord

Tot slot wil ik deze laatste pagina's gebruiken om een aantal mensen te noemen die mij de afgelopen jaren hebben gesteund en geholpen met het tot stand brengen van dit proefschrift.

Allereerst zijn dit mijn twee 'dagelijkse' begeleiders Jean in 't Zand en Erik Kuulkers. Jean, ik weet niet hoeveel rode pennen jij hebt leeggeschreven op de vele versies van mijn artikelen die je langs hebt zien komen. Maar ik hoop dat je in de afgelopen jaren toch hebt kunnen constateren dat ik langzaam vooruitgang boekte. Erik, ik hoop dat jij de 3,5 jaar dat je een kamer met mij moest delen toch hebt weten te overleven. Uiteraard wil ik ook mijn promotoren bedanken. Frank, ik ben blij dat je mij verplichtte om minimaal eens per dag een koffiepauze te nemen. Deze hebben een grote bijdrage geleverd aan mijn algemene sterrenkunde ontwikkeling. John, bedankt dat je tijdens mijn onderzoek professor wilde worden zodat je ook promotor van me kon worden. Jouw visie op sommige van mijn resultaten hebben er voor gezorgd dat ik daar op een heel andere wijze naar ging kijken.

Ook de bijdrage van de Jaap Schuurmans en Gerrit Wiersma, de softwaremensen van de groothoekcameras mag zeker niet onvermeld blijven. Ik kan me zeer goed voorstellen dat ze wel eens erg moe van mij werden als ik weer op de stoep stond met de mededeling dat ik een probleem had.

Voor het tot stand laten komen van een proefschrift moet een instituut toch meer zijn dan alleen maar een werkplek. Gelukkig was dit ook het geval, en een aantal mensen die hiervoor hebben gezorgd wil ik dan ook nog noemen. Marten bedankt voor je bijna dagelijkse trip naar het SRON om daar mijn koffiepauze op te vrolijken, maar vooral ook de maffia-avonden die je organiseerde (en die ik helaas nooit helemaal heb kunnen uitspelen). Joeri en Ferdi bedankt voor het delen van het lot om promovendus bij Frank te zijn. Rob, Mariano, Taka, Kurt, Katrien, Peter, Jelle, Else, and many others, thanks for the entertaining and sometimes even interesting discussions during lunch and coffee time. Anne Grete, bedankt dat je vele van mijn dagelijkse treinreizen sneller hebt doen verlopen met een boeiend gesprek. Nico, ik was altijd erg blij met de onzinnige discussies die we voerden, deze hebben wel geholpen om mijn werk te relativeren.

Dan zijn er uiteraard nog de vrienden die er voor hebben gezorgd dat ik er toch nog iets van een sociaal leven op na bleef houden. Frodo, Vincent, Harm, David, Petra en Jaron ik ben erg blij geweest met de vele ontspannende avonden en bordspelletjes die ik nagenoeg altijd mocht verliezen. Planters, jullie zijn met te veel om iedereen bij naam te worden genoemd. Maar uiteraard bedankt

voor de kerstdiners, spaarzame borrels en koninginnedagen. Ik hoop dat we die kunnen blijven voortzetten. Mien, bedankt voor de vele roddels zodat ik toch nog een beetje op de hoogte bleef. Willemarij, bedankt voor de wel heel milde kritiek die je had op mijn nederlandse samenvatting.

Maar bovenal wil ik mijn moeder en vader bedanken zonder wiens onaflatende steun en vertrouwen in mij dit proefschrift er nooit zou zijn gekomen.